CHARACTERISTICS AND MECHANICS OF SUBAQUEOUS DEBRIS FLOWS

ABDELMAGID MAHGOUB

Characteristics and Mechanics of Subaqueous Debris Flows

By
Abdelmagid Mahgoub

A thesis submitted to the
School of Graduate Studies
in partial fulfilment of the
requirements for the degree of
Master of Science

Department of Earth Sciences
Memorial University of Newfoundland

August 1998

St. John's Newfoundland

Abstract

Debris flows are gravity-driven mixtures of sediment and water that have considerable yield strength. Deposits of debris flows are common features of many modern and ancient continental margins. In this thesis, an integrated approach of marine, outcrop, and laboratory investigation is used to study the character and behaviour of the subaqueous debris flows.

Marine seismic data, obtained from the Northeast Newfoundland Slope, Baffin Bay, Delaware Slope, and South China Sea, were used to unravel certain geometrical aspects such as the overall shape of the deposits, slope angles, basal erosion, and relation to surrounding sea floor. Generally the deposits appear as well defined, seismically transparent lenses aligned downslope for a distance of 70-1700 km from the shelf edge. These lenses have central thickness ranging from few meters to few tens of meters. They are 0.5-75 km long and 0.5-25 km wide. Flows appear to have travelled on very gentle slopes (1.5° to about 0.1°) without significantly eroding the underlying sediments. Piston cores from debris-flow deposits reveal structureless, poorly sorted pebbly mud with numerous lithic fragments and few soft mud clasts.

More detailed information pertaining to structures, fabric, grain-size distribution and the mineralogy of the fine fraction is obtained from outcrops of the Cow Head Group, Western Newfoundland and Fraser River Valley, Central Interior of British Columbia. Deposits typically exhibit extremely poorly sorted massive diamict beds. These are mostly matrix supported with the matrix being mostly sand. A few beds are

clast-supported and show crude inverse grading at their bases. Most beds show no preferred clast orientation and exhibit weak positive correlation between bed thickness and maximum particle size

Variables such as shear strength and pore-fluid pressure, necessary to an understanding of flow support mechanisms, are reported from laboratory experiments using reconstituted slurries of seawater and debris from marine cores. Reconstituted debris-flow slurries develop high values of excess pore-fluid pressure (0.7-2.5 times hydrostatic pressure, depending on depth and sediment concentration). These high values, which are maintained for several hours, are mainly due to poor sorting and high amount of fines. High pore-fluid pressure effectively mobilised debris flows by reducing the total normal stress and consequently the shear strength of the debris material.

Acknowledgements

I would like to thank Professor R.N. Hiscott for his supervision, support and patience. Without his help this project would not have been possible. I would also like to thank the faculty and staff of the Earth Sciences Department especially Professor Ali Aksu for his help and encouragement during the course of this research.

I am grateful to the officers, crew and scientific staff of CSS Dawson 91-029, and CCS Hudson 87-033, 90-007, and 92-045 for their assistance in data collection used in this thesis. I also thank the Ocean Drilling Program, Texas A&M University and Lamont Doherty Observatory of Columbia University for providing seismic data on the Delaware Slope and South China Sea areas.

I would like to thank Dr. N. Eyles of the Geology Department, University of Toronto for suggesting the Fraser River Valley study. The field assistance of Mr. Allan Jones in the Fraser Valley area is greatly appreciated.

The technical staff of the Centre for Cold Ocean Resources Engineering (C-CORE), Memorial University of Newfoundland, are thanked for providing some of the equipment used to carry out some of the experiments conducted during this research. The research was funded by the Stratigrapic Service Section of British Petroleum, London, United Kingdom, and Natural Sciences and Engineering Research Council grants to Professor R. Hiscott. Financial support was also provided by the School of Graduate Studies, Memorial University of Newfoundland, in the form of graduate fellowships and bursaries.

Finally, I would like to extend special appreciation to my friend and colleague Sherif Awadallah for invaluable support and encouragement.

Table of Contents

List of Tables

List of Figures

List of Symbols

Quantity	Symbol
Angle of internal friction (static)	ϕ
Angle of internal friction (dynamic)	ϕ_d
Angle of repose	ϕ_r
Grain size (phi units)	ϕ
Force	F
Pressure	P
Pre-failure bed thickness of non-cohesive, loosely-packed granular sediments	D
Supplied water discharge per unit width near the initiation site of the flow	q_o
Degree of bed saturation	s
Normal dispersive pressure	P_n
Hydraulic head	h_h
Hydrostatic pressure	P_h
Pore-fluid pressure	μ
Pore-fluid pressure (excess)	μ_e
Density (bulk)	ρ_b
Density of pore fluid	ρ_f
Density of solids	ρ_s
Gravitational acceleration	g
Unit weight	γ
Unit weight (submerged)	γ'
Unit weight (debris)	γ_d
Unit weight (solids)	γ_s
Unit weight (fluid)	γ_f
Shear stress	τ
Critical shear stress	τ_c
Internal resistive stress	τ_L
Shear strength	k
Slope angle	θ
Slope angle (lower and upper thresholds)	θ_l , θ_u
Slope angle of flow surface	θ_s
X-ray diffraction goniometer angle	2Θ
Normal stress	σ_n
Effective stress	σ'
Critical thickness	T_c

Chapter 1

INTRODUCTION

1.1 Thesis Scope and Objectives

Since the 1980's, systematic high-resolution seismic surveying of the deep ocean basins has revealed ubiquitous debris-flow deposits (e.g., Damuth, 1980a; Embley, 1980; Damuth and Embley, 1981; Coleman and Prior, 1988; Aksu and Hiscott, 1989, 1992). Beyond the academic desire to better understand this important subaqueous transport process, evaluation of the hazards associated with subaqueous mass movements is critical to the safe seabed disposal of industrial wastes, installation of seabed structures, and coastal development (Brunsden and Prior, 1984; Hampton *et al.*, 1993). Debris-flow deposits have also attracted the attention of the oil industry as potential seals and local sources of hydrocarbons.

Because of the remote and hostile setting in which most submarine debris-flow deposits accumulate and the unpredictable and infrequent timing of the flows, it has proved impossible to observe and quantify flow behaviour in the field. Instead, studies of subaqueous debris flows are based entirely on description of the associated deposits long after their emplacement e.g., detailed side-scan sonar images of the Saharan debris-flow deposit and its surface flow patterns which suggest viscous flow (Masson *et al.*, 1993).

Because of the lack of field monitoring of subaqueous debris flows, flow processes have been interpreted mainly by using unrelated studies of subaerial debris flows in mountainous regions as analogues.

The approach in this thesis is to examine a number of primary deposit characteristics (Table 1), and is similar to the method that Johnson (1970, 1984) used in his seminal studies of the flow dynamics of subaerial debris flows. This approach can be employed successfully only now that large areas of the modern sea floor have been mapped thoroughly, including complete mapping of several large debris-flow deposits. The main objectives of the thesis are as follows:

1. To determine the physical and morphological characteristics of large subaqueous debris-flow deposits, and to compare these with subaerial deposits.

2. To determine flow behaviour (e.g., velocity, viscosity, fluid content, strength, competence, triggering process, transport distance) from characteristics of well-mapped deposits.

3. To evaluate the relative importance of support mechanisms in facilitating the long-distance transport of debris (e.g., matrix strength, grain interactions, buoyancy, prevention of grain settling by overpressured pore fluids, turbulence). In particular, how do the mineralogy and texture of the failed material influence debris-flow behaviour?

Table 1 Debris-flow deposits described in detail in this thesis

Location	Geological Unit	Type of Data	Information Obtained
Northeast Newfoundland Offshore	Quaternary Continental Slope and Rise sediments	Seismic, 3.5 kHz & Piston Cores	3-D Geometry, composition, texture, structure.
Baffin Bay	Quaternary Continental Slope and Rise sediments	Seismic, 3.5 kHz, Piston Cores, Drill Core	3-D Geometry, composition, texture, structure.
Delaware Slope	Quaternary Continental Slope and Rise sediments	3.5 kHz & Piston Cores	2-D Geometry, composition, texture, structure.
South China Sea (northwest of Luzon)	Quaternary Continental Slope and Rise sediments	3.5 kHz & Piston Cores	2-D Geometry, composition, texture, structure.
Fraser River Valley, Central Interior British Columbia	Quaternary glaciolacustrine sediments	Outcrop Data	2-D Geometry, composition, texture, structure.
Cow Head Peninsula, western Newfoundland	Cow Head Group (Cambro-Ordovician carbonate slope apron)	Outcrop Data	2-D Geometry, composition, texture, structure.

1.2 Terminology

The term **debris flow** may have a different connotation for the geologist, the engineer, and the geomorphologist. Even within the same discipline, this process is commonly imprecisely defined, partly because flows show wide range of rheological behaviour, sediment type, water content, support and transport mechanisms, composition, speed, etc. *In this thesis, the term debris flow is used to indicate a gravity-driven flow of a mixture of sediment and water (plus air in subaerial flows). Particles in a debris flow show a wide range in grain size (from clay to large rafts and boulders) and percentage. Water content is typically less than 25% by weight but may approach 50% (Pierson, 1986). The concentration required for particular behaviour cannot be uniquely specified, because flow behaviour is also a function of the composition (fluid chemistry and type of clay) and the grain-size. In contrast with normal stream flow and so-called "hyperconcentrated" flow, debris flows have considerable yield strength and consequently do not behave as Newtonian fluids (Pierson and Costa, 1987).*

Particles in a debris flow can be supported by a variety of mechanisms. These include strength produced by intergranular friction and/or cohesion of clay-size particles, buoyancy, dispersive pressure, excess pore-fluid pressure and, in exceptional cases turbulence. That is why a simple theoretical definition of debris flow is so elusive.

Based on flow character, Postma (1986) divided debris flows into cohesive (plastic) debris flows (clay fraction provides cohesive strength), and cohesionless (fluidal) debris flows (internal friction and dispersive pressure are the dominant mechanisms). Following Postma (1986), cohesionless debris flow is used here to include fluidised, liquefied and

density-modified grain flows (sensu Lowe, 1976). Unless grains are separated from one another in mobile debris, frictional resistance persists even during flow so that cohesionless flows cannot move on low slopes. In contrast, cohesive forces between clay particles are generally broken under shear and do not fully return until the debris has come to rest. Therefore, muddy debris flows are mobile on very low slopes and can travel for long distances.

Some additional terms, defined below, have been applied to particular types of debris flows. **Mud flow** is used by some authors for cohesive flows containing at least 25% clay (Friedman and Sanders, 1978), or 50% mixture of sand, silt and clay (Varnes, 1978). The term mud flow will not be used in this thesis since it has been applied to many other processes (Pierson and Costa 1987). **Debris avalanche** is a term that has been used to described high-velocity debris flow (US Geological Survey, 1982). However, its use is not recommended because avalanche motion is very different from debris flow (Innes, 1983). **Flowtill** is a name applied to supraglacial till that has been modified, transported and resedimented mainly by mass flow (Hartshorn, 1958, Boulton, 1968). It is not used even for ice-marginal deposits in this thesis because, as Lawson (1982) argued, the primary glacigenic character of the deposit is destroyed during the subsequent resedimentation. **Diamict** is a general term to describe a poorly sorted mixture of clasts and matrix regardless of their origin or depositional environment (Frakes, 1978, Eyles *et al.*, 1983). Lithified equivalents are known as diamictites. **Lahar** is a debris flow formed by water saturation and failure of mainly volcaniclastic material on the flanks of volcanoes.

1.3 Organization of the Thesis

Following this introductory chapter, the reminder of this thesis is divided into six chapters. Chapter 2 consists of a review of published research on both subaqueous and subaerial debris flows. Chapter 3 describes outcrop studies, methods for marine data acquisition and laboratory analysis. Chapter 4 provides background information for the case studies used in this thesis. Chapters 5 and 6 represent the contribution of this thesis to understanding subaqueous debris flows. In chapter 5, information related to deposit geometry, composition, fabric, textural and internal structures are extracted from case studies and presented. This information is used ito determine flow character, behaviour and support mechanisms. Finally, chapter 6 summarises the results presented in earlier chapters and recommends areas for further research.

Chapter 2

PREVIOUS WORK ON DEBRIS FLOWS

2.1 Introduction

Although debris-flow deposits are common and widespread in many marine environments, the process of subaqueous debris flow has received less attention from geologists than have other types of sediment gravity flows. In contrast, subaerial debris flows have received considerable attention because of their destructive nature and because they are more accessible; in addition, most laboratory experiments model subaerial flow processes (e.g., Johnson, 1970, Pierson, 1981, Davies, 1988). The lack of detailed knowledge of subaqueous debris flows can also be attributed to their unpredictable and catastrophic nature, which prevents field monitoring. Some useful information regarding the motion and the behaviour of subaqueous debris flows comes from flume experiments and laboratory simulation (e.g., Hampton, 1972); however, these observations are not properly scaled, geometrically nor dynamically, to actual marine environments.

Due to monitoring problems, the available literature on subaqueous debris flow is sparse and mainly descriptive. Rheology and dynamic behaviour are rarely addressed. Deposits are generally interpreted through analogy with their subaerial counterparts and other well studied gravity flows such as pyroclastic flows. The validity of comparisons

with other types of flows needs to be substantiated through independent studies of subaqueous flows and their deposits.

A review of the literature most relevant to this thesis is presented below. Both subaerial and subaqueous debris flows are considered. This review will serve as a foundation for a subsequent evaluation of the emplacement of full-scale subaqueous debris flows, based on newly compiled data and samples from modern ocean basins, drained Pleistocene glacial lakes in British Columbia, and outcrops of ancient deposits in western Newfoundland (Chapters 5 and 6). Variables are defined at their first occurrence in the text and in the list of symbols (page x-xi).

2.2 Review of Research on Subaerial Debris Flows

Although debris flows and their deposits have been described in the literature since the early part of this century (Table 2), much of the geological knowledge of this phenomenon comes from the pioneering work of Bull (1963), Johnson (1965, 1970, 1984), Hampton (1970, 1972, 1975, 1979), Rodine & Johnson (1976), Takahashi (1978, 1981), and Pierson (1980, 1981). More recent process-related collections of papers have been edited by Costa & Sieczorek (1987) and French (1990).

2.2.1 Contributions of Arvid Johnson

The research of Johnson (1965, 1970, 1984, Rodine & Johnson, 1976) includes field observations, laboratory experiments and theoretical analysis. Six major contributions are summarised below.

Table 2 Examples of some early observations of debris flows.

Source	Environment	Triggering mechanism	Slope (Deg.)	Composition	Bulk density (g/cm^3)	Water content (wt %)	Viscosity (Pa)	Velocity (m/s)	Comments
Blackwelder (1928)	semiarid alluvial fan	heavy rain storm	4-6	"till like", clay to large block	-----	-----	------	-----	Resembles lava flow, steep snout, blocks up to 15 m and boulders up to 5 m are fully suspended.
Sharp & Nobles (1953)	semiarid alluvial fan	occurred daily for a week due to snow melting	9 at the upper canyon to < 1	-----	2.4	25-30	200-600	3 (average)	Surges of flow confined to pre-existing channels, thickness decreases rapidly downstream, boulders up to 1 m, transport distance about 25 km.
Curry (1966)	semi arid alluvial fan	heavy rain fall	Initiated on steep slope (31-41)	less than 10 % clay	2.53	< 10 %	3000	16 (max.)	Flow occurred as surges, boulders up to 0.8 m.
Broscoe & Thomson (1969)	"alpine" environment	rain fall & snow melting	13	from clay to boulder size, clay is mainly montmorillonite	-----	-----	-----	----	Flow is channelised, cohesionless, erosive & pulsating. Fan-shaped & lobate nature, thickness 2-3 m. Support mechanisms: matrix strength & buoyancy.

1. Johnson's papers describe the movement of debris flows and similarities among the processes and morphology of debris flow, lava flow and glacier flow. Although they involve movement of quite different material. Johnson indicated that all three types of flow (a) are mainly laminar flows with a non-deforming rigid plug that progressively thickens downward as shear stress decreases until the entire mass ceases to move, (b) have a lobate form with steep fronts (snouts), (c) form lateral ridge deposits, and (d) can be broadly described by similar rheological models.

2. Johnson developed a rheological model that is widely used today to describe flow behaviour, as well as the properties of the deposits. He started by assuming that debris flows exhibit plastic behaviour. Plastic substances will deform only when the applied shear stress exceeds a certain yield value (i.e., $|\tau| > k$, where k is the yield strength). In parts of the flow where this inequality holds, the velocity gradient away from the boundary (the rate of shear strain; du/dy) is given by:

$$|\tau| = k + \eta_b \frac{du}{dy} \qquad (Bingham\ Model) \tag{2.1}$$

where η_0 is Bingham viscosity. Johnson further proposed that the flow can be described in more detail using a combination of the Coulomb Equation (describing the strength factor, k) and Newton's law of Viscosity. In parts of the flow where shear stress exceeds strength:

$$|\tau| = c + \sigma_n \tan\phi + \eta \frac{du}{dy} \qquad (Coulomb\text{-}Viscous\ Model) \tag{2.2}$$

where c is the cohesion, σ_n is the normal stress, and ϕ is the static angle of internal friction, equivalent to the angle of repose.

3. Johnson used Bingham and Coulomb-Viscous models (Eqns 2.1 and 2.2) to estimate the strength of debris by three methods:

a) Critical deposit thickness on a slope:

$$k = T_c \gamma_d \sin\theta \tag{2.3}$$

where T_c is the critical thickness of the deposit behind the snout, γ_d is the unit weight of the debris, and θ is the slope angle.

b) Critical dimensions of channels plugged by debris-flow deposit:

$$k = \frac{D_c \gamma_d \sin\theta}{[2D_c / W_c]^2 + 1} \tag{2.4}$$

where W_c & D_c are the critical width and depth of the plugged channel, respectively.

c) Submerged volume of a large boulder:

$$k = \frac{b}{4} \left| \gamma_b - \left(\frac{\gamma_d}{n}\right) \right| \tag{2.5}$$

where b, γ_b and 1/n are height of the boulder, its unit weight and the volume fraction of the boulder submerged in the top of the debris-flow deposit, respectively.

4. Johnson integrated equation 2.1 and substituted equation 2.3 in order to calculate velocity profile of a steady flow in a semicircular channel using the Bingham model and an equilibrium equation of balanced forces:

$$U_Y = \frac{1}{\eta_b}\left[\frac{H^2-Y^2}{2}\gamma\sin\theta - k\,(H-Y)\right] \qquad [Y \geq T_c] \qquad (2.6)$$

where H is the flow depth at the center of the channel, and Y is the depth below the surface of the flow (Y=0 at flow surface, Y=H at the bed). For $Y < T_c$, $U_Y=U_{max}$.

5. Johnson explained why debris flows and glaciers form U-shape valleys in contrast to the common V-shape valleys formed by stream flow (Johnson, 1970: chapter 15), based on the shape of both contours of equal velocity and cross-sectional profiles of shear stress.

6. Rodine and Johnson (1976) attributed the high transporting ability of debris flow even on gentle slopes to the strength of the fluid phase (water + mud) and the small density contrast between coarse clasts and the enclosing mixture (or "matrix") of water, mud and finer clasts. They advocated a pyramid effect in which the coarser clasts have their buoyant support enhanced by the presence abundant, high-density yet smaller clasts (including silt and sand) in the surrounding matrix. Based on experimental and theoretical analysis of various slurries, Rodine and Johnson concluded that poorly sorted debris can maintain high mobility even with as much as 95 volume percent solids.

2.2.2 Contributions of Tamotsu Takahashi

Utilising the dispersive pressure concept of Bagnold (1954), Takahashi (1978, 1980, 1981) introduced a "dilatant fluid model" that differs from Johnson's models. The formula which Bagnold (1954) derived, based on shearing of a dispersion of neutrally buoyant particles in a Newtonian fluid, can be written as:

$$\left.\begin{aligned} P_n &= a_i \rho_s \lambda^2 \left(\frac{du}{dy}\right)^2 \cos\phi_d \\ \tau &= P_n \tan\phi_d \end{aligned}\right\} \qquad (2.7)$$

where P_n is the normal dispersive stress, τ is the shearing stress, ρ_s is the grain density, ϕ_d is the dynamic internal angle of friction, a_i is a constant, and λ is the linear concentration given by $\lambda = [\,(C_* / C_d)^{1/3} - 1]^{-1}$, where C_* and C_d are the grain concentration in the static bed and the flow, respectively.

Takahashi's model describes the conditions required for both the initiation of flow under heavy rainfall, and final deposition of the debris in terms of particle concentration of the static bed, C_*, and slope angle, θ (Figure 1). Lower and upper threshold values of slope, θ_L and θ_U, provide limits for the conditions of no movement (even if bed is fully saturated) and landslide (i.e., when failure occurs before bed is fully saturated), respectively. If $\theta \leq \theta_L$, then there is no movement. If $\theta > \theta_U$, then landsliding occurs. If $\theta_L \leq \theta < \theta_U$, then debris flow occurs. These threshold slopes are given by:

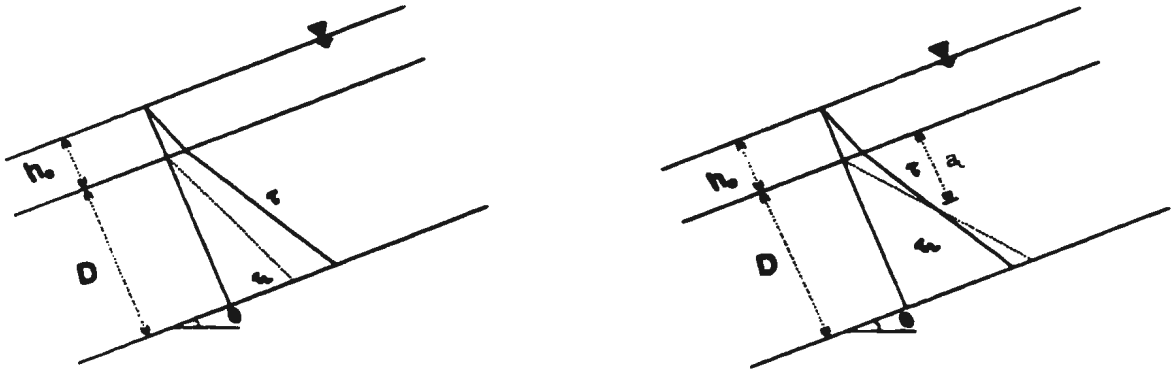

Figure 1 Distribution of shear stress in thick uniform bed of loosely packed non-cohesive grains (after Takahashi, 1978). D is the original bed thickness. Movement starts when the applied stress (τ) exceeds is the internal resistive stress (τ_L). In Case (1), the entire bed will move; in Case (2), only the part of the bed above a_L, will move.

$$\tan\theta_L = \frac{C_*(\rho_s-\rho_f)\tan\phi}{C_*(\rho_s-\rho_f) + (1 + h_o d^{-1})} \quad ; \quad \tan\theta_U = \frac{C_*(\rho_s-\rho_f)\tan\phi}{C_*(\rho_s-\rho_f) + \rho_f} \tag{2.8}$$

where h_o is depth of any overriding surface water flow, ϕ is the angle of internal friction, and ρ_f is the density of the pore fluid.

The critical slope, θ_L, predicted by Takahashi (1978) for the initiation of major downslope transport is much lower than actual slopes observed in subaerial settings. This can be attributed to the fact that equation 2.8 does not account for the stabilizing effects of cohesion. Moreover, natural debris flows are extremely poorly sorted in contrast with Takahashi's (1978, 1981) simplistic assumption of a homogeneous dispersion of uniform grains.

Takahashi (1978, 1981) developed the following equations that describe the frontal height, model the quasi-steady propagation of debris flow and define its equilibrium concentration. Respectively, these are:

$$\frac{h}{h_o} = \frac{U}{U_o} \frac{C_*}{C_* - [s+(1-s)C_*]\,C_{d_*} + \left(\frac{h_o}{D}\right) C_{d_*}\left(1-\frac{U_c}{U}\right)} \tag{2.9}$$

$$\frac{\left(\frac{U}{\sqrt{gd}}\right)^{0.3}}{\left(\frac{q_o^2}{gd^3}\right)} = \frac{0.693\,\sin^{0.2}\theta_s}{(a_i \sin\phi_d)^{0.2}} \frac{\left[\left(\frac{C_*}{C_d}\right)^{\frac{1}{3}} - 1\right]^{0.4}\left[C_d + (1-C_d)\frac{\rho_f}{\rho_s}\right]^{0.2}}{\left[1 - \frac{[s + (1-s)\,C_*]\,C_d}{C_*}\right]^{0.6}} \tag{2.10}$$

$$C_{max} = \frac{\rho_f \tan\theta}{(\rho_s - \rho_f)(\tan\phi_d - \tan\theta)} \qquad \tan\phi_d = \tan\phi_r \qquad (2.11)$$

where C_{max} is the maximum grain concentration in the flow at quasi-steady equilibrium. d is the representative grain diameter, ϕ_r is the angle of repose, s is the degree of bed saturation, U is the propagational velocity of the debris front, θ_s is the slope angle of the flow surface, h is the depth of the flow, g is gravitational acceleration, and q_o is the supplied water discharge per unit width near the initiation site of the flow.

2.2.3 Contributions Emphasizing the Role of Pore Fluid Pressures

Pierson (1981) conducted field and laboratory investigations to determine the dominant particle support mechanism in subaerial debris flow. His study showed that all of the previously proposed mechanisms combined contribute very little to clast support (less than 2%). Due to the high density contrast between boulders and the fluid, buoyancy alone can only account for a maximum of ~ 79% of the dry weight of a boulder even if the entire slurry (including all smaller grain size) is considered to form the supporting matrix (as suggested by Rodine and Johnson, 1976). Field observations show that even at very late stages of flow (i.e., nearly static conditions), debris can still keep large boulders in suspension. This is why Pierson (1981) disregarded the effect of other mechanisms such as dispersive pressure and turbulence and investigated other supplementary mechanisms which might be in operation at that stage. Laboratory measurements indicated that debris slurries exhibit high pore fluid pressures (i.e., pressures above the expected hydrostatic pressure) attributed to the loading effect of

suspended solids on the interstitial fluid phase. Depending on its magnitude and its dissipation rate, this excess pore fluid pressure can provide a substantial grain support by preventing consolidation of the inflated mass (see also Chapter 5).

Subsequent investigations by Lawson (1982) affirmed the importance of excess pore fluid pressure in mobilizing debris flows in a glacial environment. In the vicinity of Matanuska Glacier, Alaska, sediments are virtually cohesionless. Flows were initiated by slumping, backwasting and ablation of ice and the overlying sediments. Measurements of water volume in oversaturated sediments indicated that thawing of the underlying ice and the downslope movement of meltwater through sediments generated and maintained high pore fluid pressures.

2.3 Review of Subaqueous Debris Flow Research

It was not until about 1960 that debris flows were recognised as a major transporting agent of marine sediments, specifically pebbly mudstones (Crowell, 1957, Dott, 1963). The disorganised texture of such deposits attracted the attention of geologists for a long time, but their exact origin was controversial. Some of the mechanisms thought to be responsible for such deposits included ice rafting, ablation of glaciers, selective deep weathering of *in situ* conglomerates, seaward sliding and slumping of coastal clays and nearshore conglomerates (Crowell, 1957 and references therein).

Crowell (1957) strongly suspected mass flow as an origin of pebbly mudstones; however, he proposed a complicated scenario as a prerequisite for their movement:

(1) transportation and deposition of graded gravel by turbidity currents on a pre-existing layer of water-saturated soft mud, (2) sinking of gravel into the mud by loading. (3) failure of unstable sediments as slumps and mass flows which range from sluggish and viscous to more fluidal and turbulent flows.

Dott (1961) suggested subaqueous mass flow of rapidly deposited volcanic-rich sediments as an alternative hypothesis for the origin of the Squantum Tillite of Massachusetts. Dott (1963) further emphasised the importance of understanding the fundamental differences in the dynamics of subaqueous gravity processes. He recognised a continuum of subaqueous gravity flows, in particular to distinguish between plastic mass flow and the more fluidal turbidity currents. According to Dott (1963), the stability of marine sediments is mainly due to a combination of cohesion (mainly in clay-rich sediments) and particle packing (in coarser sediments). Therefore, rapidly deposited (e.g., deltaic) silt and fine sand (being weakly cohesive and loosely packed) are the least stable. They are very susceptible to mass movement. Moreover Dott (1963) explained that excess pore-fluid pressure reduces the critical shear stress (τ_c) needed to fail marine sediments as follows:

$$\tau_c = c + (\gamma'_s z - \mu_e) \tan\phi \qquad (2.12)$$

where μ_e is the excess hydrostatic pressure of Terzaghi (1956), γ'_s is the submerged unit weight of sediments and z is the depth below the depositional interface.

Fisher (1971) described submarine mass-flow deposits up to 9 m thick. The emplacing flows fully supported sub-horizontal siltstone and sandstone slabs up to 3 m

long. The deposits show inverse grading and limited erosional features. Fisher suggested an origin similar to that of laminar subaerial debris flows transitional to Newtonian flows. Depending on the scale of observation and maximum particle size. Fisher (1971) considered debris flows to have two phases: (a) a continuous phase called matrix (water, clay and sand), and (b) a dispersed phase (larger clasts).

Hampton (1972) indicated that the incorporation of only a few percent of water can transform a subaqueous slide into a debris flow analogous to subaerial flows studied by Johnson (1970). This process can ultimately lead to the generation of turbidity currents due to the erosion of sediments from the surface of the debris front and the ejection of this material into the overlying water to form a more dilute suspension. According to Hampton (1972), little water can be incorporated into the body of the moving debris flow; mixing is inhibited by the presence of clay and solids.

By considering the equilibrium forces acting on a clast, Hampton (1975) calculated flow competence (largest supported grain-size, d_{max}) as follows:

$$d_{max} = \frac{8.8\ k}{g(\rho_s - \rho_f)} \qquad (2.13)$$

This analysis only considered clast weight, buoyancy and matrix strength. Experiments confirm that in fine-grained debris flows values for k and d_{max} vary with the amount and type of fines. Although addition of only a few percent water can drastically reduce strength and therefore competence, Hampton (1975) showed that even very dilute slurries (clay content 1.5-19 %) are capable of supporting sand.

Subsequent experiments by Hampton (1979) indicated that competence is further enhanced in heavily loaded debris flows. In these flows the weight of clay and coarse particles is transferred to the fluid causing an increase in pore fluid pressure which in turn effectively increases buoyant support of large clasts by the flow.

Enos (1977) used plots of velocity versus yield strength for experimental flows to differentiate between laminar and turbulent flows. Experiments indicated to Enos (1977) that variables such as the Reynolds and Froude numbers are less significant in determining the flow regime in debris flows. Instead, strength is the main factor that determines the flow behaviour of Bingham materials. Field observations indicate that materials of high strength (highly concentrated and muddier) tend to flow in a laminar fashion.

Hiscott and Middleton (1979) plotted data of Hampton (1972) to show that turbulence in subaqueous debris-flows depends on both the Reynolds number, R, and the Bingham number, $B = \tau_c H/\eta\bar{U}$, where $\bar{U}$ is the average velocity. A conservative criterion for turbulence is $R \geq 1000\ B$.

Many natural debris-flow deposits exhibit inverse grading. Popular explanations for this phenomenon include Bagnold's dispersive pressure (section 2.2.2), the kinetic sieving mechanism of Middleton (1970) and Hampton's (1972) demonstration that competence of slurries decreases after prolonged vigorous shear, which is of greater intensity near the base of debris flows (Naylor, 1980).

Unlike most other gravel deposits, debris-flow deposits show positive correlation between bed thickness (BTh) and maximum particle size (MPS). Nemec and Steel

(1984) explained this commonly observed phenomenon in terms of the Coulomb-viscous model (Eqn. 2.2), and Hampton's force-equilibrium relationship (Eqn. 2.13). According to Nemec and Steel (1984), plots of BTh versus MPS, if carefully used, can be useful in distinguishing between cohesive and cohesionless debris flow. Furthermore, the high correlation of these variables suggests equilibrium between competence and flow thickness which is typical of flows with important grain support from dispersive pressure.

Deep-water carbonate debris-flow deposits of the Cow Head Group, western Newfoundland, resemble subaerial debris-flow deposits in many geometrical and textural aspects (e.g., snout shape, clast fabric, etc.). Hence, Hiscott and James (1985) justified the application of Johnson's formulae (Eqns. 2.3 & 2.5) to calculate strength and paleoslope for these deposits. Calculated values for static strength range from 10^2-10^4 kPa, within the range of values reported by Johnson (1970). Calculated values of paleoslope were rather high (10°-18°), but could be reduced to more reasonable values of 1°-2° if excess pore fluid pressures characterised these flows (based on application of experimental results of Pierson, 1981).

On the Northwest African continental margin and in the vicinity of the Canary Islands, two large debris-flow deposits (the so-called Saharan and the Canary debris-flow deposits) cover vast areas of the slope. Masson *et al.* (1992, 1993) surveyed these deposits using a combination of seismic profiles (3.5 kHz) and side-scan sonar. The side-scan sonar images add a new dimension to traditional echo-character mapping and provide a more complete picture of the deposits. While long-range side-scan sonar images outline the aerial extent of the flows, higher resolution images show surficial

details that were interpreted as: (a) longitudinal shear bands which parallel flow direction, (b) fine-scale flow banding (compositional) resulting from clast streaming, (c) lateral ridges (levees) marking the boundaries of several flow pulses, and (d) large rafted blocks up to 3 km in diameter and few tens of meters in thickness. Masson *et al.* (1993) speculated that these features are products of non-turbulent viscous flow that had strength and flowed in laminar fashion.

Recent deep ocean drilling of the Amazon Fan (ODP site 941; Flood *et al.*, 1995) sampled a 125 m-long section through a Quaternary mass-transport deposit. The core shows a remarkable clast-supported breccia (clasts centimetres to several metres in dimension) that contains only a little muddy matrix. This deposit, which has a volume of 4000 km3, is one of a number of similar deposits that cover about 40% of the fan surface. Piper *et al.* (1997) interpret this and other similar deposits on Amazon Fan to be slides of large blocks encased in only a small amount of matrix. More matrix-rich units atop some of the block-rich units are interpreted as the deposits of true debris flows.

2.4 Requirements for a Better Understanding of Subaqueous Debris Flows

The wide range of variables that influence the behaviour of debris flows complicates the task of modelling them. Any attempt must allow for, reflect and even emphasise these variations.

Comparative models derived from subaerial settings must be first evaluated and then calibrated for use in the marine environment. Evaluation of support processes in

water-rich and fine grained debris, the role of pore-fluid pressure and the unique effects of marine environments on the stability/mobility of sediments are but a few aspects that need to be addressed.

Our understanding of subaqueous debris flow processes is hindered by a lack of adequate outcrops on land and deficiencies, until recently, in marine sampling and imaging techniques. For example, problems of obtaining long gravity or piston cores in cohesive and pebbly mud generally restrict information to the uppermost few meters. Limitations in resolution and/or penetration of seismic profiling techniques and the spacing of survey lines often limit recognition of the details of the deposits and preclude accurate mapping of deposit geometry. These limitations also restrict correlation between field and marine data and the establishment of a common database.

Observations and experiments conducted by researchers such as soil and hydraulic engineers operating outside the field of geology (for example, numerous papers in *Hydraulics/Hydrology of Arid Lands*, edited by R. French, 1990) must be incorporated into any synthesis of processes.

Targeted *in situ* studies of slope stability would be particularly helpful in developing models for subaqueous sediment slides and debris flows.

This thesis takes the approach that the small number of well imaged and mapped subaqueous debris-flow deposits from the modern seafloor and Quaternary outcrops can provide important constraints on flow processes. These existing data have not previously been consistently analysed to extract all the critical data on which to base general conclusions.

Chapter 3

METHODS AND DATA SOURCES

3.1 Introduction

This study utilises several lines of inquiry to extract as much information as possible from observations that scale over several orders of magnitude. First, marine seismics are used to unravel certain geometrical aspects such as the overall shape of the deposits, slope angles, basal erosion, relation to surrounding sea floor, etc. These data are augmented by more detailed information obtained from outcrops and sediment cores pertaining to structures, fabric, grain-size distribution and the mineralogy of the fine fraction. Variables such as shear strength and pore-fluid pressure, necessary to an understanding of flow support mechanisms, are reported from laboratory experiments using reconstituted slurries of seawater and debris from marine cores. This integrated approach of marine, outcrop and laboratory analysis is used to clarify the character and behaviour of the flows (chapters 5 and 6).

3.2 Methods for the Analysis of Marine Data

3.2.1 Seismic Data

Seismic data and piston cores were collected with the author's participation from the Northeast Newfoundland Slope during cruise 92-045B of CSS Hudson between October 25 and November 20, 1992. The survey included about 1500 line-km of high-

resolution 3.5 kHz and 40 in^3 airgun reflection profiles acquired using 30.5 m and 6 m streamers (Seismic Engineering streamer and a Nova Scotia Research Foundation Corporation hydrophone array, respectively). Bathymetry data were collected using a 12 kHz echosounder. Data from earlier seismic surveys (including 3.5 kHz and airgun profiles) in the same area were obtained from marine data repository of Memorial University (cruises 90-007 and 91-029; Aksu and Hiscott, 1992).

Seismic data from Baffin Bay are mainly 3.5 kHz and airgun profiles collected during CSS Hudson cruise 87-033 (Aksu and Hiscott, 1989). Additional 3.5 kHz seismic profiles from other parts of the world ocean were obtained from Lamont-Doherty Earth Observatory data base. These profiles were collected in the South China Sea (cruises Conrad 14-04, 17-10, 20-06, 26-04, -12 & -14 and Vema 28-17, 33-09, 34-04, 36-08 & -14) and Delaware Slope (cruises Conrad 19-03, -07, -19 & 20-01 and Vema 30-02 & 33-09).

3.2.2 Core Samples

Piston cores were raised from the Northeast Newfoundland Slope during cruise 92-045B. The upper parts of four shallow debris-flow deposits were cored (cores 92-045-07P, -08P, -12P & -13P). Due to the stiff nature of the deposits, these cores range in length from 3.7 m to 7.2 m, including debris-flow deposits 0.2 m to 2.0 m thick. Cores were first visually described for lithology and sedimentary structures by the author, then photographed, X-rayed and sampled for further analysis.

Table 3 Core sub-samples used for grain-size analysis. (*) denotes sample also used for clay-mineral analysis; mbsf = meter below sea floor.

Sample #	Case study	Location of the sample	Interval	Remarks
8X1-108	Baffin Bay	core 645B-8X, section 1	108-112 cm (63.1 mbsf)	ODP Leg 105, site 645, hole B
8X1-83		core 645B-8X, section 2	83-87 cm (64 .3 mbsf)	
9X1-52 *		core 645B-9X, section 1	52-57 cm (72.2 mbsf)	
9X2-30		core 645B-9X, section 2	30-34 cm (73.5 mbsf)	
47-75	Delaware Bay	19-47P	75-77 cm	Cruise: Conrad 19, core: 47P
47-302 *		19-47P	302 -304cm	
47-502		19-47P	502-507 cm	
47-703		19-47P	703-705 cm	
47-1044		19-47P	1044 -46cm	
48-54		19-48P	54-56 cm	Cruise: Conrad 19, core: 48P
48-255		19-48P	255-257cm	
48-504		19-48P	504-506 cm	
48-754		19-48P	754 -756cm	
48-954		19-48P	954 -956cm	
07-280	North-east Newfoundland Slope	core 92045B-07P	280-283 cm	Cruise: Hudson 92045B
07-340 *		core 92045B-07P	340-343 cm	
08-360		core 92045B-08P	360-363cm	
12-430		core 92045B-12P	430-443 cm	
12-480		core 92045B-12P	480-482 cm	
12-530		core 92045B-12P	530-533 cm	
12-575 *		core 92045B-12P	575-577 cm	
13-627		core 92045B-13P	627-630 cm	
13-660 *		core 92045B-13P	660-663 cm	
13-693		core 92045B-13P	693 -696cm	
29-945	South-China Sea	34-29P	945-947 cm	Cruise: Vema 34 , core: 29P
29-1045		34-29P	1045-47 cm	
29-1135 *		34-29P	1135-37cm	

Additional core subsamples were obtained from repositories for grain-size and clay mineral analysis (Table 3). Baffin Bay subsamples were obtained from the Ocean Drilling Program repository at Texas A & M University (cores 105-645B-8X and -9X). Delaware Slope and South China Sea subsamples were obtained from Lamont-Doherty Earth Observatory (cores Conrad 19-47P & -48P, and Vema 34-29P, respectively).

3.3 Outcrop Studies

Fabric measurements were completed at lacustrine Quaternary outcrops at Gang Ranch (16 sites), Farwell Canyon (2 sites), and Quesnel (2 sites). The orientation (long-axis azimuth and plunge) of 40 clasts larger than 2 cm were measured within a 1 m^2 area of freshly exposed vertical outcrop. In each debris-flow deposit, only prolate clasts with axial ratios of $b/a < 2/3$ and $c/b > 2/3$ were used for fabric study. In a few cases where the desired number of clasts could not be obtained, the grid area was slightly expanded. Clasts which were perceived to be shielded or locked in the interstices of larger clasts (i.e., not freely dispersed) were not considered. Clast fabrics of the Cambro-Ordovician Cow Head debris-flow deposits were measured by Hiscott and James (1985), and were not repeated for this thesis.

Field data are plotted as lower-hemisphere equal-area stereographic projections (Figure 19, section 5.5). Orientation statistics were calculated using the computer program Quickplot (Van Everdingen *et al.*, 1992). Following the eigenvalue method (Mark 1973, Woodcock 1977), the three eigen vectors V1, V2 and V3 represent the principal (dominant), the intermediate, and the minor orientation axes. The

corresponding eigenvalues S1, S2 and S3 quantify the strength (C), and the clustering (K) around the eigen vectors (see Table 7 and Figure 20, section 5.5). The shape of the distribution can be one of the following:

Cluster $S1 > S2 \approx S3$

Girdle $S1 \approx S2 > S3$

Uniform $S1 \approx S2 \approx S3$

Theoretically, the principal eigenvalue (S1) can range from 0.33 (indicating a uniform distribution) to 1.0 (indicating a perfectly clustered unimodal distribution). Field results are discussed in section 5.5.

3.4 Laboratory Techniques

3.4.1 Grain-size Analysis

Several methods and techniques were applied to determine the full distribution of grain size in outcrop and core subsamples. In outcrops, the size of each boulder, cobble and pebble larger than 2 cm was estimated by outlining these clasts on field photographs of cleaned two-dimensional faces. Clasts were first assigned to grain-size classes using, as characteristic dimension, the diameter of a sphere with the same cross-sectional area. Then, the volume proportion of each class was estimated by the area percent covered by all such clasts on the photograph. Finally, the weight percentage of each size fraction was calculated assuming quartz mineral density.

The fraction of the sample approximately less than 2 cm was analysed with sieve and Sedigraph techniques. In some cores, the grain size and volumetric abundance of

clasts approximately larger than 0.5 cm was determined in a similar way from X-radiographs (Figure 2).

Samples weighing 10 to 100 g (depending on the nature of the sample) were first treated with 10 ml 30% hydrogen peroxide for 24 hours to remove any organic material. Samples were then dispersed in 1% sodium hexametaphosphate (calgon) solution and further dissaggregated using an ultrasonic probe for about one minute. The treated samples were then split by wet sieving at 4.0 ϕ (63 μm). The coarse fraction was dried and sieved at 1/2 ϕ intervals, and the fine fraction up to 11 ϕ (0.49 μm) was analysed with an automated grain-size analyzer (Sedigraph 5100).

Results (in weight percent) from the sieve and Sedigraph analyses were combined and plotted as histograms, pie diagrams and cumulative frequency curves (Folk, 1980, Appendix A). The break around 5Φ, which is always observed whenever Sedigraph and sieve data are merged, is artificial. It should not be misinterpreted as natural feature of the deposit. Some duplicate sampling and duplicate analyses were performed to delineate any sampling bias and analytical errors (i.e., sieve losses, temperature variations for Sedigraph, etc.). A more complete estimate of the entire grain-size population was obtained by merging data from sieving and the Sedigraph with pebble to boulder proportions measured directly from core X-radiographs and field photographs (Appendix A). Results of grain size analyses and their implications are discussed in section 5.4.

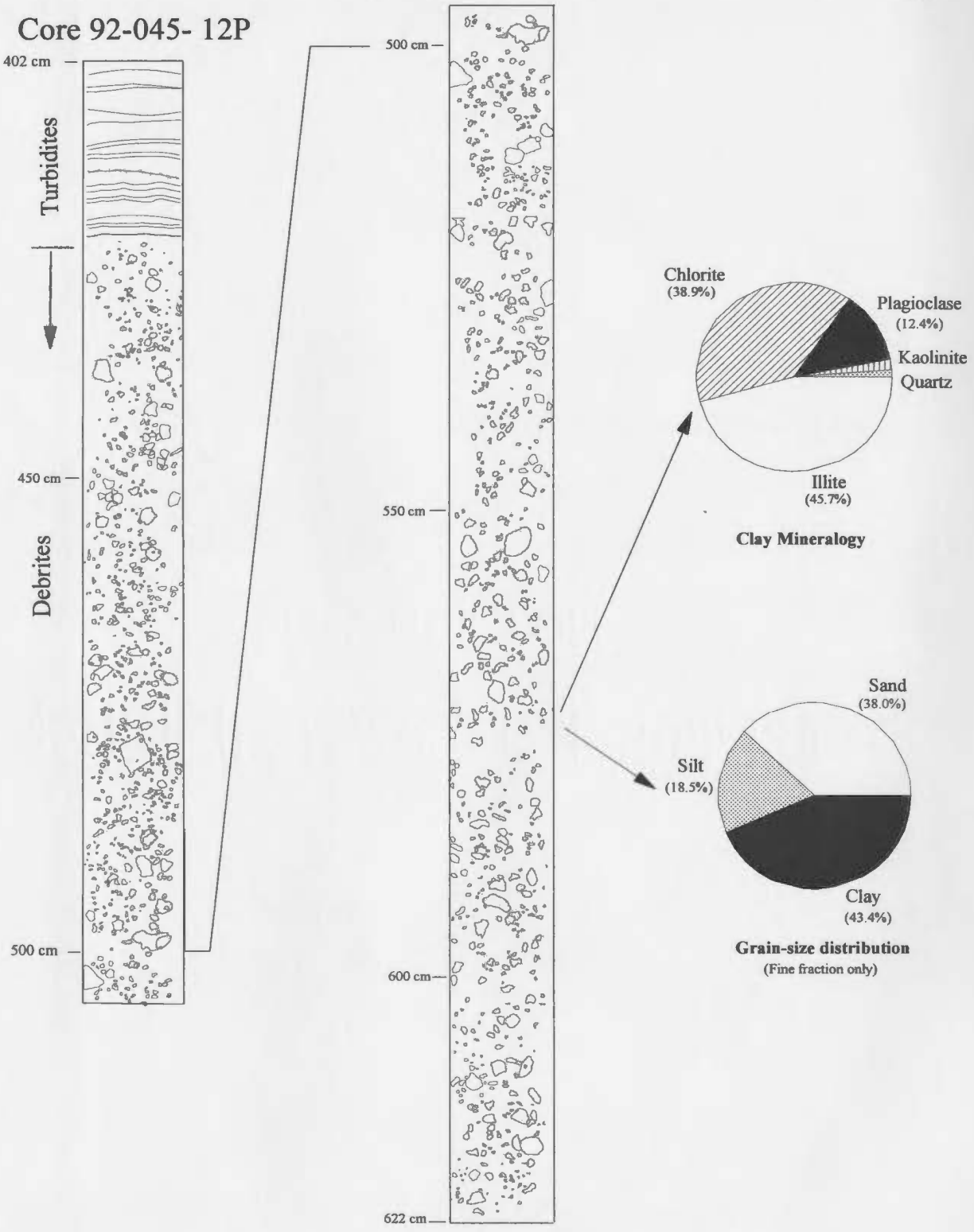

Figure 2 Size, shape, and distribution of clasts in a piston core sample of a debris-flow deposit plotted from X-radiograph. Core is from the Northeast Newfoundland Slope (see Figure 6 for location).

3.4.2 Clay Mineralogy

Some outcrop and core subsamples (Table 4) were chosen for a semi-quantitative determination of their clay-mineral contents using X-ray diffraction (XRD). The analysis was performed on clay-size material (<2 μm).

The fine fraction (< 63 μm: already treated for organic removal) was subjected to ultrasonic treatment for a time not exceeding 3 minutes. The sample was then put in a 1000 ml graduated cylinder and left to settle for 16 hours. A < 2 μm sample was obtained by drawing off the upper 20 cm of the suspension. The suspension was then centrifuged, treated with 5% acetic acid (for carbonate removal), centrifuged again, washed with distilled water, centrifuged a final time and decanted. Iron was removed following a procedure described by Mehra and Jackson (1963). The clay fraction was then washed in 20ml of a saturated calcium chloride solution, centrifuged, washed with distilled water, centrifuged again and decanted.

The paste of the < 2μm minerals was smeared on frosted glass slides and dried in a desiccator at room temperature to obtain an oriented mount. Three sets of mounts were analysed using a Rigaku Ru-200 X-ray diffractometer with Cu kα as a radiation source at the following setting: 40 kV/50 mA, 1° divergence slit, 0.3 mm receiving slit, sampling interval of 0.03°.

The first set of mounts was run at 3° 2θ per minute between 3° and 35° in order to identify the principle clay-size minerals (Thorez, 1974). The same slides were rerun from 24.5°-25.5° 2θ at a lower scanning speed of 0.25° 2θ per minute in order to differentiate between chlorite (3.54Å) and kaolinite (3.58Å) (Biscaye, 1964).

The second set of mounts was placed in a desiccator containing ethylene glycol for several hours in a 60°C oven. The slides were scanned at 1° 2θ per minute from 3°-35° 2θ in order to distinguish between smectite and chlorite, because ethylene glycol has the effect of expanding smectite to a basal spacing of about 17Å (Carroll, 1970).

The third set of mounts was heated to 375°C for one hour, and run at a scanning speed of 1° 2θ per minute to differentiate smectite (and mixed layer illite-smectite) from other clay minerals. Heating to this temperature causes the smectite to collapse to 10Å while leaving the other clay minerals unaffected (Thorez, 1974). Samples were then heated at 550°C for one hour, and rerun at a scanning speed of 1° 2θ per minute in order to differentiate kaolinite from the other clay minerals. Heating to this temperature causes the kaolinite and some chlorite to collapse (Thorez, 1974).

Diffractograms showing various mineral peaks were obtained. Minerals were identified by their lattice spacings (Biscaye, 1965; Carroll 1970; Tucker 1988). Peaks representing major clay and clay-size minerals include montmorillonite (17Å), illite (9.9-10.1Å), quartz (4.26Å), feldspar (3.18Å), amphibole (8.4-8.5Å), chlorite & kaolinite (7Å), and montmorillonite (17Å). Semi-quantitative relative abundances of each clay-size mineral were obtained by multiplying peak height, by peak width at half height, by a characteristic intensity factor(I), different for each mineral (quartz = 1, plagioclase = 2.8, amphibole = 2.5, montmorillonite =1, illite = 4 and chlorite & kaolinite =2; Biscaye, 1965). The ratio of chlorite to kaolinite was determined by measuring the area under the 3.54Å peak (chlorite) and the 3.58Å peak (kaolinite) obtained by slow scanning (Biscaye, 1964). Results are discussed in section 5.4.

3.4.3 X-radiography

Piston cores containing debris-flow deposits were X-rayed using an industrial Picker X-ray source (model 6321). Placing cores on specially designed aluminium "channel" (Figure 3) prevented dark-edge effect produced by overexposure at core edges. This provided a uniform and clear image across the entire core width (10.5 cm). Best results were obtained when the cores were exposed for 2 minutes at a voltage of 70 kV and a current of 50 mA.

3.4.4 Rheology of reconstituted slurries

About 2 kg of debris-flow deposit were taken from the core catcher of core 92-045-7P, raised from the Northeast Newfoundland Slope. Water content, average wet bulk density, density of dry solids, and grain-size distribution were determined first. The whole sample was placed in 4-liter glass container. Reconstituted slurries with different water content were made by adding known volumes of sea water. Immediately after thoroughly mixing each slurry, undrained shear strength was measured using a small laboratory vane shear device (Wykeham Farrance, model WF2350). Then pore-fluid pressure was measured at different depths using a miniature pore pressure transducer (Druck, type PDCR 81) provided by the Centre for Cold Ocean Resources Engineering (C-CORE), Memorial University of Newfoundland.

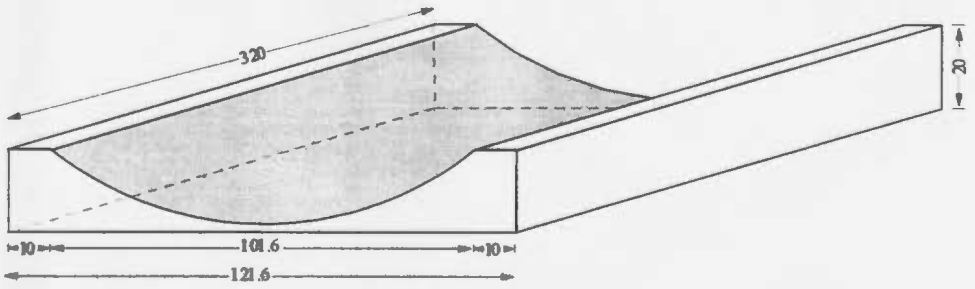

Figure 3 Diagram of aluminium "channel" designed to compensate for the dark edge effect produced by overexposure to X-rays at core edges. Dimensions are in millimeters. Central thickness is 2 mm.

The transducer is a very small (11.4 mm long & 6.4 mm in diameter), sensitive, fast, and reliable device. It can detect changes as little as 1 Pa and consistently provides a linear pressure profile in clear water columns (Figure 4). The transducer is made of a single-crystal silicon diaphram with a fully active strain gauge bridge which is protected by a porous filter plate. The transducer requires a steady excitation voltage of 5 V. This was ensured by using a voltage reference (steady within $\pm 10^{-5}$ V) attached to an AC\DC adapter. The output voltage for each pore-fluid pressure measurement was recorded by multimeter with an accuracy of $\pm 10^{-6}$ V ($\pm$ 1 Pa). To ensure that the transducer was working properly, it was immersed in boiling water for a few minutes and then calibrated before being implanted into each experimental slurry. Measurements were taken every minute for the first half-hour, every 5 minutes for the next 2 hours and then occasionally for the next 12 hours. Twelve unique experimental runs and 4 duplicate runs were completed in vibration- and noise- free environment to prevent interference and minor disturbance of the slurry (Figure 22). Results of experiments are discussed in section 5.6.

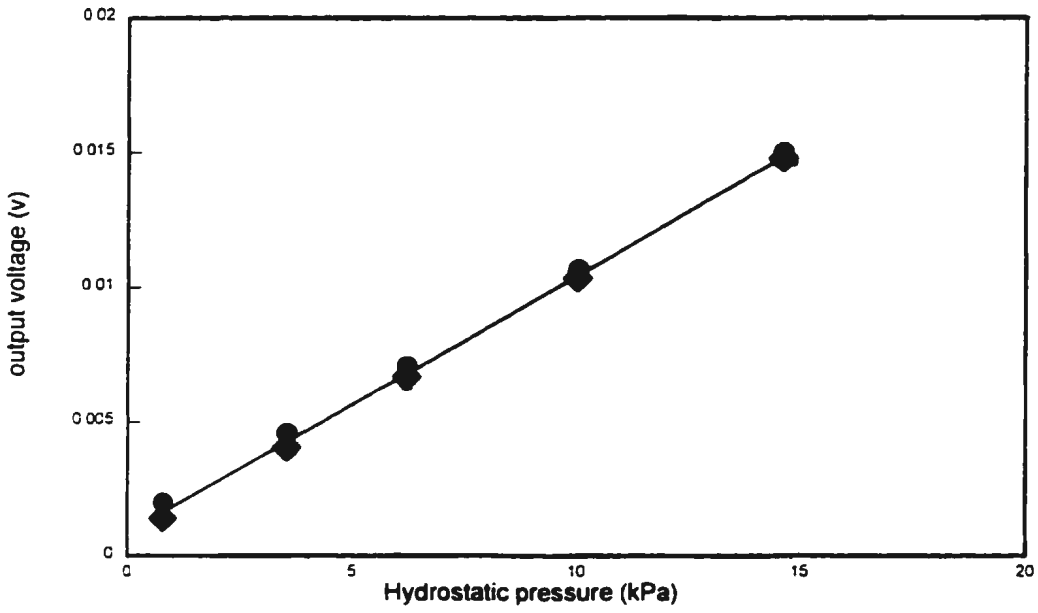

Figure 4 Calibration of pore-pressure transducer using clear water columns.

Chapter 4

BACKGROUND FOR CASE STUDIES

4.1 Introduction

This chapter provides background information for each case study used in this thesis, including location, geological and environmental settings, geological history, relevance to this study and the related pertinent previous work.

4.2 Marine case studies

4.2.1 The Northeast Newfoundland Slope

The study area is situated on the northeastern continental slope of Newfoundland between long. 47°-52°W and lat. 48°-51°N (Figure 5, Figure 6). The slope is devoid of submarine canyons and valleys. To the west lies a broad shelf (about 300 km wide) and to the east lies a small semi-enclosed basin (2500-3500 m water depth) known as Orphan Basin. Three segments of the slope can be recognised: An upper slope which begins at about 300 m isobath and has a gradient of 1.5°, a middle slope which averages 0.7° and extends between the 700-2000 m isobaths, and a lower slope which is generally < 0.5° and extends down to the 2500 m isobath. Below the 2500 m isobath lies the continental rise.

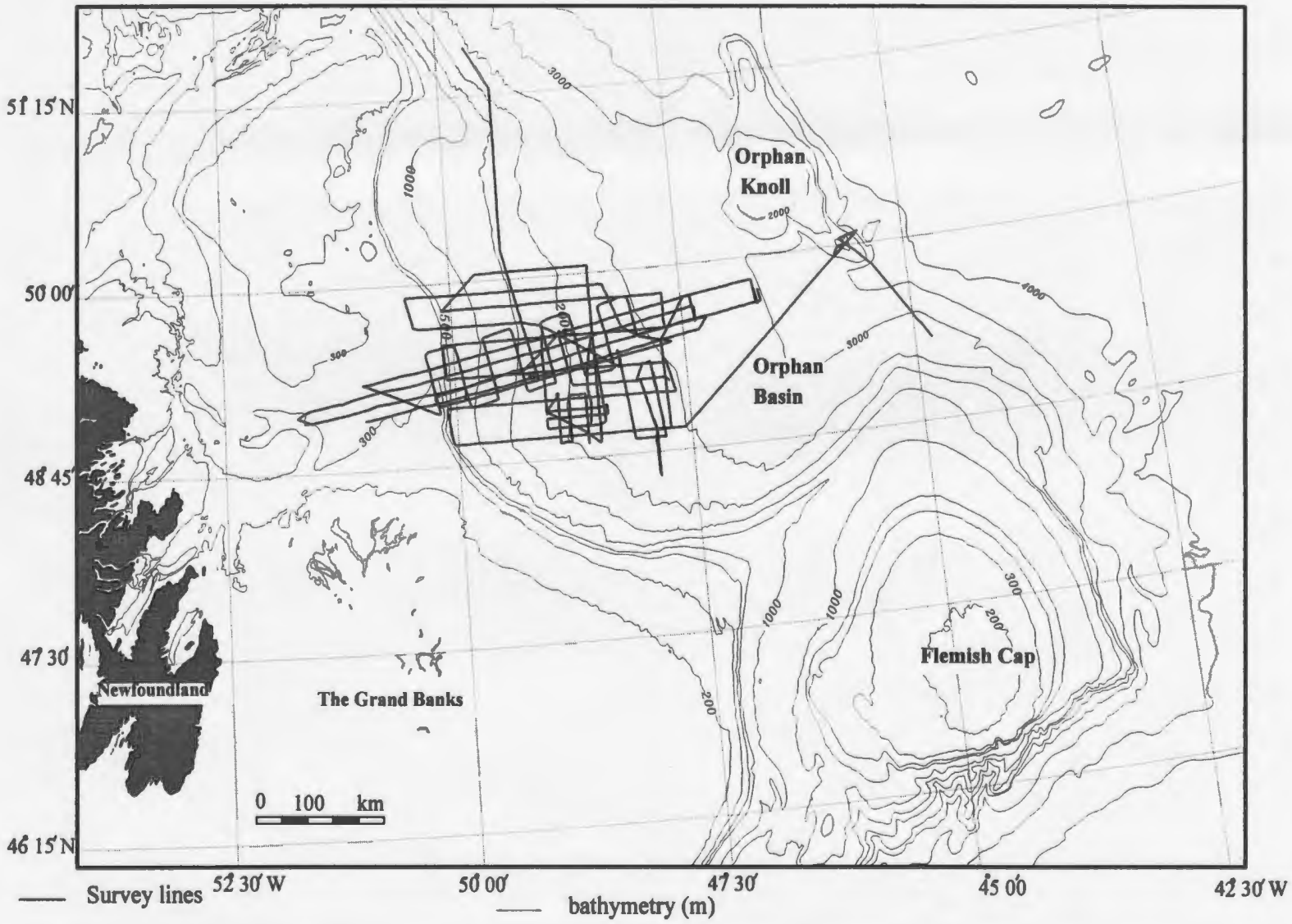

Figure 5 Physiography of eastern Newfoundland offshore (modified from Aksu and Hiscott, 1992). Details of study area are shown in Fig. 9.

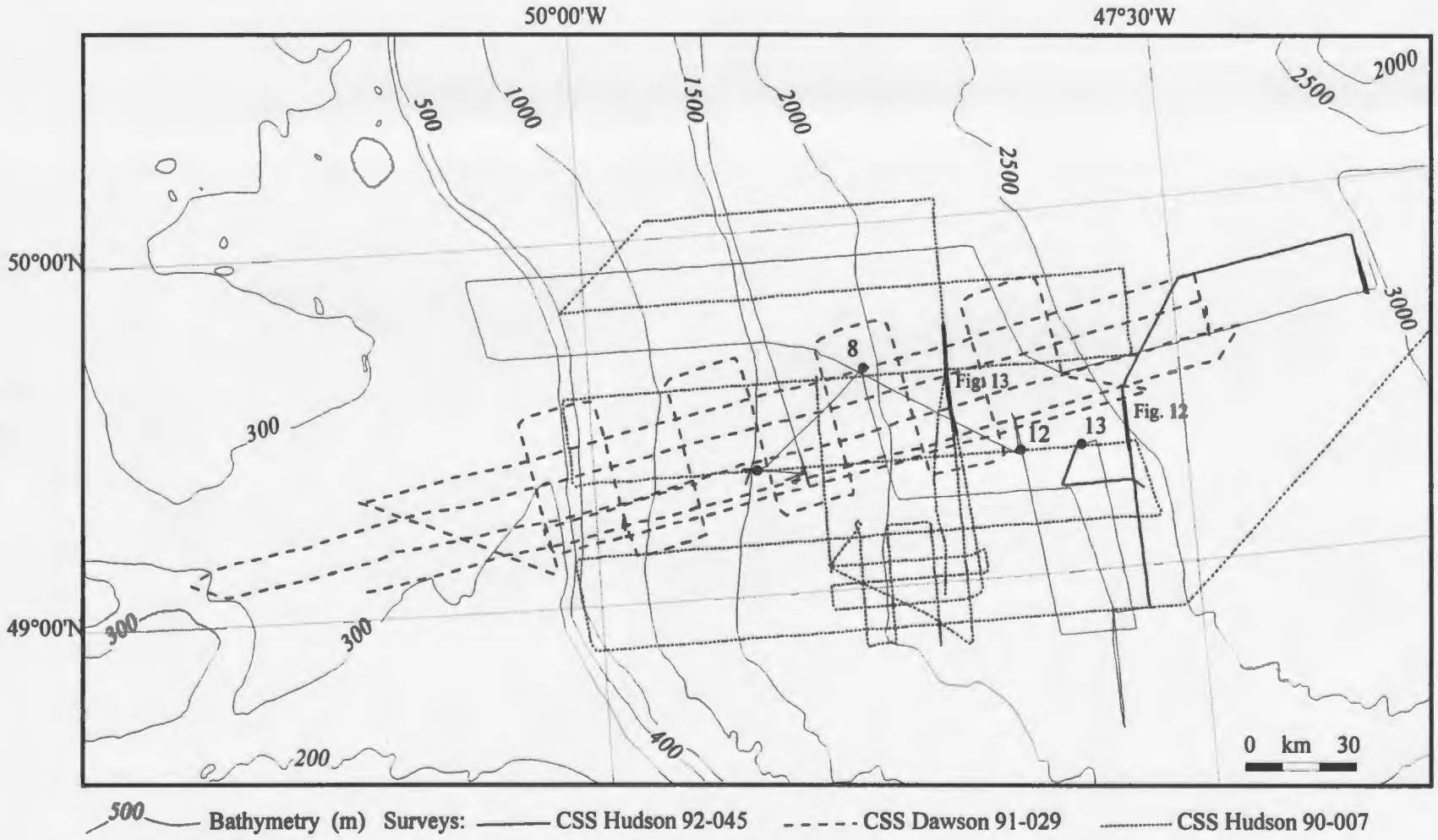

Figure 6 Detailed survey area. Numbered heavy line segments indicate location of seismic reflection profiles shown in corresponding figures. Solid dots indicate cores containing debris-flow deposits.

Carter *et al.*(1979) studied the morphology, sedimentology and faunal content of surficial sediments on the slope and the rise. According to Carter *et al.* (1979), the upper slope features hummocks (< 10 m high) and a terrigenous gravely muddy sand cover with low average concentrations of organic carbon (0.37 wt %), $CaCO_3$ (< 10 wt %) and foraminifera . Both upper slope and shelf sediments are reworked by the Labrador Current, a southward-flowing surface current. The middle slope is smoother (except for a few undulations) and has finer sediment cover (mainly clayey mud) that is richer in organic carbon (0.41 wt %), $CaCO_3$ (20 wt %) and foraminifera. The lower slope has a similar morphology to the middle slope but slightly coarser surficial sediments (sandy mud), lower organic carbon (0.30 wt %) and higher $CaCO_3$ content (27 wt %). Wavy bedforms on the lower slope and parts of the middle slope were probably generated by the southeast-flowing Western Boundary Undercurrent (WBUC). Surficial sediments become coarser (gravely sands) towards the continental rise of Orphan Basin, where prominent wavy bedforms indicate a greater influence of the WBUC.

The area was investigated by Aksu and Hiscott (1992) who mapped and described the Quaternary sediments of the slope using seismic surveys and piston cores. Their study indicates that the slope is constructed of sediments which were delivered directly and continuously to the slope during much of the Quaternary by mass-wasting of shelf-edge glacial and pro-glacial deposits. The majority of these sediments were deposited by large debris flows. The debris-flow deposits appear as seismically transparent lenses, shingled and aligned down the slope.

4.2.2 Baffin Bay

Baffin Bay is a relatively small (~1200 km long & 100-500 km wide) but deep (2300 m in the center) semi-enclosed basin north of the Labrador Sea between Baffin Island and Greenland (Figure 7). A narrow shelf (~50 km wide, ~ 200 m deep) lies to the west, followed by a slope which averages 2-3°, leading to a central abyssal plain. The eastern shelf off Greenland is wider (~150 km) and deeper (average ~450 m). Baffin Bay is connected to the Labrador Sea by Davis Strait. The central basin floor generally flattens northward and finally progressively shallows up to the north.

The study area is located in the western slope of Baffin Bay. Relevant background information comes from: (a) a sedimentological study by Aksu (1984) of 40 piston cores containing thin bedded debris-flow deposits from the entire basin, (b) continuous coring of parts of the slope by the Ocean Drilling Program (ODP Site 645: Srivastava *et al.*, 1987), and (c) a seismic study of this area by Aksu and Hiscott (1989) and parallel study by Hiscott and Aksu (1994) in the vicinity of Home Bay, south of the study area.

The slopes of Baffin Bay, which lack submarine canyons, are characterised by abundant slide and debris-flow deposits. Hence, Aksu and Hiscott (1989) and Hiscott and Aksu (1994) propose a line-source style of sedimentation whereby large amounts of sediment were supplied to the shelf edge during Pleistocene glaciations. Mass movement of these sediments created an erosional upper slope and a constructional lower slope. Mass wasting along the ice margin periodically reshaped the slope of the seafloor and

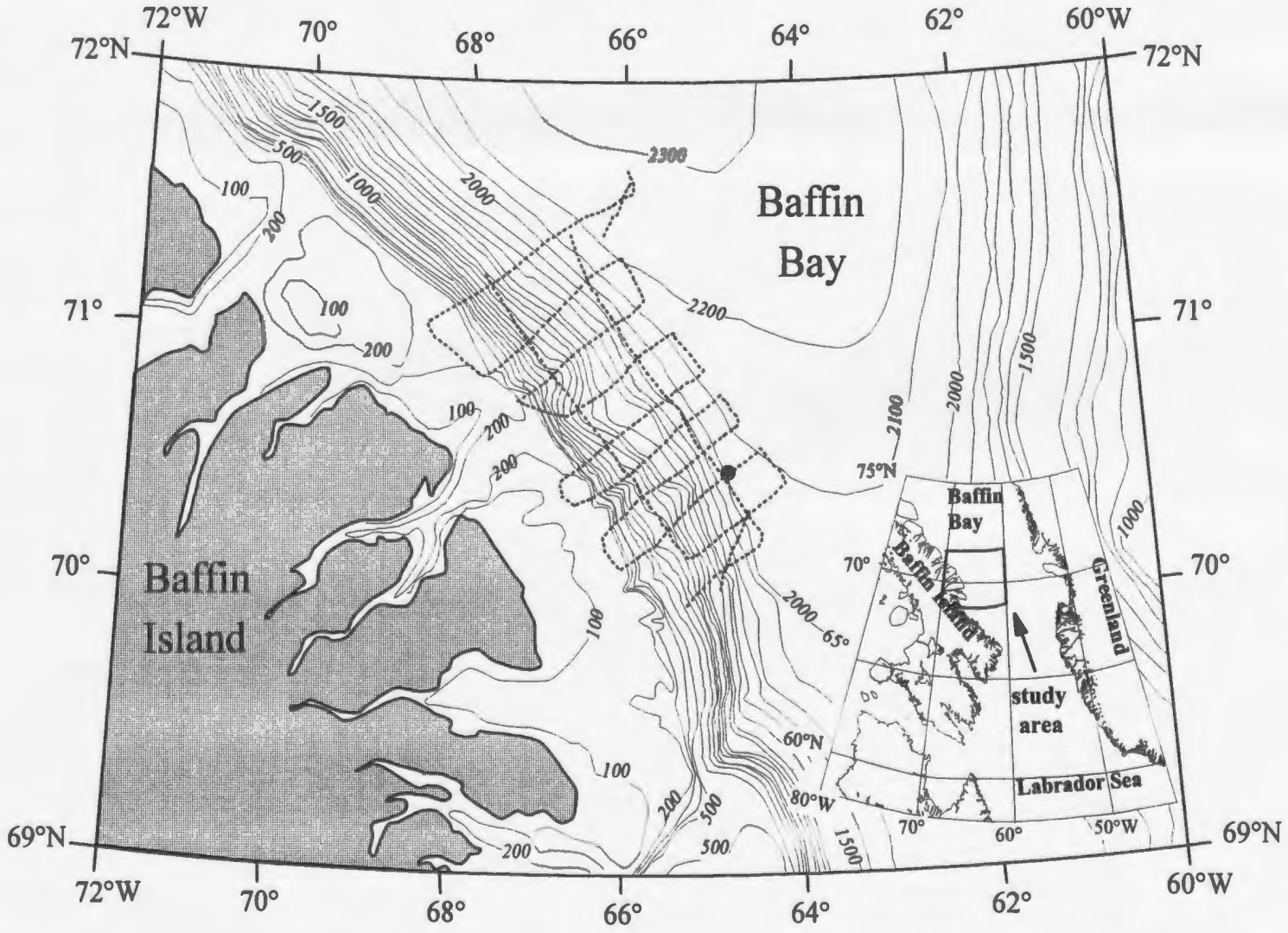

Figure 7 Bathymetric map of Baffin Bay showing CSS Hudson 87-033 survey tracks. Solid circle denotes ODP Site 645. Bathymetric contours are in metres (based on Canadian Hydrographic Service chart 7053

consequently the overall sedimentation pattern (Hiscott and Aksu, 1994).

4.2.3 South China Sea

The study area (between long. 117°-120°E & lat. 19°-20°N) is a small area situated just to the northwest of Luzon, the largest of the Philippine Islands (Figure 8). It is part of the South-China Basin, a marginal sea bounded by the Philippine Islands to the east, Vietnam to the west, Taiwan and mainland China to the north and Borneo to the south. The basin depth averages 4100 m. There is a broad abyssal plain in its center with scattered seamounts and basement ridges. It is bordered to the north and the west by a passive continental margin (continental shelf of mainland Asia) and to the east by the Manila Trench which is a part of an active subduction zone just off the west coast of Luzon (Damuth, 1980a).

The tectonic history, evolution, morphology, structures and stratigraphy of the basin are relatively well studied (Hayes 1980, 1983), but Quaternary sedimentology and geology of the basin have been addressed in only a few papers (e.g., Chen 1978; Damuth 1980a). Chen (1978) examined types and distribution of clay minerals in the surficial sediments throughout the basin. He recognised six provenance-controlled clay-mineral assemblages. The mineral assemblage of the study area is dominated by illite (42-55%) and chlorite (20%) derived from the Asian continent, and smectite (12-23%) and kaolinite (12-15%) derived from the archipelagoes to the west and south.

Damuth (1980a) studied the types and regional distribution of Quaternary sediments using 3.5 kHz echograms, piston cores and bottom photographs.

Figure 8 Location of South-China Sea study area . Distribution of Quaternary surficial sediments based on Damuth (1980a) echo character mapping verified by core sampling. Echo types are:

Type I: Distinct echo — I_B silt/fine sand (turbidites).

Type II: Indistinct echoes: II_A semi-prolonged with intermittent parallel sub-bottoms.
II_B very prolonged with no sub-bottoms (slumps, debris flows).

Type III: Hyperbolic echoes: III_A seamount/rugged basement.
III_B basement with pelagic cover.
III_C "migrating" sediment waves of turbidity current origin.
III_D "non-migrating" sediment waves of turbidity current origin.

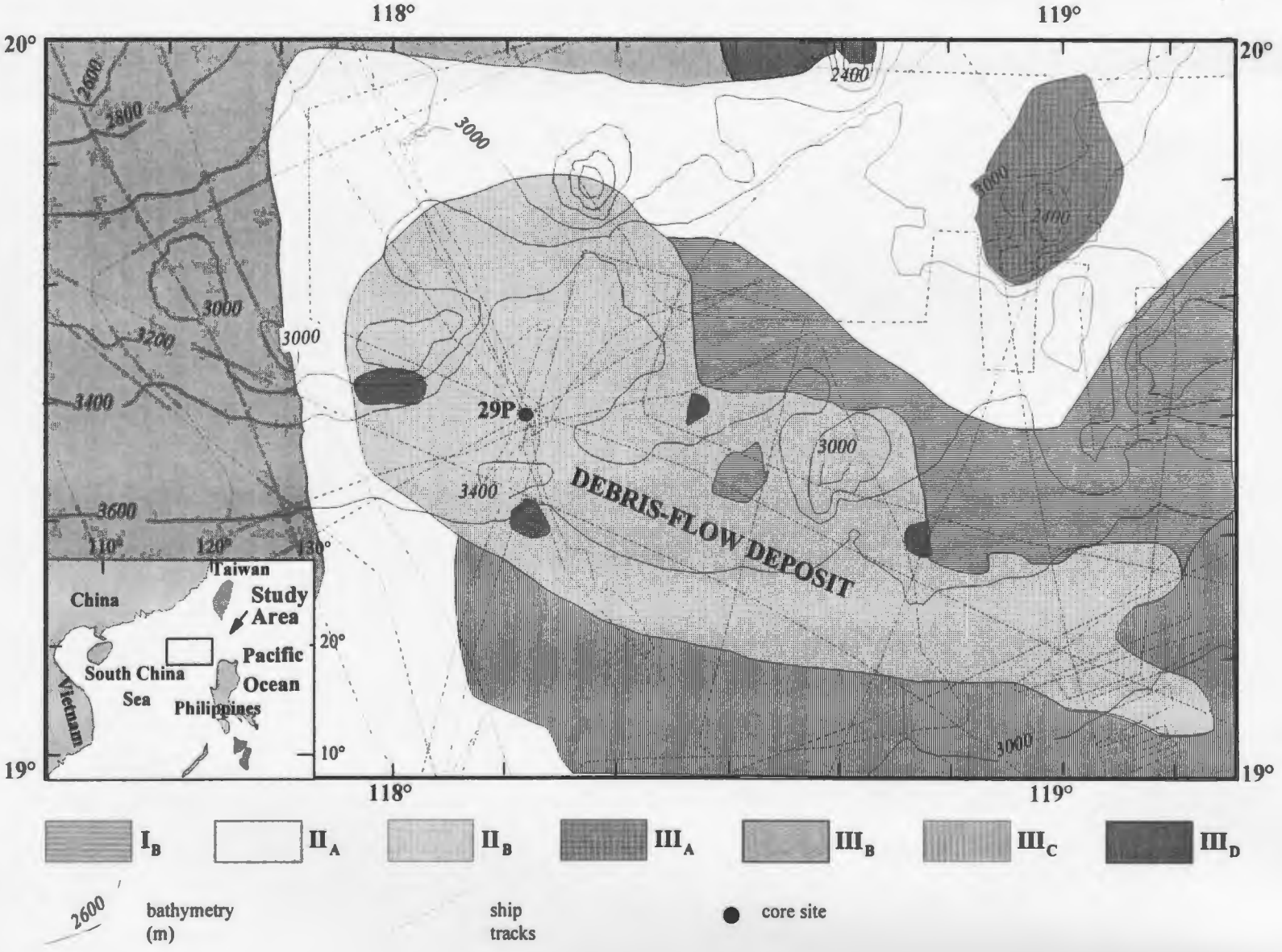
118°
119°
20°
19°
2600
2800
3000
3200
3400
3600
2400
29P
DEBRIS-FLOW DEPOSIT
110°
120°
130°
10°
Taiwan
China
Study Area
Pacific Ocean
South China Sea
Philippines
Vietnam
I_B
II_A
II_B
III_A
III_B
III_C
III_D
bathymetry (m)
ship tracks
core site

Echo character mapping (verified by piston cores) indicates the existence of slumps and debris-flow deposits kilometers to a few tens of kilometers in extent and up to 100 m in thickness. One large slump/debris-flow deposit complex covers more than 125000 km^2 (Fig. 8). These deposits were initiated as slides and slumps on the upper slope. They flowed to the south and southeast down a slope of as little as 1° and now rest on the continental rise overlying stratified sediments of pelagic and hemipelagic origin.

4.2.4 Delaware Slope

This study area is part of the eastern U.S. continental slope and rise where slides, slumps and debris-flow deposits are common features (Embley and Jacobi, 1977). It is located off Delaware Bay (long. 72°30'-73°45' W & lat. 37°-38°N) at water depths of 1400-3200 m (Figure 9). The average slope ranges between 0.25° at the lower slope/rise and about 5° at upper slope canyons and valleys.

This area has been the site of many investigations, including: (a) numerous seismic surveys (mainly 3.5 kHz profiles) by Lamont-Doherty Earth Observatory (LDEO) vessels, (b) sea-floor mapping using sidescan sonar and seismic surveys by the USGS Exclusive Economic Zone Scientific Staff (EEZ-SCAN, 1991), and (c) detailed studies which involve seismic surveys and piston and box cores (Embley, 1980; Malahoff *et al.*, 1980). The study area is mainly covered with a large slide/slump, debris-flow complex, collectively known as the Baltimore-Accomac Slide. The available 3.5 kHz profiles

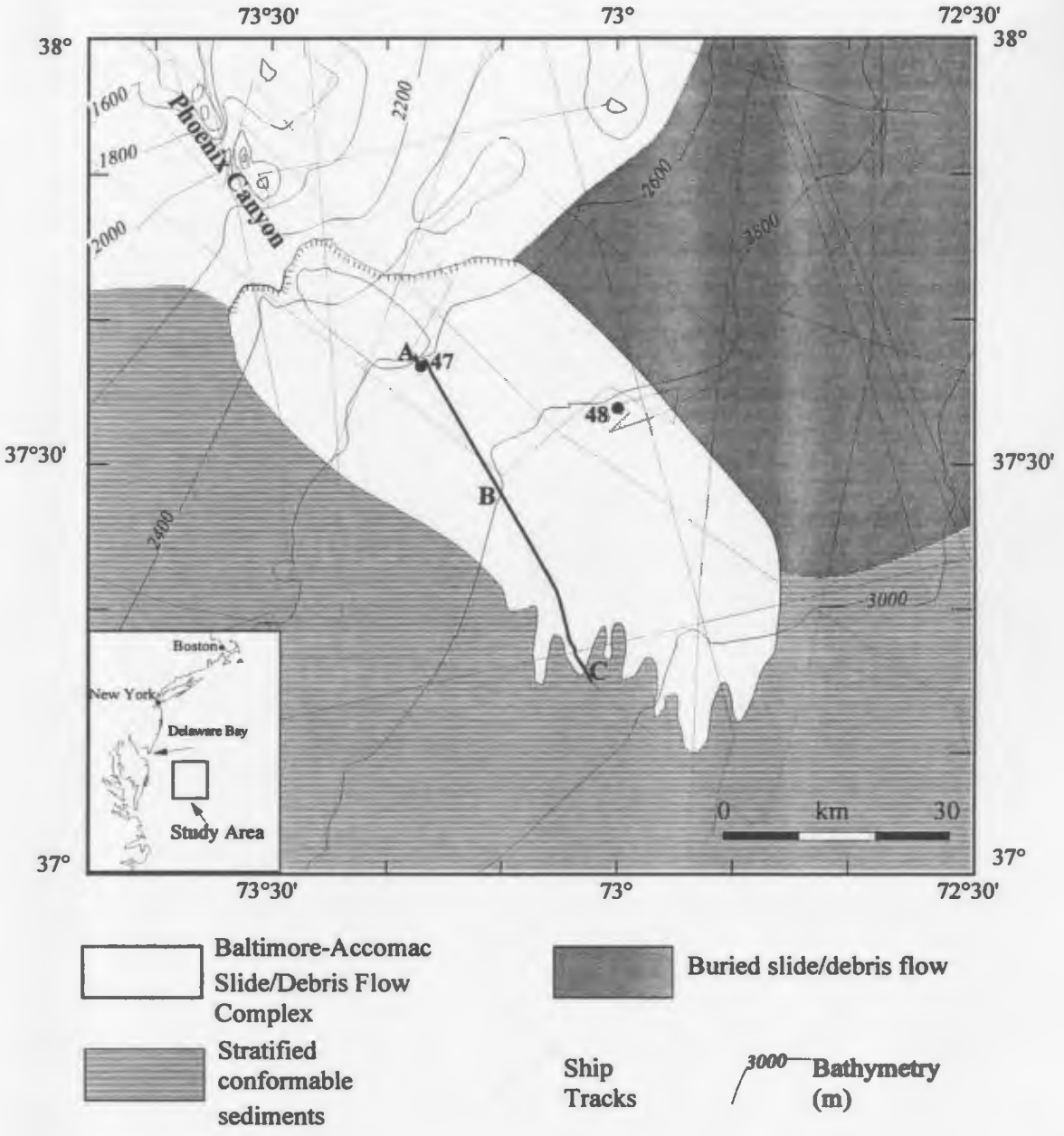

Figure 9 Map showing the location of Delaware Slope study area and illustrating the distribution of surficial sediments as interpreted from seismic surveys. Solid dots indicate core sites. Heavy line segment corresponds to the 3.5 kHz profile shown in figure 15.

indicate that the complex covers about 2700 km^2 although this figure is limited by incomplete survey lines and the fact that large part of the complex lie beneath a thick cover of hemipelagic sediments. The mass movement began when the upper 50 m of sediments started moving southeast down slope canyons as small slides (Embley, 1980). It stopped about 150 km downslope, where the toes of debris-flow deposits terminate on a large field of sediment waves formed by bottom currents. Core samples (described by LDEO personnel) indicate that debris-flow deposits are predominantly sandy marls. The coarse fraction (> 63 μm) ranges between 3-10 %, and is mainly composed of foraminifera mixed with detrital quartz, feldspar, amphibole, pyroxene and plant debris.

4.3 Outcrop case studies

4.3.1 The Cow Head Group, Western Newfoundland

The Cambro-Ordovician Cow Head Group (Figure 10) is a part of the Humber Arm Allochthon (Williams, 1975), emplaced during Taconic Orogeny (Middle to Late Ordovician; Rodgers and Neale, 1963). The group consists of about 300-500m of predominantly deep-water carbonates, which are believed to have been deposited as a base-of-slope apron in front of a shallow carbonate platform and a bypass slope (James and Stevens, 1986). There is an interdigitation of pelagic/hemipelagic sediments and gravity-flow deposits. The former consists of a mixture of shale (black, green and red),

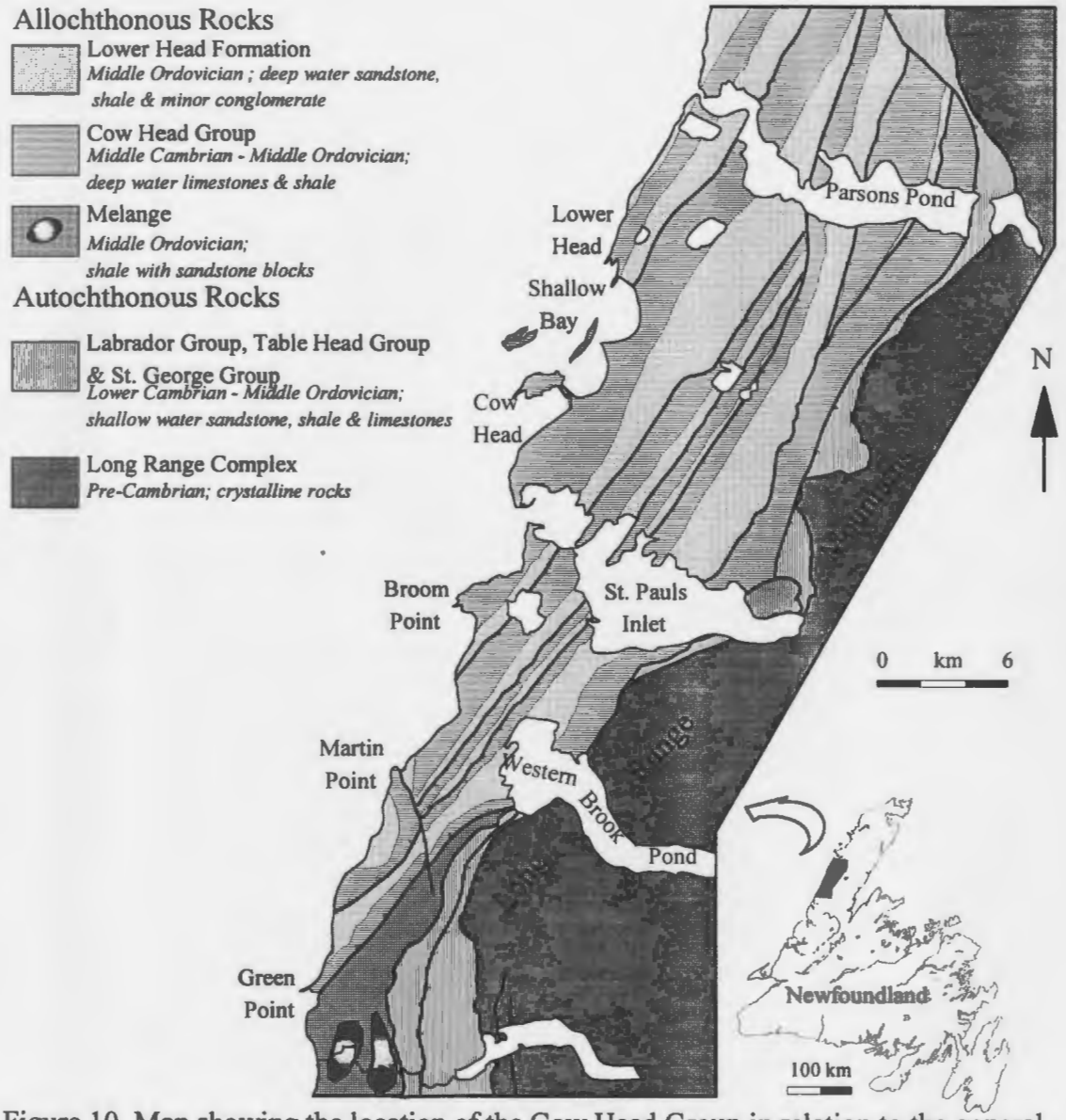

Figure 10 Map showing the location of the Cow Head Group in relation to the general geology of western Newfoundland (modified from Williams *et al.*, 1985).

siltstones, grainy to muddy locally silicified limestone rhythmites (parted and ribbon limestone), dolomite and chert. Gravity-flow deposits include sandstone and quartzose calcarenite forming massive beds (grain-flow origin) or graded beds (turbidity-current origin) or caps on top of conglomerates. Sedimentological characteristics of conglomerates are summarised in Table 4.

Rapid change in facies between the Cow Head rocks and the adjacent shallow platform rocks led Johnson (1941) to propose that the sequence is allochthonous. Early paleontological studies by Kindle and Whittington (1958) of trilobite and graptolite fauna resulted in the systematic division of Cow Head strata into 14 beds that range in age from late Middle Cambrian to Middle Ordovician.

Hubert *et al.* (1977) studied the paleogeography and the sedimentary history of the Cow Head Group. They used synsedimentary slump sheets, soft sediment folds and what they called "synsedimentary boudin" to resolve paleoslopes and hypothesise the significance of paleocurrents. They recognised two narrow carbonate platforms trending northwest-southeast and a regional paleoslope dipping northeast. Southeast-flowing contour currents were proposed to explain an apparent 90° difference between paleocurrent indicators and slope indicators. However, Hiscott and James (1985) questioned the methods used by Hubert *et al.* (1977) to determine paleoslope and disagreed with their interpretations. Instead, they suggested a paleoslope to the southeast,

Table 4 Some typical features of conglomerates from Cow Head Group (based on Hiscott and James, 1985).

Facies	Thickness (m)	Composition (clasts & matrix)	Structures	Remarks	Origin
A	<1.0	**Grainy** (mainly peloid sand, minor quartz, ooids & bioclasts), commonly quartzose cobble to pebble **conglomerates**.	Graded-stratified. Cross-bedded, rippled and laminated tops.	No mud matrix. Grade into calcarenite along the strike.	Turbidity currents
B	<2.0	Poorly sorted **limestone plate conglomerates**. Cobble to boulder to large rafts (up to several meters). 10-20 % matrix (argillaceous and/or carbonate mud).	Chaotic fabric, except some wave forms (wave length, 1-6 m) at the top of some beds. Flat bases.	Mostly pieces of parted and ribbon limestone, identical to the intervening hemipelagites.	Debris flows
C	<2.0	**Limestone chip conglomerates**. Pebble to cobble sized clasts. > 10 % matrix (fine calcite, dolomite or argillaceous lime mud).	Chaotic fabric, except some clast alignment sub-parallel to bedding. Sharp tops and bases.	Clasts of both shallow and deep-water origin. Some boulders project from bed.	Debris flows
D	<5.0	**Boulder conglomerates.** Like facies c, but contain abundant exotic shallow water, cobble to boulder size clasts. Muddy matrix. Some have calcarenite cap.	Chaotic fabric. Cross-bedded or ripple-laminated grainy caps. Flat bases except some minor erosional bases.	Some boulders project from the top, some rest at the base. Clasts are calcified algae boundstone.	Debris flows
E	<30.0	**Megaconglomerates**. The thickest and muddiest. Matrix of green terrigenous mud.	Most chaotic fabric. Most have flat bases. Some show huge load casts, loaded boulders and basal injections of substrate.	Some beds are 100 m thick, contain huge blocks of shallow water limestone and rafts of slope deposits up to 200 m x 50 m.	Debris flows

which is also in agreement with the proximal-distal facies polarity, the graded-stratified deposits (re-interpreted as turbidites and not contourites), and the fabric of the conglomerates. Based on their geometry (mound tops, frontal snouts, etc.), disorganised fabric and the presence of large floating and projecting boulders, Hiscott and James (1985) also concluded that the Cow Head conglomerates were deposited by viscous debris flows. They also provided a detailed account of the mode of emplacement and the geotechnical properties of the flows. Soon after, James and Stevens (1986) meticulously documented the details of stratigraphy, palaeontology and sedimentology of the Group.

The studied debris-flow deposits for this thesis are all located in the Cow Head Peninsula. They are part of beds 2-14 (Kindle and Whittington, 1958) which correspond to the Shallow Bay Formation of James and Stevens (1986).

4.3.2 Fraser River Valley, Central Interior of British Columbia

During major Pleistocene glaciations, most of British Columbia was covered by the Cordilleran Ice Sheet (Clague, 1975). In the central interior part of the province, the northward advance and retreat of ice lobes frequently obstructed the southward and eastward flowing rivers of the former Fraser Valley System. As a result, vast areas were covered by glacial lakes. This is recorded by extensive and thick sequences of glaciolacustrine sediments which were deposited at the end of the penultimate glaciation (at least Early Wisconsin, >50 ka) and during the subsequent Fraser Glaciation (Late Wisconsin, <20 ka; Eyles, 1987; Eyles *et al.*, 1987; Eyles and Clague, 1991). The

glaciolacustrine deposits are best exposed along the deeply incised valleys of the Fraser and the Chilcotin River and their tributaries.

The oldest glaciolacustrine sequence (> 50 ka) overlies Tertiary basalts of the Chilcotin Group, Tertiary sediments including diatomite, lignite, poorly lithified clastic and pyroclastic rocks, and granites of Jurassic age. These glaciolacustrine sediments lie beneath a major unconformity which is overlain by fluvial gravels and sands deposited during the Olympia Nonglacial Interval (Middle Wisconsin; Fulton, 1971). The oldest glaciolacustrine sequence indicates deposition in a supraglacial environment. It consists of thick normally graded gravels and sands that fill subaqueous outwash channel feeders. Trough cross-bedded, horizontally-bedded and massive sands and diamicts are also common. Suspension deposits including massive and laminated mud. Silts and silty sands are preserved only along the lower Chilcotin River.

The Late Wisconsin glaciolacustrine sequence consists mainly of massive and crudely stratified diamict of debris-flow origin and interbedded silts. These deposits accumulated in valleys that were deeply cut during the Olympia Nonglacial Interval, and later deepened by advancing glaciers. Diamicts contain a variety of rafts and boulders from older lithologies; some are largely composed of material resedimented from the older glaciolacustrine sequence.

Both glaciolacustrine sequences are capped by Late Wisconsin till deposits (Fraser Till) which are blanketed by a thin deglacial sequence marking the final melting of the Cordilleran Ice Sheet (< 11 ka; Eyles and Clague, 1991).

Based on previous studies by Eyles (1987) and Eyles and Clague (1991), selected sections containing debris-flow deposits at Quesnel, Gang Ranch and Farwell Canyon were chosen for this study (Figure 11).

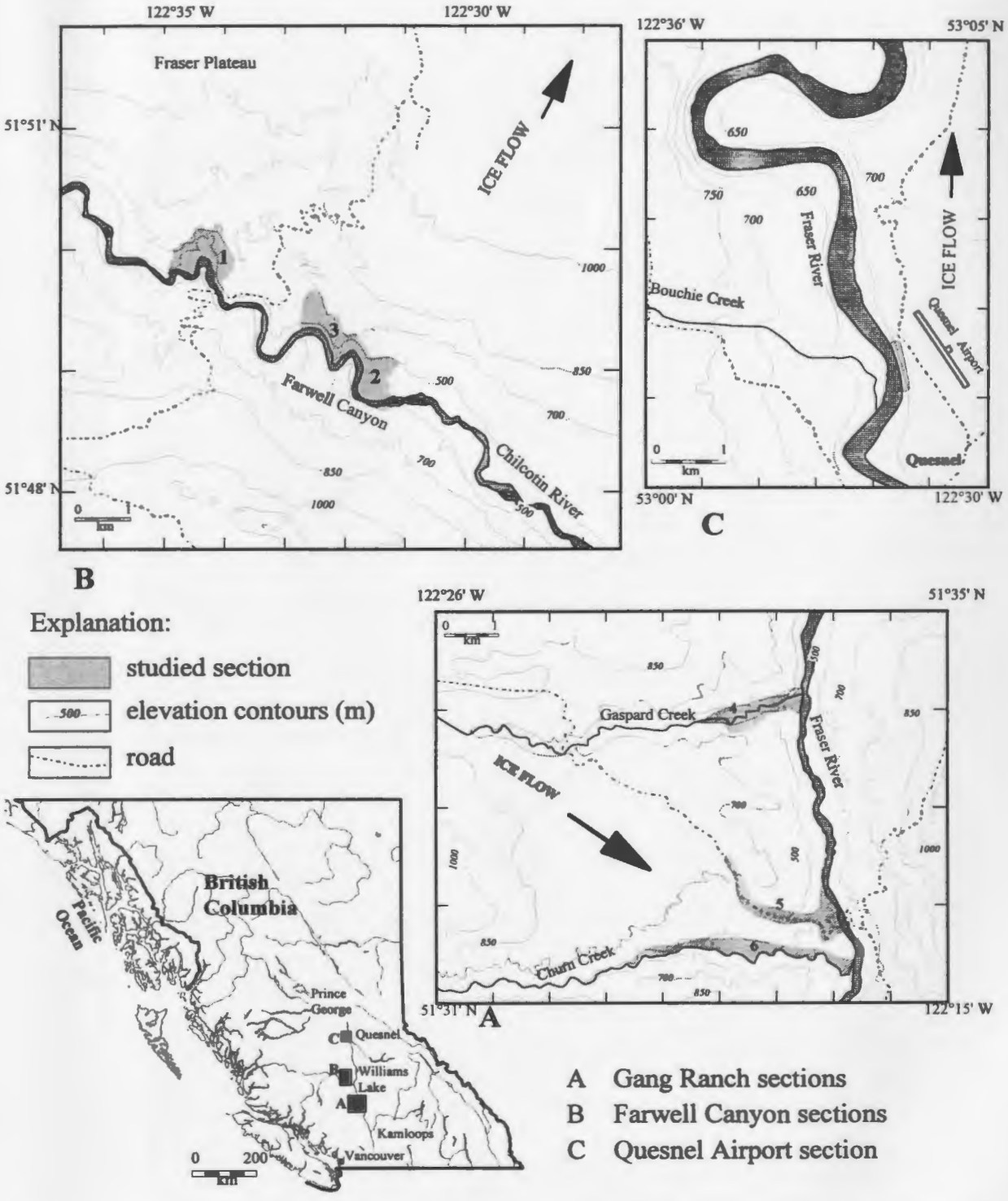

Figure 11 Location of the studied glaciolacustrine sediment sections along the Fraser and Chilcotin Rivers, Central Interior of British Columbia (modified from Eyles,1987; Eyles and Clague, 1991).

Chapter 5

CHARACTERISTICS AND MECHANICS OF SUBAQUEOUS DEBRIS FLOWS

5.1 Introduction

The transport mechanism and behaviour of subaqueous debris flows can be deduced from certain characteristics of their deposits. Characteristics such as deposit shape and geometry are best observed in seismic reflection profiles because large exposures on land are too limited to yield this type of information. Characteristics related to the composition of the deposits are best described from outcrops because cores from subaqueous debris-flow deposits are limited in number and many have limited penetration. The result is a blending of observations from different deposits as the basis for an improved understanding of depositional processes. This is not an ideal situation. Instead, it would be better to rely on a number of broadly based case studies for which all possible types of data are available. A similar compromise is made for other types of deep-marine deposits, however, like submarine-fan deposits. Specifically, submarine-fan models depend on modern fans for information on morphology and geometry of depositional elements, and ancient deposits for details of facies and textures, particularly for the coarser grained facies (Mutti and Normark, 1987).

In this chapter, characteristics measured both in the field and in the laboratory are

described. The common elements of various deposits are synthesised and discussed together with experimental data in Chapters 5 and 6.

5.2 Acoustic Characteristics

Submarine debris-flow deposits are easily recognised in seismic-reflection profiles as acoustically transparent bodies with discrete and continuous top and bottom reflectors (Figure 12). The acoustically transparent and indistinct patterns indicate massive, homogeneous and disorganised deposits. This is in contrast to other well-stratified marine sediments such as turbidites, pelagites and hemipelagites. Due to their massive internal nature, debris-flow deposits typically lack internal reflectors although local weak discontinuous and disorganised reflection patterns are observed (Figure 12). The discrete and laterally continuous echoes at the base and top of debrites indicate sharp contacts, at least at the scale of resolution of the acquisition system (>1 m for small airgun; ~50 cm for 3.5 kHz profiles). Some of these acoustic properties characterise submarine slide and slump deposits as well, and in some cases resolution of the acquisition systems does not allow distinction of these other deposits from debris-flow deposits. In such cases, a distinction may be achieved when the distribution and the overall geometry of the deposit are considered.

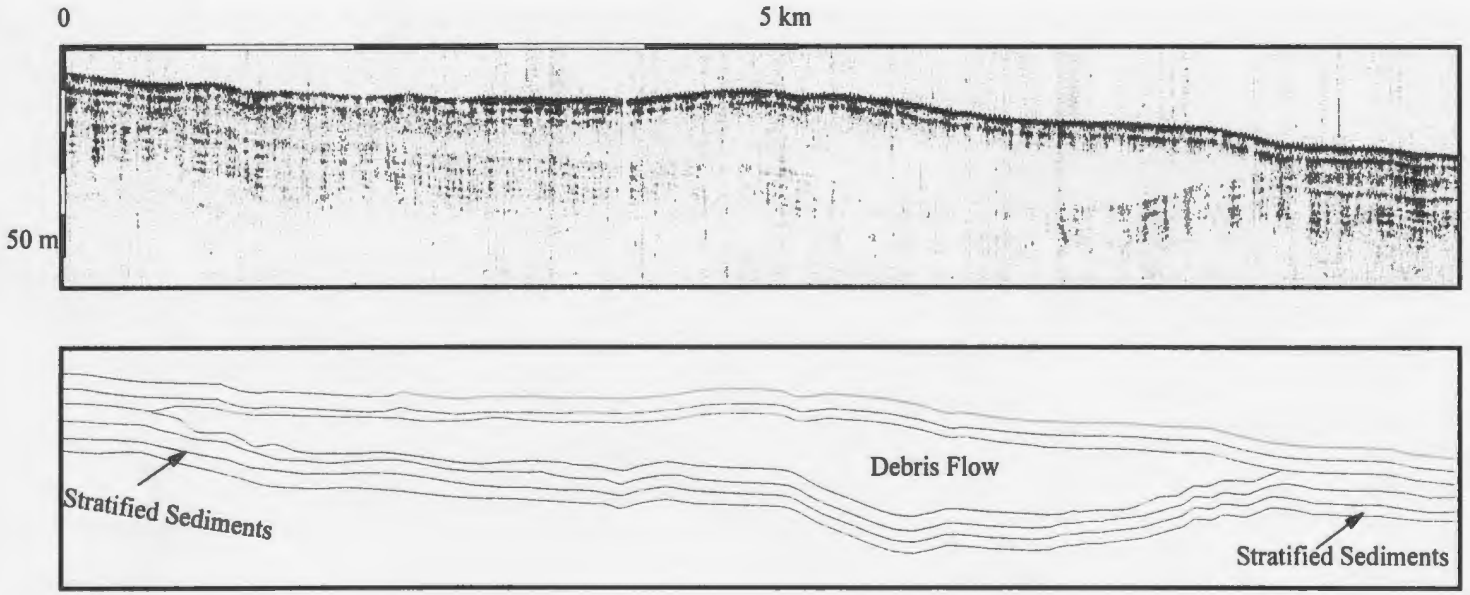

Figure 12 Seismic profile of a debris-flow deposit (recorded with N.S.R.F. hydrophone array). This is a cross-sectional profile of one of the Northeast Newfoundland deposits (see Figure 6 for location).

5.3 Distribution and shapes of deposits

Only the higher resolution 3.5 kHz profiles are used in this thesis to study the geometrical aspects of individual debris-flow deposit. This is necessary to avoid erroneous interpretation based on vague or in some cases false representation of deposit boundaries and dimensions in lower resolution data. Figure 13, which shows an airgun and a 3.5 kHz profile of the same deposit(s) clearly illustrates this problem.

In 3.5 kHz reflection profiles, debris-flow deposits often have the appearance of elongated, mound-shaped lenses aligned downslope. They have maximum thickness of a few meters to few tens of meters and can be kilometers to several tens of kilometers long. On the Northeast Newfoundland Slope, deposits have length to width ratio of 1:1 to 12:1, although typically the length is about 4 times the width (Figure 14; Table 5). Sometimes irregular sea-floor morphology can have a profound effect on the geometry and distribution of the deposit. The Delaware/Accomac deposit on the Delaware Slope provides a clear illustration of this effect. The debris flow appears to have over-filled some pre-existing bathymetric lows, but also had enough momentum to override some highs before finally blanketing a pre-existing field of sediment waves (Figure 15)

Johnson's (1970) formula (Eqn. 2.3) establishes the relation between shear strength, critical (maximum) thickness, unit weight and slope angle of subaerial debris-flow deposits on relatively smooth slopes. Applying equation 2.3 to the debris-flow deposits of the Northeast Newfoundland Slope indicates no apparent relation between the

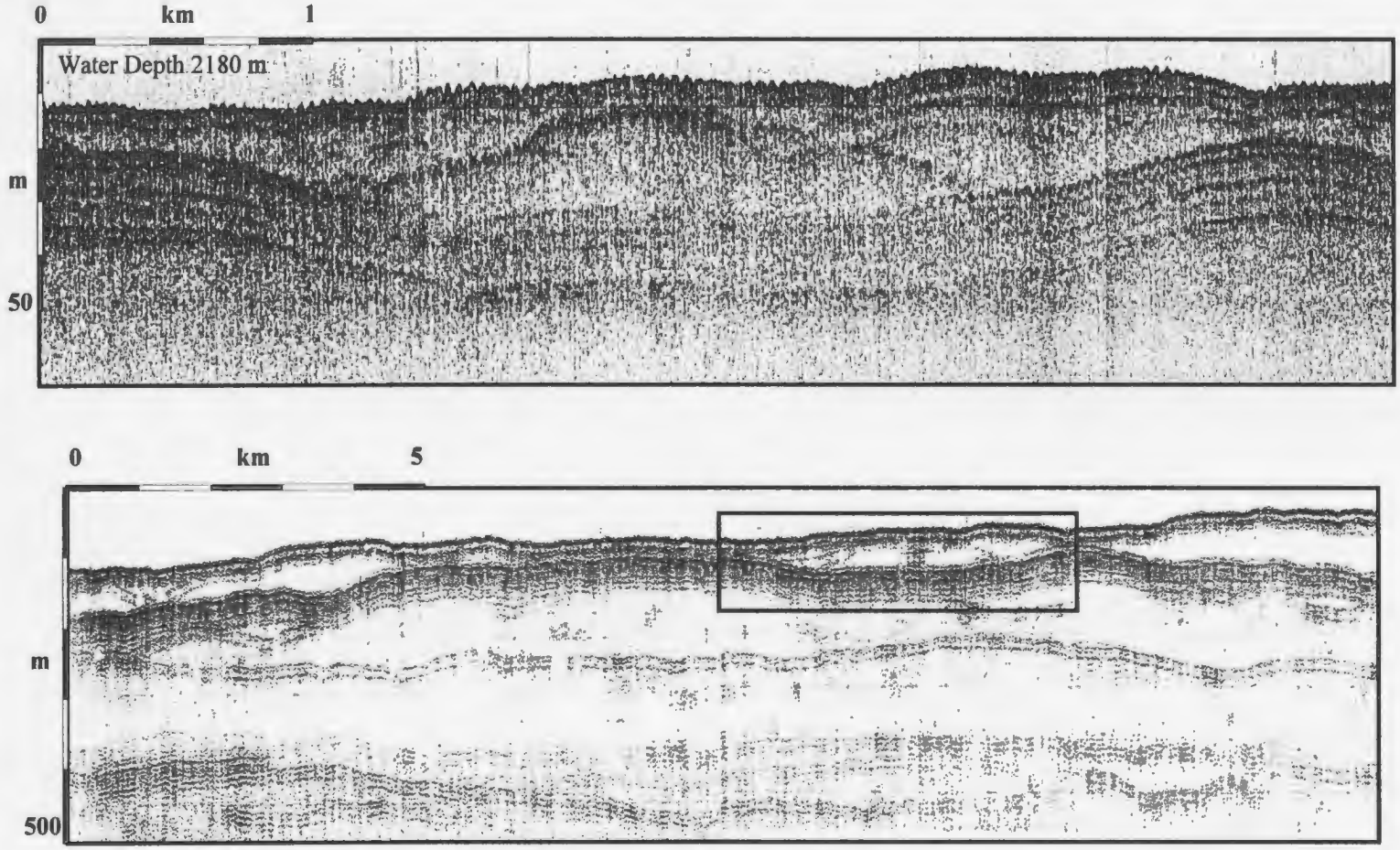

Figure 13 Comparison between seismic (with N.S.R.F. hydrophone array) and 3.5 kHz reflection profile. The 3.5 kHz profile (top) has limited penetration but higher resolution. Example from the Northeast Newfoundland Slope (see Figure 6 for location).

Table 5 geometrical parameters of 40 debris-flow deposits. T is the maximum thickness in meters. Slope angle is in degrees. L & W are deposits length and width (in km). k is the strength of the debris in (kPa) as calculated from equation 2.3 using a density of 1.95 g/cm^3 (measured from piston core samples). Data, which come from the Northeast Newfoundland Slope, include only those deposits where the geometrical parameters are clearly identified in 3.5 kHz profiles.

Flow #	Cruise #	T(m)	Slope (°)	L(km)	W(km)	W/T	L/W	L*W	K(kPa)
1	90007	27.8	0.45	75.13	16.65	599	4.5	1250.91	4.18
2	91029	18.1	0.30	30.00	17.80	983	1.7	534.00	1.81
3	90007	25.0	0.34	26.57	15.17	607	1.8	403.07	2.84
4	90007	27.3	0.20	35.00	10.45	383	3.3	365.75	1.82
5	90007	24.8	0.42	38.65	6.31	254	6.1	243.88	3.48
6	91029	12.8	0.63	20.00	8.96	700	2.2	179.20	2.69
7	91029	26.6	0.60	24.16	7.41	279	3.3	179.03	5.33
8	91029	22.0	0.60	21.00	7.70	350	2.7	161.70	4.41
9	90007	22.0	0.44	16.22	8.06	366	2.0	130.73	3.23
10	90007	20.0	0.23	30.40	3.80	190	8.0	115.52	1.54
11	90007	18.4	0.35	12.24	9.05	492	1.4	110.77	2.15
12	91029	18.3	0.80	10.88	9.52	520	1.1	103.58	4.89
13	90007	16.7	0.73	18.66	5.46	327	3.4	101.88	4.07
14	90007	23.7	0.14	16.95	6.00	253	2.8	101.70	1.11
15	90007	13.5	0.35	26.78	3.79	281	7.1	101.50	1.58
16	90007	18.0	0.61	32.55	3.07	171	10.6	99.93	3.66
17	90007	20.3	0.37	21.15	4.49	221	4.7	94.96	2.51
18	91029	16.0	0.50	15.43	5.80	363	2.7	89.49	2.67
19	91029	16.6	1.03	11.78	7.08	427	1.7	83.40	5.71
20	92045	26.0	0.70	12.50	5.18	199	2.4	64.75	6.07
21	90007	11.3	0.19	27.50	2.29	203	12.0	62.98	0.72
22	91029	15.4	0.57	16.01	3.84	249	4.2	61.48	2.93
23	91029	15.0	0.42	16.13	3.39	226	4.8	54.68	2.10
24	90007	31.8	0.67	18.00	3.00	94	6.0	54.00	7.11
25	90007	19.0	1.00	19.00	2.52	133	7.5	47.88	6.34
26	90007	9.2	0.14	11.88	3.83	416	3.1	45.50	0.43
27	90007	16.5	0.95	13.58	3.13	190	4.3	42.51	5.23
28	90007	16.9	0.80	8.63	4.61	273	1.9	39.78	4.51
29	90007	11.1	0.29	10.52	3.60	326	2.9	37.87	1.07
30	90007	5.9	0.26	9.42	3.75	632	2.5	35.33	0.51
31	91029	6.4	0.46	6.44	4.16	650	1.5	26.79	0.98
32	90007	13.0	0.23	5.87	3.79	292	1.5	22.25	1.00
33	91029	11.2	1.20	5.80	3.39	303	1.7	19.66	4.49
34	90007	13.0	0.23	5.87	2.75	212	2.1	16.14	1.00
35	90007	15.5	0.61	8.36	1.73	111	4.8	14.46	3.16
36	91029	8.3	0.62	4.50	2.87	346	1.6	12.92	1.72
37	90007	13.2	0.28	5.15	2.43	184	2.1	12.51	1.23
38	91029	8.0	1.00	6.46	1.63	204	4.0	10.53	2.67
39	90007	4.5	0.15	5.90	1.57	349	3.8	9.26	0.23
40	90007	28.6	0.35	4.82	1.78	62	2.7	8.58	3.34

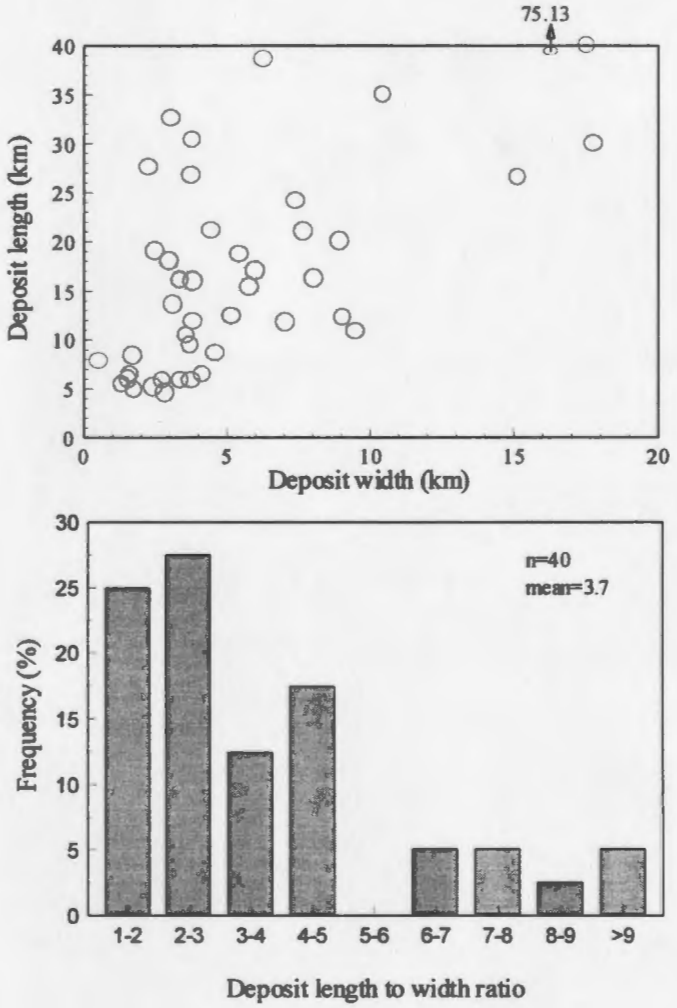

Figure 14 Geometrical parameters of 40 debris-flow deposits from the Northeast Newfoundland Slope as measured from 3.5 kHz profiles (see Table 5 for the data set).

thickness of the deposit and the slope angle. This is mainly because an unusually large flow will leave a thick deposit and in this case, the thickness may not relate to the slope angle or the strength of the flow. The other reason is that in areas of high debris flow activity such as the Northeast Newfoundland Slope the geometry of each deposit is greatly influenced by the behaviour of all preceding flows and the geometry of their deposits. These can significantly alter sea-floor morphology and force succeeding flows to fill newly formed topographic lows. Flow size effect can be accounted for by considering the aerial distribution of the deposits, whereas, true deposit thickness is obtained by excluding the infill part from thickness measurement. After these considerations, slight negative correlation is observed when the ratio of deposit width to thickness or deposit area to thickness is plotted against slope angle (Figure 16).

In the Fraser Valley outcrops, individual debris-flow deposits form very thick diamicton beds that range in thickness from 1 m to 25 m. Slope angles for these deposits range from 1 to 20° and are typically less than 5°. Most beds have sheet-like appearance with limited lateral change in thickness as observed in most of the exposed sections.

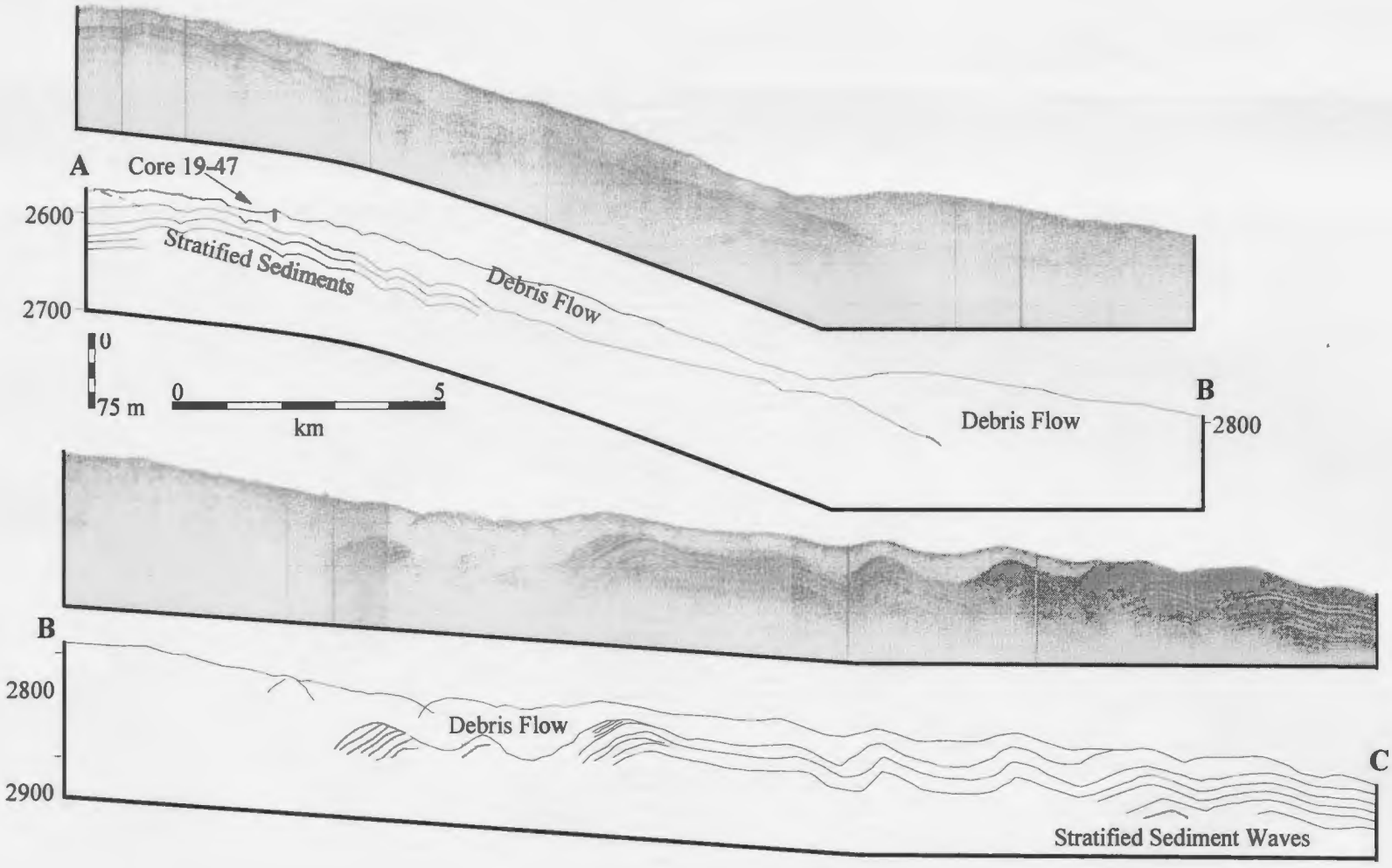

Figure 15 Influence of sea-floor morphology on the shape and distribution of the deposits. An example from the Delaware/Accomac debris-flow deposit on the Delaware Slope. See Figure 9 for location.

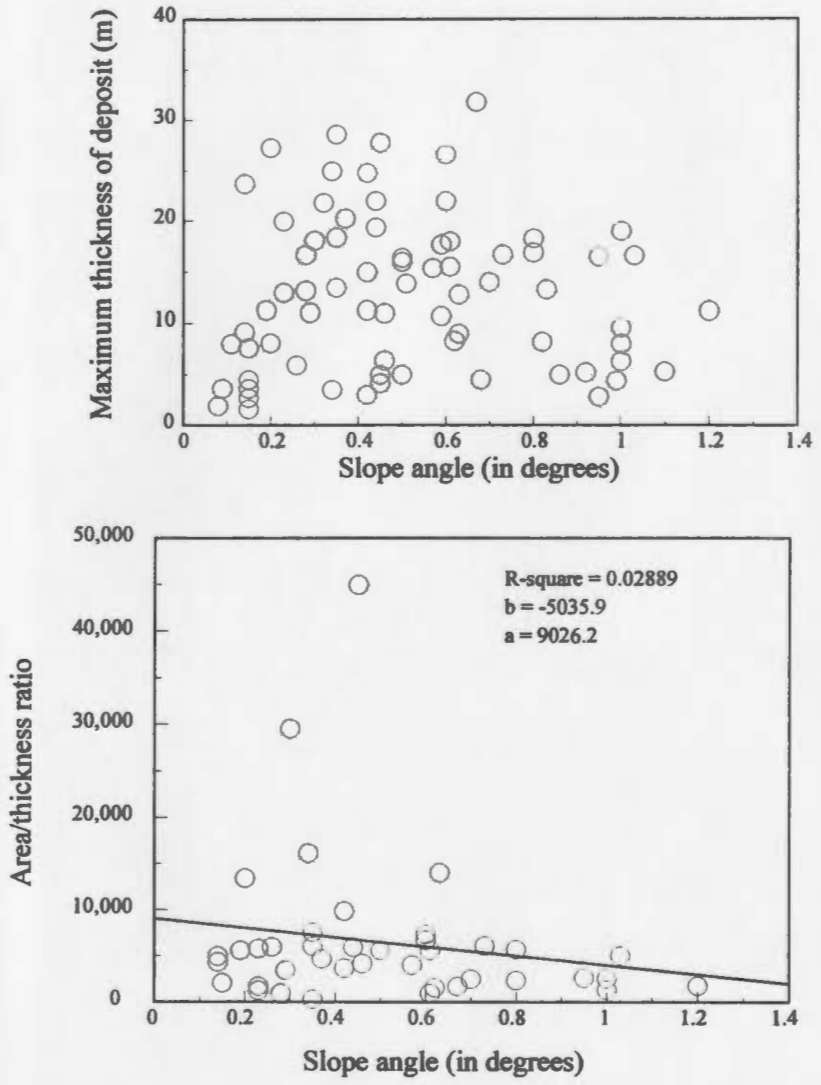

Figure 16 Relation between deposit geometry and slope angle. Data from the Northeast Newfoundland Slope

Except for the widely exposed outcrop at Quesnel, snouts and lateral contacts are rarely exposed; consequently, the lenticular nature of the deposits cannot be deduced. Most of the studied debris-flow deposits lack significant scours and basal undercutting. A few inferred amalgamated debrites marked by trails of coarser clasts are present in some sections (Figure 17). However, similarities in the texture and appearance of the component parts of the amalgamated beds inhibit their recognition as deposits of one pulsating flow or different flows.

Debris-flow deposits from the Cow Head Group have thicknesses that range from 0.1 m to 20 m. They are non-channelised and have sheet-like geometry except at their margins. Loading and basal erosion are commonly insignificant.

The maximum transport distance for debris flow is variable: about 1700 km for the South China Sea flows, 200 km on the Northeast Newfoundland Slope, 150 km for Delaware Slope flows and about 70 km for Baffin Bay flows. These transport distances are comparable to transport distances of other subaqueous debris-flow deposits described in the literature (e.g., Embley 1976, Masson *et al.*, 1992). Apparently bottom slope rather than length of the transport path determines where deposition will occur. This observation has implications for the time scales over which elevated pore fluid pressures likely persist in mobile debris (see section 5.6).

Figure 17 Thick diamicton beds exposed at Gaspard Creek, Gang Ranch, Central Interior British Columbia (section 4 in Figure 11). Crude inverse grading and the concentration of large boulders at certain horizons are used to infer the deposit of each debris flow. Sheet-like beds (up to 25 m thick) form the majority of sediments in the section. Some boulders are up to 3m in diameter. Total section is 70-80m high.

5.4 Composition, Textures and Internal Structures

Piston cores of Quaternary debris-flow deposits typically show a firm and poorly-sorted sandy mud with numerous clasts. Grain-size distribution characteristically deviates from a log-normal shape, instead being bimodal to multimodal. This suggests minimal hydrodynamic sorting during transportation and deposition. Breaks in the grain-size population may allow distinction of "clast " and "matrix" phases.

Commonly, the deposits exhibit sharp tops and bases, although basal contacts are usually not observed due to limited core penetration. Most of the studied deposits are matrix-supported gravels that lack sedimentary structures or grading. They are mainly terrigenous in nature. Some deposits have low to moderate carbonate content that is attributed to the presence of foraminifera tests.

The fine fraction of these debris-flow deposits consists predominantly of clay (40-65%), silt (15-25%) and sand (10-40%). The clay-size fraction consists of 33-54% illite, 16-39% chlorite, 0-10% kaolinite, 0-7% montmorillonite, 1-6% quartz, 0-25% feldspar and 0-14% amphibole (Table 6). Because the studied deposits come from several widely separated areas around the globe, these mineralogical proportions should show a range of composition reflecting variable source rocks. In all but one case, however, illite and chlorite happen to predominate, and likely control cohesive properties of the mud-water interstitial phase (see Hampton, 1972).

As also shown in X-radiographs, clasts are mainly sub-angular to sub-rounded. They range in size from 0.2 to 6 cm and have variable composition (e.g., igneous mineral and rock fragments, limestone, dolomite, shale, and shell fragments).

Debris-flow deposits of the Fraser Valley consist of extremely poorly sorted massive diamict beds. These diamictites are mostly matrix supported with the matrix being mostly sand. A few beds are clast-supported and show crude inverse grading at their bases. In some outcrops, several debris-flow deposits may be stacked and form a succession that may reach several tens of meters in thickness.

A greater variability in grain size was observed in these deposits than in the marine piston cores; particles range from clay-size to boulders over 3 m long and rafts of semi-indurated sediments more than 6 m long. Either the continental slope deposits do not contain outsize clasts of these dimensions (because of greater distance from source or granulometry of the proglacial-failed material), or the restricted sampling by piston coring did not intersect large clasts, which may in fact be present. The clasts in the Fraser Valley deposits range in shape from well rounded (e.g., large basaltic & granitic boulders at Gang Ranch and Farwell Canyon sections) to angular (e.g., large sediment rafts at Quesnel section). Maximum particle size (MPS) weakly correlates to bed thickness (BTh).

At Gang Ranch and Farwell Canyon, the fine fraction of the deposits consists mainly of 65-95% sand and 1-20% silt. The percentage of clay size minerals in the matrix

Table 6 Clay-mineral content of debris-flow deposits in weight % of the <2 micron fraction. Samples G-6-6, G-4-3, and I-2-M are from Gang Ranch and Quesnel deposits, British Columbia. The remaining samples are from piston cores (see Table 3 for location).

Sample	Illite	Chlorite	Kaolinite	Amphibole	Feldspar	Quartz	Montmorillonite
92045-07P-CC	43.45	37.12	3.17	13.77	0.50	1.90	-
92045-12P-575	45.64	38.9	1.83	-	12.4	1.20	-
92045-13P-660	40.65	32.5	3.60	3.73	13.54	2.79	3.18
645B-9X1-57	32.91	15.58	10.38	10.41	25.56	5.12	-
RC-19-47P-302	53.61	30.00	-	3.94	9.84	2.61	-
VM-34-29P-1135	48.72	19.16	2.10	-	17.50	5.94	6.57
G-6-6	33.41	31.00	2.78	-	24.44	8.35	-
G-4-3	20.7	17.24	1.91	13.41	32.14	8.29	6.29
I-2-M	41.61	1.75	1.80	11.29	15.37	5.01	23.17

is usually less than 3%, and 30-50% of this size fraction is actually very fine quartz, feldspar and amphibole (Table 6; Appendix A). The fine fraction in Quesnel deposits is considerably more rich in clay minerals (15-67%).

Composition and internal structures of the Cow Head debris-flow deposits are summarised in section 4.3.1 (Table 4). Like the Fraser Valley deposits, Cow Head debris-flow deposits exhibit weak correlation between MPS and BTh. (Figure 18.).

5.5 Clast Fabric

Clast fabric analysis is an important sedimentological tool that can be used to deduce paleoflow directions. It has been used also to infer the behaviour of the transporting flow, and the associated depositional processes (e.g., Lawson, 1979a). When clast fabric is analysed using the three-dimensional eigenvalue method (Mark, 1973; Woodcock, 1977), diamicts of Fraser and Chilcotin Valleys indicate no preferred orientation (values for strength parameter, C <2; Table 6). Only two data sets (S511 and S612) show weak preferred orientation (C is slightly > 2). The fabric mainly follows a girdle distribution; i.e., S1 ≈ S2 > S3 (Figure 20). Dip values for the principal eigen vector (V_1) are typically less than 20° (except 42° for sample SQ11). S1 values range from 0.4 to 0.6 (Table 7). Figures in Appendix B are graphical representations of the results.

These fabric results are comparable with other published results for subaqueous debris-flow deposits (e.g., Hampton, 1972, Lawson, 1979b, Jong and Rappol, 1983) and subaerial debris-flow deposits (Boulton, 1971). For example, the subaerial debris-flow

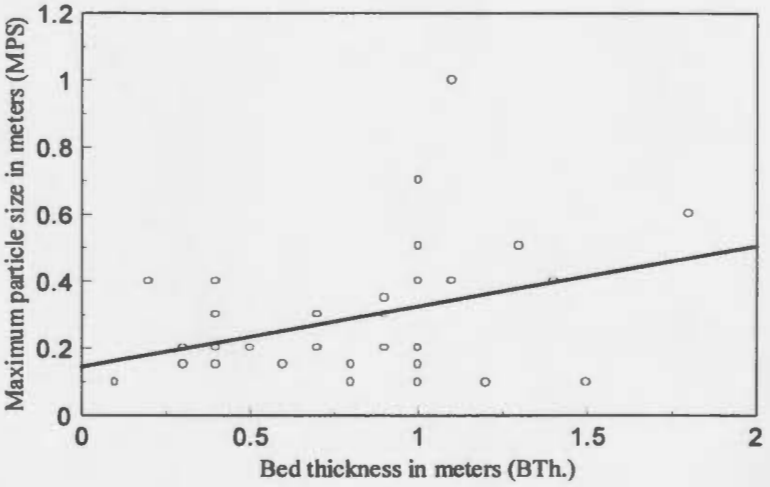

Figure 18 Data from 33 debris-flow beds from the Cow Head Group, western Newfoundland indicate weak correlation between bed thickness and maximum particle size (R-square = 0.128; b = 0.18; a = 0.144).

deposits from a glacially-influenced alluvial fan at the mouth of Cinquefoil Creek south of the study area have similar fabrics i.e., weakly-clustered (S1 between 0.45 and 0.73) with long axes of clasts dipping up or downfan at shallow angles (Eyles and Kocsis, 1988). Elsewhere, Eyles *et al.* (1988) report identical results from subaerial debris-flow deposits near Banff, Alberta. Subaqueous debris-flow deposits from Baffin Bay show a sub-horizontal clast orientation (Aksu, 1984).

These fabrics differ significantly from those obtained from lodgement and basal melt-out till (Boulton, 1971, Domack and Lawson, 1984). Lawson (1979a) suggested that lodgement and basal melt-out till fabrics have S1 values ranging from 0.7-0.9, whereas debris-flow deposit have lower S1 values.

In the case of ice rafted debris, clasts show weak preferred orientation with some clasts even vertically oriented (Anderson 1983). These criteria should be used with caution, however, as other authors have found less well oriented fabrics in basal tills, and better oriented fabrics in debris-flow deposits (Mark, 1974; Mills, 1984; Rappol, 1985).

The strength of the fabric is inversely proportional to the strength of the depositing flow, clast size and concentration (collision effect). These factors control the movement of the clasts during the flow. Thus, it is expected that deposits from the snout area, which is characterised by a high concentration of clasts, will have less oriented fabric than the rest of the deposit.

It should be noted here that the fabric formed in the deposits might only reflect flow conditions at or near the site of deposition, which may be different from the

Table 7 Statistical parameters describing the strength and the cluster around the 3 eigen vectors of Mark (1973) and Woodcock (1977). K is the shape parameter [K = ln (S1/S2)/ln ((S2/S3)]; C is the strength parameter [C = ln (S1/S3)].

Data Set	S1	S2	S3	ln (S1/S2)	ln (S2/S3)	K	C
S111	0.5197	0.2776	0.2027	0.6272	0.3145	1.9944	0.9417
S411	0.4996	0.4158	0.0846	0.1835	1.5918	0.1153	1.7753
S422	0.6214	0.2840	0.0945	0.7829	1.1002	0.7116	1.8831
S431	0.4510	0.3692	0.1798	0.2001	0.7197	0.2780	0.9197
S511	0.5590	0.3705	0.0705	0.4114	1.6590	0.2480	2.0704
S521	0.6014	0.3101	0.0885	0.6625	1.2536	0.5285	1.9161
S531	0.4889	0.3928	0.1183	0.2188	1.2005	0.1823	1.4193
S532	0.5323	0.3035	0.1641	0.5618	0.6149	0.9136	1.1766
S533	0.6087	0.2835	0.1078	0.7642	0.9672	0.7901	1.7315
S611	0.4635	0.3839	0.1525	0.1885	0.9229	0.2042	1.1114
S612	0.5011	0.4377	0.0612	0.1353	1.9674	0.0688	2.1027
S623	0.5597	0.3603	0.0799	0.4404	1.5057	0.2925	1.9460
S631	0.5148	0.3172	0.1680	0.4842	0.6353	0.7621	1.1194
S641	0.6001	0.3123	0.0876	0.6531	1.2707	0.5140	1.9238
S651	0.5022	0.3542	0.1436	0.3490	0.9030	0.3866	1.2520
S661	0.5547	0.3351	0.1101	0.5040	1.1126	0.4530	1.6167
S662	0.5595	0.3114	0.1291	0.5858	0.8807	0.6651	1.4664
SQ11	0.4263	0.3346	0.2392	0.2423	0.3357	0.7219	0.5780

S511

Eigen values:
.519 .277 .2026
Eigen vectors:
Dip-Dir Dip
286.8 16.142
25.18 26.58
169.0 58.20
Confidence Radius
95% Signif.: 25.6 deg.
Axis:
Azim = 286.
Plng = 16.1

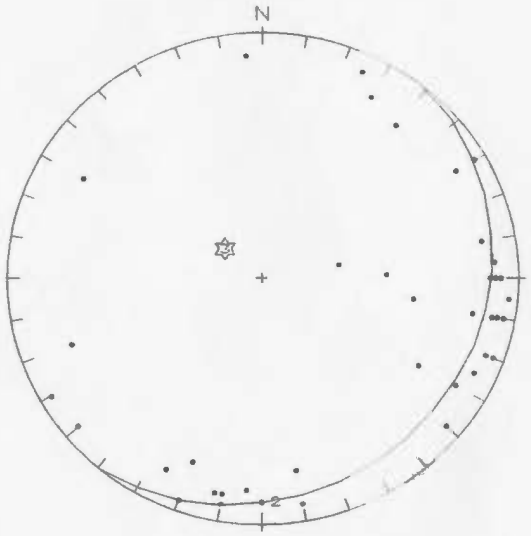

N = 40

S111

Eigen values:
.559 .375 .065
Eigen vectors:
Dip-Dir Dip
84.58 11.02
176.6 10.45
309.0 74.71
Confidence Radius
95% Signif.: 21.8 deg.
Best Fit Girdle:
Azim = 265
Dip = 78.9

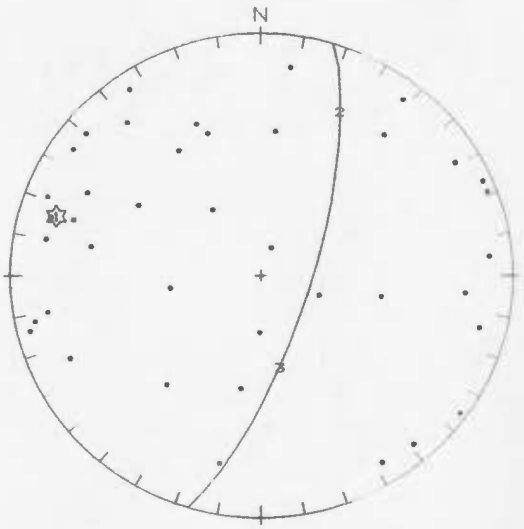

N = 40

Figure 19 Examples of fabric data from the Fraser Valley debris-flow deposits.plotted as lower-hemisphere equal-area stereographic projection. See Appendix B for complete data set.

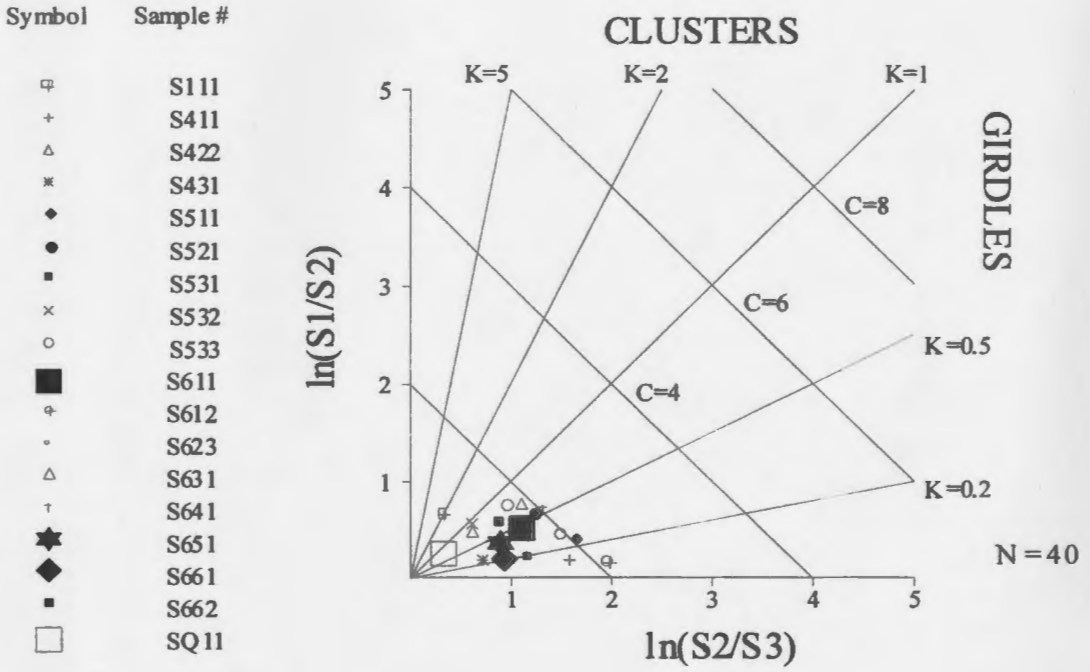

Figure 20 Fabric data from Gang Ranch, Farwell Canyon, and Quesnel deposits plotted as Modified Flinn Diagram. Data sets show no preferred orientation except S511 & S612 which show weak preferential orientation. See Appendix B for the complete data.

conditions during most of the flow history. For example, if the flow becomes laminar during the final stages of deposition a subhorizontal fabric may develop. It should also be noted that post-depositional phenomena could effect the original fabrics. Of great importance is the affect of consolidation and compaction, which tend to flatten the girdle patterns.

5.6 Support Mechanisms

This section deals with the result of the laboratory experiments described in chapter 3. In these experiments, shear strength and pore-fluid pressure of a series of reconstituted slurries were measured. Techniques used in these experiments are discussed in section 3.4.4.

The sediment used in the experiments (core catcher sample 92045-07P) consists of 44.1% clay, 18.4% silt, 33.4% sand, and 4.1% gravel. The clay-size fraction consists of 43.5% illite, 37.1% chlorite, 13.8% amphibole, 3.2% kaolinite, 2% quartz, and 0.5% feldspar. Slurries with water content of 30%, 40%, 50%, and 60% by weight were reconstituted by mixing with seawater. The volume of the material used was limited by the availability of core sample. Because of that, measurements could only be done to a maximum depth of 12 cm into the slurry.

Measurements of undrained shear strength were made immediately after thoroughly mixing each slurry. The results, which are shown in figure 21, indicate values between 20-35 kPa at 30% water content (by weight). These values drop sharply to about 2-4 kPa at 40% water and to about 1 kPa at 50% water. At 60% water content, the slurry

is too diluted and has a strength that is below the detection limit of the vane shear device (Figure 21).

Profiles of pore-fluid pressure indicate that the slurries develop high values of excess pore-fluid pressure. Initially values were mainly 0.7-4 times the hydrostatic pressure for most experimental runs. Initial values were exceptionally high in run 1 and 2 (up to 7 times). They dropped very sharply in the first 2 hours of measurements, but more crucial is the fact that in almost all experimental runs, slurries maintained elevated pore-fluid pressure values for very long time (0.5-2 times the hydrostatic; for up to 24 hours). Slurries with high concentration of solids were able to sustain excess pore-fluid pressure for longer time and the rate of dissipation of excess pore-fluid pressure decreased with depth in the slurry. This is mainly the result of settling and consolidation. In few experimental runs the normal dissipation profile was preceded by an initial increase in pore-fluid pressures. This is mainly due to temporary blockage of pore spaces, which hinder the escape of pore fluids.

The measured values for excess pore-fluid pressures are higher than those obtained by Pierson (1981) from cohesionless slurries (with > 3% clay). This clearly indicates the strong influence of composition (mainly clay content) on the observed pore fluid-pressures. Experiments showed that elevated values of pore-fluid pressure, which can be as large as the normal stress of the slurry, could provide the necessary lift mechanism for the debris. This results in sediments with very low values of effective stress.

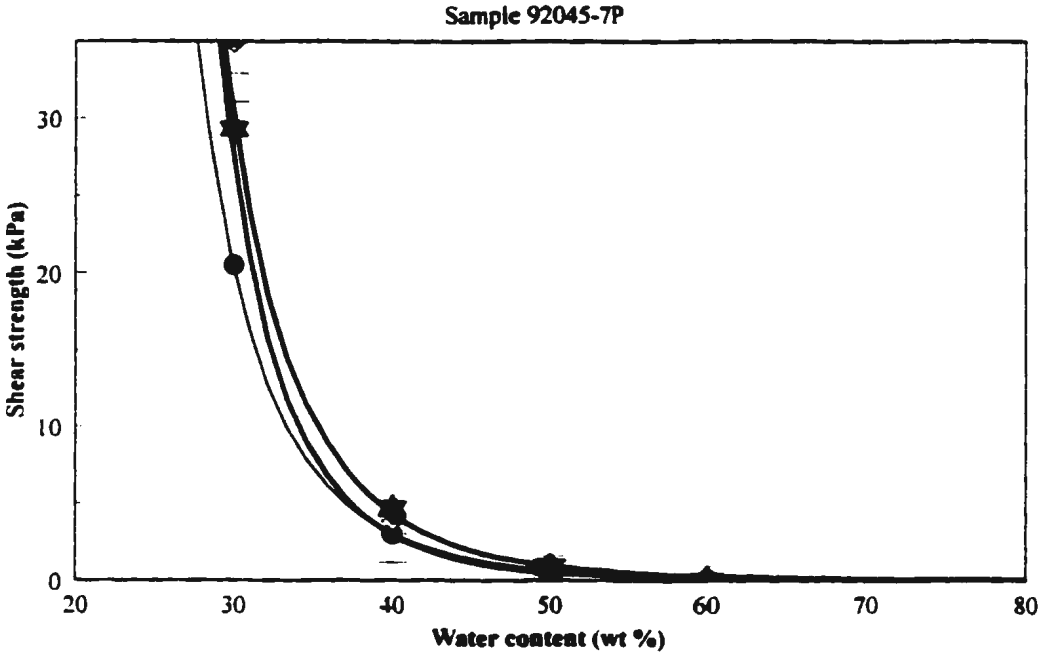

Figure 21 Measurements of undrained shear strength of reconstituted slurries.

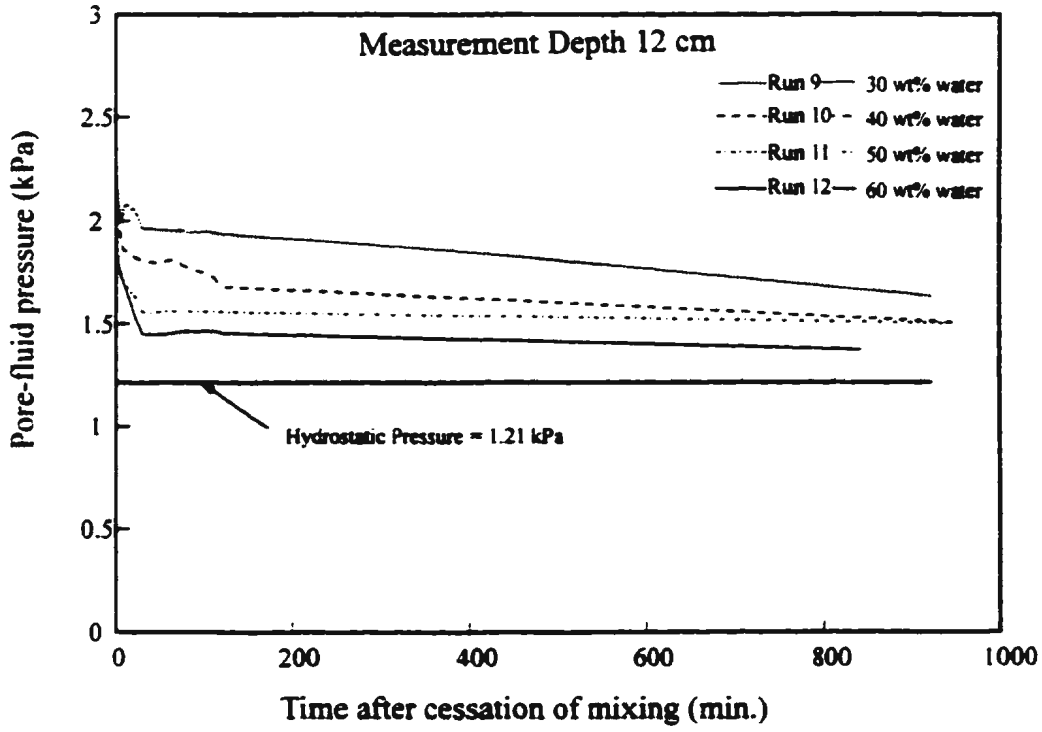

Figure 22 Pore-fluid pressure measurements of reconstituted slurry (sample 92045-07P).

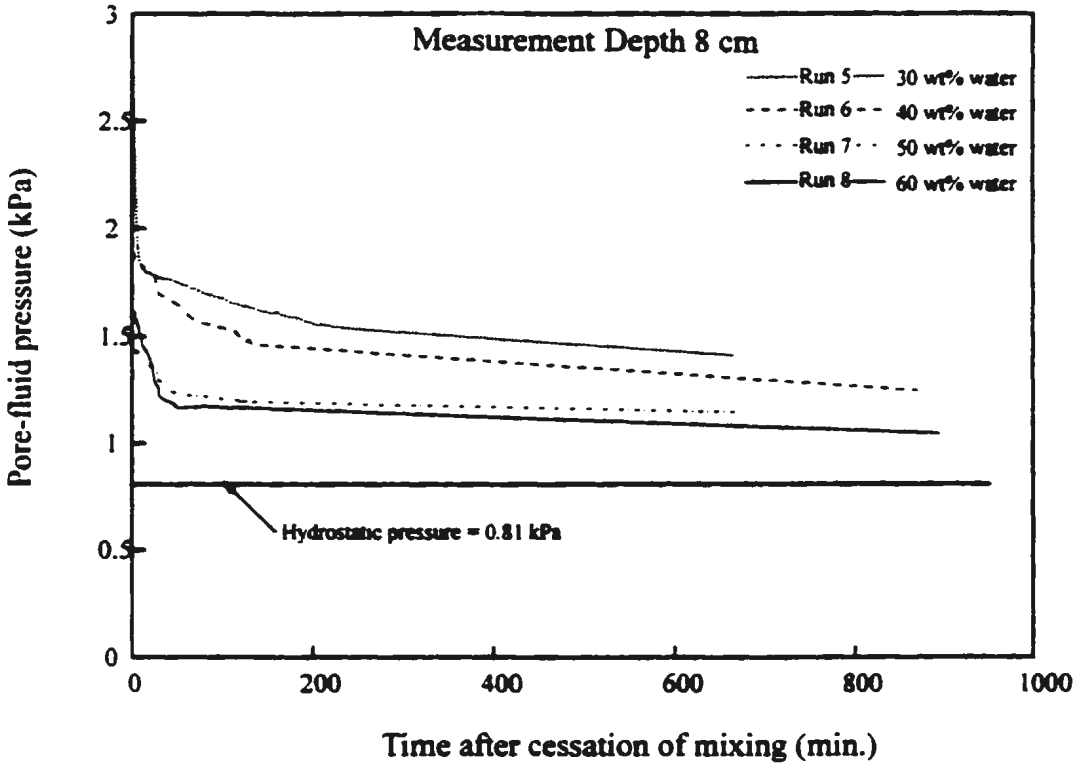

Figure 22 (continued).

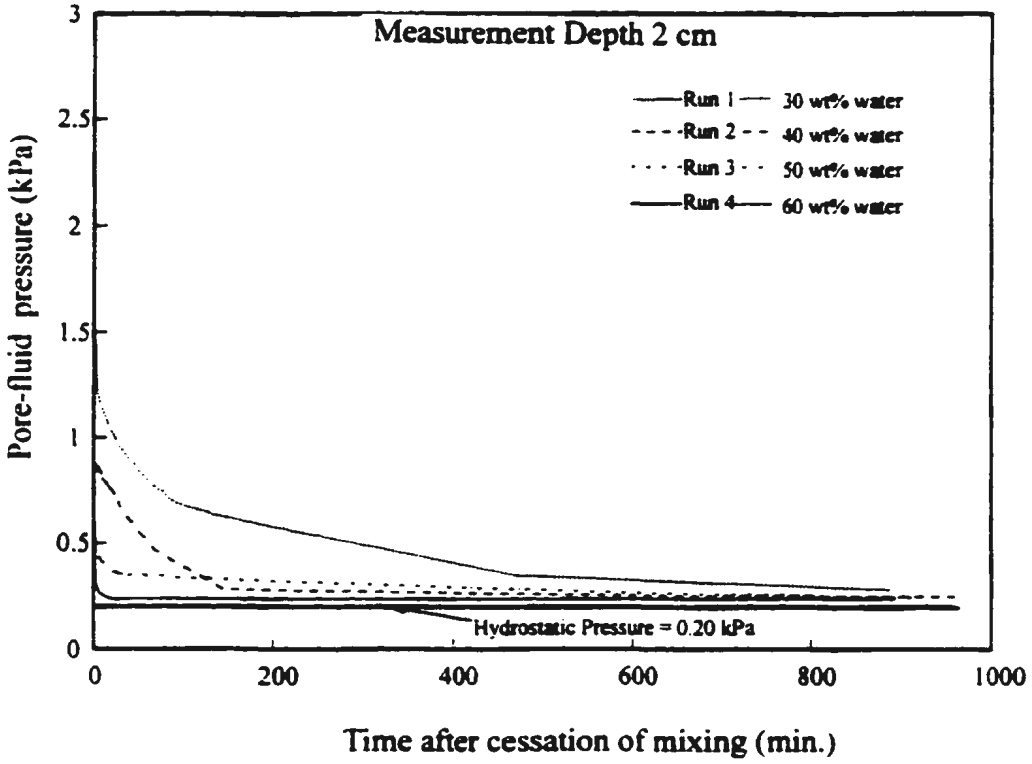

Figure 22 (continued).

Chapter 6

DISCUSSION AND CONCLUSIONS

6.1 Discussion of the Results

The observed acoustic characteristics are typical of debris-flow deposit as described in the literature. Accurate geometrical parameters are best obtained using closely spaced high-resolution 3.5 kHz seismic profiles. Of all case studies examined in this thesis, the survey area on the Northeast Newfoundland Slope has the most detailed and comprehensive seismic coverage. Hence, the dimensions of more than forty individual flows were accurately measured and incorporated in the study. However, it should be noted that data from this specific case study only represent clastic deposits of non-channelised debris flows produced by line source discharge of fine-grained glacigenic sediments. Parameter used to indicate flow behaviour should be used only within that geographic basin and only for qualitative comparison with other deposits of different source and depositional environment.

The wide range in grain size and composition (e.g., clay content of < 1% in the Fraser Valley deposits compared with > 40% in the Northeast Newfoundland deposits) should also be considered. Unlike the Northeast Newfoundland deposits, the Fraser Valley deposits show some inverse grading. Although clast fabric alone is not an indicator of flow process nor depositional environment, it is clear that those measurements do not indicate lodgement or melt-out till which would generally have stronger fabric and consistent mean orientation.

Pore pressure transducer and laboratory vane shear provide accurate measurements of pore-fluid pressures and shear strength of a small sample of true but static debris-flow material. The nature of the experiments and the amount of the sample did not allow for a simulation of moving debris and hence parameters such as velocity and dynamic viscosity could not be measured.

6.2 Conclusions

In this thesis several approaches were employed to evaluate the mechanics and dynamics of subaqueous debris flows. First the geometry of well-mapped debris-flow deposits from the modern sea floor was used to infer travel path, transport distance, slope angle, and strength of the flow. This was augmented by examination of composition, fabric, and internal structures from outcrop and piston core samples. Finally, the role of pore-fluid pressure as a particle support mechanism was investigated using series of small-scale experimental measurements on reconstituted slurries.

Case studies used in this thesis indicate that debris-flow deposits cover significant portions of modern continental slopes. Generally the deposits appear as well defined, seismically transparent lenses aligned downslope to a distance of 70-1700 km from the shelf edge. These lenses have central thickness ranging from few meters to few tens of meters. They are 0.5-75 km long and 0.5-25 km wide. Flows appear to have travelled on very gentle slopes (1.5° to about 0.1°) without significantly eroding the underlying sediments.

Cores from debris-flow deposits reveal structureless, poorly sorted pebbly mud with numerous lithic fragments and few soft mud clasts. The studied outcrops of debris-flow deposits typically exhibit extremely poorly sorted massive diamict beds. These are mostly matrix supported with the matrix being mostly sand. A few beds are clast-supported and show crude inverse grading at their bases. Most beds show no preferred clast orientation and exhibit weak positive correlation between bed thickness and maximum particle size.

Laboratory measurements of pore-fluid pressure indicate that reconstituted debris-flow slurries develop high values of excess pore-fluid pressure (0.7-2.5 times hydrostatic pressure, depending on depth and sediment concentration). These high values, which are maintained for several hours, are mainly due to poor sorting and high amount of fines. High pore-fluid pressure effectively mobilised debris flows by reducing the total normal stress and consequently the shear strength of the debris material.

6.3 Recommendations

1. Attempts to study and model subaqueous debris flows should consider the wide range of variables that control the behaviour of flows and the wide variety of resulting deposits.
2. An integrated approach of marine, outcrop and laboratory analysis remains the best option for studying the character and behaviour of debris flows.
3. Marine surveys are more appropriate in studying the origin, triggering mechanism, travel paths, and geometrical aspects of debris-flow deposits. To accurately map the

target deposits. line spacing and vertical resolution of such surveys should be carefully considered.

4. Rheological properties are better measured directly from accurately designed and properly scaled debris flow experiments. For example slope angle. water content. clay type and the proportion of sand. silt. and clay must be carefully determined since they have a great influence on the behaviour of the flow.
5. The role of pore-fluid pressure as a support mechanism and the unique effects of marine environments on the stability/mobility of sediments are but a few aspects that require further investigation.

References

Aksu, A.E. (1984) Subaqueous debris flow deposits in Baffin Bay. *Geo-Mar. Letts.*, 4, 83-90.

Aksu, A.E. and Hiscott, R.N. (1989) Slides and debris flows on the high-latitude continental slopes of Baffin Bay. *Geology*, 17, 885-888.

Aksu, A.E. and Hiscott, R.N. (1992) Shingled Upper Quaternary debris flow lenses on the NE Newfoundland slope. *Sedimentology*, 39, 193-206.

Aksu, A.E. and Piper, D.J.W. (1987) Late Quaternary sedimentation in Baffin Bay. *Can. J. Earth Sci.*, 24, 1833-1846.

Anderson, J.B. (1983) Ancient glacial-marine deposits: Their spatial and temporal distribution. In: *Glacial-Marine Sedimentation* (Ed. by B.F. Molnia), pp 3-92, Plenum Press, New York.

Bagnold, R.A. (1954) The flow of cohesionless grains in fluids. *Phil. Trans. Roy. Soc. Lond. Series A*, 249, 235-97.

Blackwelder, E. (1928) Mudflow as a geological agent in semiarid mountains. *Bull. geol. Soc. Am.*, 39, 465-484.

Biscaye, P. E. (1964) Distinction between kaolinite and chlorite in Recent sediments by X-ray diffraction. *Am. Mineralogist*, 49, 1281-1289.

Biscaye, P. E. (1965) Mineralogy and sedimentation of recent deep sea clay in the Atlantic Ocean and adjacent seas and oceans. *Bull. geol. Soc. Am.*, 76, 803-832.

Boulton, G.S. (1968) Flowtills and related deposits on some Vestspitsbergen glaciers. *J. Glaciology*, 7, 391-421.

Boulton, G.S. (1971) Till genesis and fabric in Svalbard, Spitsbergen. In: *Till Symposium* (Ed. by R.P. Goldthwait), pp 41-72. Ohio State University Press, Columbus, Ohio.

Broscoe, A.J. and Thomson, S. (1969) Observation on an alpine mudflow, Steele Creek, Yukon. *Can. J. Earth Sci.*, 6, 219-229.

Brunsden, D.and Prior, D.B. (1984) *Slope Instability* (Ed.), Wiley and Sons, New York, 563 pp.

Bull, W.B. (1963) Alluvial-fan deposits in Western Fresno County, California. *J. Geol.*, 71, 243-250.

Carroll, D. (1970) Clay minerals: a guide to their X-ray identification. *Spec. Pap. geol. Soc. Am.*, 126, 273 pp.

Carter, L., Schafer, C.T. and Rashid, M.A. (1979) Observations on depositional environments and benthos of the continental slope and rise, east of Newfoundland.*Can. J. Earth Sci.*, 16, 831-846.

Chen, P.Y. (1978) Minerals in bottom sediments of the South China Sea. *Bull. geol. Soc. Am.*, 89, 211-222.

Clague, J.J. (1975) Sedimentology and paleohydrology of Late Wisconsinan outwatsh, Rocky Mountain Trench, southeastern British Columbia. In: *Glaciofluvial and Galciolacustrine Sedimentation.* (Ed. by A.V. Jopling and B.C. McDonald), *Spec. Publ. Soc. econ. Paleont. Miner.*, 23, 223-236.

Coleman, J.M. and Prior, D.B. (1988) Mass wasting on continental margins. *Ann. Rev. Earth Planet. Sci.*, 16, 101-119.

Costa, J.E. and Sieczorek, G.F (1987) *Debris Flows/Avalanches: Process, Recognition, and mitigation* (Ed.), Reviews in Eng. Geol., 8, pp 13-29, Geological Society of America, Boulder, Colorado.

Crowell, J.C. (1957) Origin of pebbly mudstones. *Bull. geol. Soc. Am.*, 68, 993-1009.

Curry, R.R. (1966) Observation of alpine mudflows in the Tenmile Range, Central Colorado. *Bull. geol. Soc. Am.*, 77, 771-776.

Damuth, J.E.(1980 a) Quaternary sedimentation processes in the South China Basin as revealed by ech-character mapping and piston-core studies. In: *The Tectonic and Geologic Evolution of Southeast Asian Seas and Islands*. (Ed. by D.Hayes), Geophysical Monograph, 23, pp 105-125, American Geophysical Union, Washington, D.C.

Damuth, J.E. (1980 b) Use of high frequency (3.5 kHz-12 kHz) echogram in the study of near-bottom sedimentation processes in the deep sea: A review. *Mar. Geol.*, 38, 51-57.

Damuth, J.E. and Embley, R.W. (1981) Mass-transport processes on Amazon Cone: western equatorial Atlantic. *Bull. Am. Ass. petrol. Geol.*, 65, 629-643.

Davies, T.R.H. (1988) Debris flow surges- A laboratory investigation. Mitteilung no. 96 der Versuchsanstat für Wasserbau, Hydrologie und Glaziologie an der ETH , 122 pp.

Domack, E.W. and Lawson, D.E. (1984) Pebble fabric in ice-rafted diamicton. *J. Geol.*, 93, 577-591.

Dott, R.J (1961) Squantum "Tillite", Massachusetts: evidence of glaciation or subaqueous mass movements? *Bull. geol. Soc. Am.*, 72, 1289-1306.

Dott, R.J. (1963) Dynamics of subaqueous gravity depositional processes. *Bull. Am. Ass. petrol. Geol.*, 47, 104-128.

EEZ-SCAN 87 Scientific Staff (1991) Atlas of the U.S. Exclusive Economic Zone. Atlantic Continental Margin. *U.S. Geological Surv. Miscell. Invest. Series*, I-2054, 174 pp. scale 1:500,000.

Embley, R.W. (1976) New evidence for the occurrence of debris flow deposits in the deep sea. *Geology*, 4, 371-374.

Embley, R.W. (1980) The role of mass transport in the distribution and character of deep ocean sediments with special reference to the North Atlantic. *Mar.Geol.*, 38, 23-50.

Embley, R.W. and Jacobi, R.D. (1977) Distribution and morphology of large submarine sediment slides and slumps on the Atlantic continental margins. *Mar. Geotechnology*, 2, 205-228.

Enos, P. (1977) Flow regimes in debris flow. *Sedimentology*, 24, 133-142.

Eyles, N., Eyles, C.H. and Miall, A.D. (1983) Lithofacies types and vertical profile models: an alternative approach to the description and the environmental interpretation of glacial diamict and diamictite sequences. *Sedimentology*, 30, 393-410.

Eyles, N. (1987) Late Pleistocene debris-flow deposits in large glacial lakes in British Columbia and Alaska. *Sediment. Geol.*, 53, 33-71.

Eyles, N., Clark B.M. and Clague, J.J. (1987) Coarse-grained sediment gravity flow facies in a large superglacial lake. *Sedimentology*, 34, 193-216.

Eyles, N., Eyles, C.H. and McCabe, A.M. (1988) Late Pleistocene subaerial debris-flow facies of the Bow Valley, near Banff, Canadian Rocky Mountains. *Sedimentology*, 35, 465-480.

Eyles, N. and Kocsis, S. (1988) Sedimentology and clast fabric of subaerial debris flow facies in a glacially influenced alluvial fan. *Sediment. Geol.*, 59, 15-18.

Eyles, N. and Clague, J.J. (1991) Glaciolacustrine sedimentation during advance and retreat of the Cordilleran Ice Sheet in Central British Columbia. *Geographie physique et Quaternaire*, 45, 317-331.

Fisher, R.V. (1971) Features of coarse-grained, high-concentration fluids and their deposit. *J. sedim. Petrol.*, 41, 916-927.

Flood, R.D., Piper, D.J.W., Klaus, A. and shipboard scientific party (1995) *Proc. ODP, Init. Repts.*, 155, College Station, Texas (Ocean Drilling Program), 1233 pp.

Frakes, L.A. (1978) Diamictite. In: *The Encyclopedia of Sedimentology*. (Ed. by R.W. Fairbridge and J. Bourgeois). pp. 262-263. Dowden, Hutchinson and Ross, Stroudsburg, Pennsylvania.

French, R.H. (1990) *Hydraulics/Hydrology of Arid lands*. ASCE, New York, 784 pp.

Friedman, G.M. and Sanders, J.E. (1978) *Principles of Sedimentology*. Wiley and Sons, New York, 792 pp.

Fulton, R.J. (1971) Radiocarbon geochronology of southern British Columbia. *Geol. Surv. Can. Pap.*,71-37, 28 pp.

Hampton, M.A. (1970) Subaqueous debris flow and generation of turbidity currents. Ph.D. thesis, Stanford University, Stanford, California.

Hampton, M.A. (1972) The role of subaqueous debris flow in generating turbidity currents. *J. sedim. Petrol.*, 42, 775-793.

Hampton, M.A. (1975) Competence of fine-grained debris flows. *J. sedim. Petrol.*, 45, 834-844.

Hampton, M.A. (1979) Buoyancy in debris flows. *J. sedim. Petrol.*, 49, 753-758.

Hampton, M.A., Lemke, R.W. and Coulter, H.W. (1993) Submarine slides that had a significant impact on man and his activities: Seward and Valdez Alaska. In: *Submarine landslides: Selected studies in the U.S. Exclusive Economic Zone*. (Ed. by W.C. Schwab, H.J. Lee and D.C. Twichell), *Bull. U.S. geol. Surv.*, 2002, 123-134.

Hartshorn, J.H. (1958) Flowtill in southeastern Massachusetts. *Bull. geol. Soc. Am.*, 69, 477-481.

Hayes, D.E. (1980) *The Tectonic and Geologic Evolution of Southeast Asian Seas and Islands (Part I)*, Geophysical Monograph, 23, American Geophysical Union, Washington, D.C., 326 pp.

Hayes, D.E. (1983) *The Tectonic and Geologic Evolution of Southeast Asian Seas and Islands (Part II)*, Geophysical Monograph, 27, American Geophysical Union, Washington, D.C., 396 pp.

Hiscott, R.N. and Middleton, G.V. (1979) Depositional mechanics of the thick-bedded sandstones at the base of a submarine slope, Tourelle Formation, Lower Ordovician, Quebec, Canada. In: *Geology of Continental Slopes* (Ed. By L.J. Doyle and O.H. Pilkey). *Spec. Publ. Soc. econ. Paleont. Miner.*, 27, 307-326.

Hiscott, R.N. and James, N.P. (1985) Carbonate debris flows, Cow Head Group, Western Newfoundland. *J. sedim. Petrol.*, 55, 735-745.

Hiscott, R.N. and Aksu, A.E. (1994) Submarine debris flows and continental slope evolution in front of Quaternary ice sheets, Baffin Bay, Canadian Arctic. *Bull. Am. Ass. petrol. Geol.*, 78, 445-460.

Hubert, J.F., Suchecki, R.K and Callahan, R.K.M. (1977) The Cow Head Breccia: sedimentology of the Cambro-Ordovician continental margin, Newfoundland. In: *Deep Water Carbonate Environments* (Ed. by H. E. Cook and P. Enos). *Spec. Publ. Soc. econ. Paleont. Miner.*, 25, 125-154.

Innes, J.L (1983) Debris Flows. *Progress in Physical Geography*, 7, 469-501.

James, N.P. and Stevens, R.K. (1986) Stratigraphy and correlation of the Cambro-Ordovician Cow Head Group, western Newfoundland. *Bull. geol. Surv. Can.*, 366, 143 pp.

Johnson, A.M. (1965) A model for debris flow. Ph.D. thesis, Pennsylvania State University, University Park, Pennsylvania.

Johnson, A.M. (1970) *Physical Processes in Geology*. Freeman, Cooper & Co., San Francisco, 577 pp.

Johnson, A.M. (1984) Debris flow. In: *Slope Instability* (Ed. by D. Brunsden and D.B. Prior), pp. 257-362. Wiley and Sons, New York.

Johnson, H. (1941) Paleozoic lowlands of northwestern Newfoundland. *The New York Academy of science Transactions, Series II*, 3, 141-145.

Jong, M.G.G. and Rappol, M. (1983) Ice-marginal debris-flow deposits in western Allagu, southern West Germany. *Boreas*, 12, 57-70.

Kindle, C.H. and Whittington, H.B. (1958) Stratigraphy of the Cow Head region, western Newfoundland. *Bull. geol. Soc. Am.*, 69, 315-342.

Lawson, D.E. (1979a) A comparison of the pebble orientations in ice and deposits of the Matanuska Glacier, Alaska: *J. Geology*, 87, 629-645.

Lawson, D.E. (1979b) A sedimentological analysis of the western terminus region of the Matanuska Glacier, Alaska: *Cold Regions Res. Eng. Lab. (Hanover, N.H.) Rept.* 79-9, 122.

Lawson, D.E. (1982) Mobilisation, movement and deposition of active subaerial sediment flows, Matanuska Glacier, Alaska. *J. Geol.*, 90, 279-300.

Lowe, D.R. (1976) Grain flow and grain flow deposits. *J. sedim. Petrol.*, 46, 188-199.

Malahoff, A., Embly, R.W., Berry, R.B. and Fefe, C. (1980) Submarine mass-wasting of sediments on the continental slope and upper rise south of Baltimore Canyon. *Earth Planet. Sci. Letts.* , 49, 1-7.

Mark, D.M. (1973) Analysis of axial orientation data, including till fabrics. *Bull. geol. Soc. Am.*, 84, 1369-1374.

Mark, D.M. (1974) On the interpretation of till fabrics. *Geology*, 2, 101-104.

Masson, D.G., Huggett, Q.J., Weaver, P.P., Brunsden, D. and Kidd, R.B. (1992) The Saharan and Canary Debris Flows, Offshore Northweast Africa. *Landslide News*, 6, 9-13.

Masson, D.G., Huggett, Q.J. and Brunsden, D. (1993) The surface texture of the Saharan Debris Flow deposit and some speculations on debris flow processes. *Sedimentology*, 40, 583-598.

Mehra, O.P. and Jackson, M.L. (1960) Iron removal from soils and clays by a dithionite-citrate system buffered with sodium bicarbonate. *Clays and Clay Minerals*, 7, 317-327.

Mills, H. (1984) Clast orientation in Mount St. Helens debris-flow deposits, North Fork Toutle River, Washington. *J. sedim. Petrol.*, 54, 626-634.

Mutti, E. and Normark, W.R. (1987) Fan valleys, channels, and depositional lobes on modern submarine fans: characters for recognition of sandy turbidite environments. *Bull. Am. Ass. petrol. Geol*, 62, 912-931.

Naylor, M.A. (1980) The origin of inverse grading in muddy debris flow deposits-a review. *J. sedim. Petrol.*, 50, 1111-16.

Nemec, W. and Steel, R.J. (1984) Alluvial and coastal conglomerates: their significant features and some comments on gravelly mass-flow deposits. In: *Sedimentology of gravels and conglomerates.*(Ed. by E.H. Koster and R.J. Steel). *Mem. Can. Soc. petrol. Geol.*, 10, 1-31.

Pierson, T.C. (1980) Erosion and deposition by debris flows at Mt. Thomas, North Canterbury, New Zealand. *Earth Surface Processes*, 5, 227-47.

Pierson, T.C. (1981) Dominant particle support mechanisms in the debris flows at Mt. Thomas, New Zealand, and implication for flow mobility. *Sedimentology*, 28, 49-60.

Pierson, T.C. (1986) Flow behaviour of channelized debris flows, Mount St. Helens, Washington. In: Hillside processes. (Ed. by: A.D. Abrahams), pp.269-296. Allen and Unwin, Boston, Massachusetts.

Pierson, T.C. and Costa, J.E. (1987) A rheologic classification of subaerial sediment-water flows. In: *Debris Flows/Avalanches: Process, Recognition, and mitigation* (Ed. by J.E. Costa and G.F. Wieczorek), Reviews in Eng. Geol., 8, pp 13-29. Geological Society of America, Boulder, Colorado.

Postma, G. (1986) Classification of sediment gravity-flow deposits based on flow characteristics during sedimentation. *Geology*, 14, 291-294.

Rappol, M. (1985) Clast-fabric strength in tills and debris flows compared for different environments. *Geologie en Mijnbouw*, 64, 327,332.

Rodgers, J. and Neale, E.R.W. (1963) Possible "Taconic" klippen in western Newfoundland. *Am. J. Sci.*, 261, 713-730.

Rodine, J.D. and Johnson, A.M. (1976) The ability of debris, heavily freighted with coarse clastic materials to flow on gentle slopes. *Sedimentology*, 23, 213-234.

Sharp, R.P. and Nobles, L.H. (1953) Mudflow of 1941 at Wrightwood, southern California. *Bull. geol. Soc. Am.*, 64, 547-560.

Srivastava, S.P., Arthur, M., Clement, B. and shipboard scientific party (1987) *Proc. ODP, Init. Repts.*, 105, College Station, Texas (Ocean Drilling Program), 971 pp.

Takahashi, T. (1978) Mechanical characteristics of debris flow. *J. Hydraulics Division, Am. Soc. civil Eng.*,104, No. HY8, 1153-69.

Takahashi, T. (1981) Debris flow. *Ann. Rev. Fluid Mech.*, 13, 57-77.

Terzaghi, K. (1956) Varieties of submarine slope failures. In: *Proceedings of the 8th Texas soil mechanics and foundation engineering conference*. Austin, Texas, 41 pp.

Thorez, J. (1974) Phyllosilicates and clay minerals: a laboratory handbook for their X-ray diffraction analysis. Lelotte, Belgium, 539 pp.

Tucker, M. (1988) *Techniques in sedimentology*. (Ed.). Blackwell Scientific, Oxford, 394pp.

Van Everdingen, D.A., Van Gool, J.A.M. and Vissers, R.L.M. (1992) QUICKPLOT: A microcomputer-based program for processing of orientation data. *Computers and Geosciences*, 18, 183-287.

Varnes, D.J. (1978) Slope movement types and processes. In: *Landslides and engineering*. (Ed. by E.B. Eckel), National Academy of Sciences, Transportation Research Board Special Report 176, 11-33.

United States Geological Survey (1982) Goals and tasks of the landslide part of a ground-failure hazards reduction program. *U.S. Geological Survey Circular 880*, 49 pp.

Williams, H. (1975) Structural succession, nomenclature, and interpretation of transported rocks in western Newfoundland. *Can. J. Earth Sci.*, 12, 1874-1894.

Williams, H., James, N.P. and Stevens, R.K. (1985) Humber Arm allochthon and nearby groups between Bonne Bay and Portland Creek, western Newfoundland. In: *Current Research, Part A. Geol. Surv. Can. Pap.*, 85-1A, 399-406.

Woodcock, N.H. (1977) Specification of fabric shapes using an eigenvalue method. *Bull. geol. Soc. Am.*, 88, 1231-1236.

Table A1. List of grain-size and clast-fabric samples collected from Fraser River Valley, Central Interior, British Colombia. Sample prefixes C are from Quesnel Airport section, prefixes G are from Gaspard Creek section, prefixes F are from Farwell Canyon sections 1,2,3, prefixes R are from Gang Ranch sections, and prefixes C are from Churn Creek sections. See Figures 6 and 11 for section locations. For samples from piston cores, see Table 3.

Q-1-1	Unit 1	Sample 1	53° 01′ 15″ N, 122° 31′ 20″ W	~15 m thick DF (unit I, section 2 of Eyles, 1987). Fabric sample SQ11.
Q-1-2	Unit 1	Sample 2	53° 01′ 15″ N, 122° 31′ 20″ W	~2 m thick DF (unit I, section 3 of Eyles, 1987).
Q-3-1	Unit 3	Sample 1	53° 01′ 15″ N, 122° 31′ 20″ W	~10 m thick DF, unit III of Eyles (1987).
F-1-1	Sect.1	Sample 1	51° 31′ 50″ N, 122° 17′ 15″ W	500 m N of Farwell Canyon bridge, lower 1m of DF1 (2.5 m thick) at the base of the section. Fabric station S111.
F-1-2	Sect.1	Sample 2	51° 31′ 50″ N, 122° 17′ 15″ W	Middle part of 2 m-thick unit, DF2.
F-1-3	Sect.1	Sample 3	51° 31′ 50″ N, 122° 17′ 15″ W	DF3, on top of DF2, exposed thickness ~2m.
G-4-1a	Sect.4	Sample 1	51° 34′ 05″ N, 122° 18′ 50″ W	Base of 11 m DF exposed by Gaspard Creek. Fabric station S411.
G-4-1b	Sect.4	Sample 1	51° 34′ 05″ N, 122° 18′ 50″ W	Base of 11 m DF exposed by Gaspard Creek.
G-4-2	Sect.4	Sample 2	51° 34′ 05″ N, 122° 18′ 55″ W	120 m west of G-4-1, base of 20 m bed (DF1). Fabric station S422.
G-4-3	Sect.4	Sample 3	51° 34′ 05″ N, 122° 18′ 55″ W	Same bed (DF1), 15 m from base.
G-4-4	Sect.4	Sample 4	51° 34′ 05″ N, 122° 18′ 55″ W	DF2, 5 m thick, on top of DF1. Fabric station S431.
R-5-1	Sect.5	Sample 1	51° 31′ 50″ N, 122° 17′ 15″ W	Along the road 300m NNW of Gang Ranch bridge, middle part of 12 m-thick DF. Fabric sample S521. Fabric sample S511 from the lower 1 m of the DF.
R-5-2	Sect.5	Sample 2	51° 32′ 15″ N, 122° 17′ 40″ W	650 m NNW of R-5-1. DF1, 2m thick. Fabric station S531.
R-5-3	Sect.5	Sample 3	51° 32′ 15″ N, 122° 17′ 40″ W	650 m NNW of R-5-1. DF2, 13m thick, overlying DF1 and 4m till unit. Fabric station S532.
R-5-4	Sect.5	Sample 4	51° 32′ 15″ N, 122° 17′ 40″ W	650 m NNW of R-5-1. DF3, 20 m thick, overlying DF1. Fabric station S533.

Table A1. Continued

C-6-1	Sect.6	Sample 1	51° 31′ 30″ N, 122° 18′ 00″ W	1 km west of bridge, DF1, lower unit in the section, thickness 1.1-2.5 m. Fabric station S611.
C-6-2	Sect.6	Sample 2	51° 31′ 30″ N, 122° 18′ 00″ W	DF2, 1-3 m thick, separated from lower unit (DF1) by two cross-bedded sand units ~ 0.5 m-thick each. Fabric station S612.
C-6-3	Sect.6	Sample 3	51° 31′ 30″ N, 122° 18′ 00″ W	DF3, 2-3 m thick, on top of DF2. Fabric station S623.
C-6-4	Sect.6	Sample 4	51° 31′ 30″ N, 122° 18′ 00″ W	DF4, 5 m thick, on top of DF3.
C-6-5	Sect.6	Sample 5	51° 31′ 15″ N, 122° 17′ 05″ W	150m N of Churn Creek bridge. 10 m-thick DF unit. Fabric station S631.
C-6-6	Sect.6	Sample 6	51° 31′ 20″ N, 122° 17′ 30″ W	300m W of Churn Creek bridge. 7m + DF unit. Fabric station S641.
C-6-7	Sect.6	Sample 7	51° 31′ 20″ N, 122° 17′ 45″ W	200m W of C-6-6, base of 3 m-thick DF2, about 5 m above creek level. Fabric station S651.
C-6-8	Sect.6	Sample 8	51° 31′ 20″ N, 122° 17′ 45″ W	the top part of DF2. Fabric station S661.
C-6-9	Sect.6	Sample 9	51° 31′ 20″ N, 122° 17′ 45″ W	on the opposite (N) side of the creek, same unit (DF2). Fabric station S662.
C-6-10	Sect.6	Sample 10	51° 31′ 20″ N, 122° 17′ 45″ W	DF1 underneath DF2, partially exposed, 10 m thick.

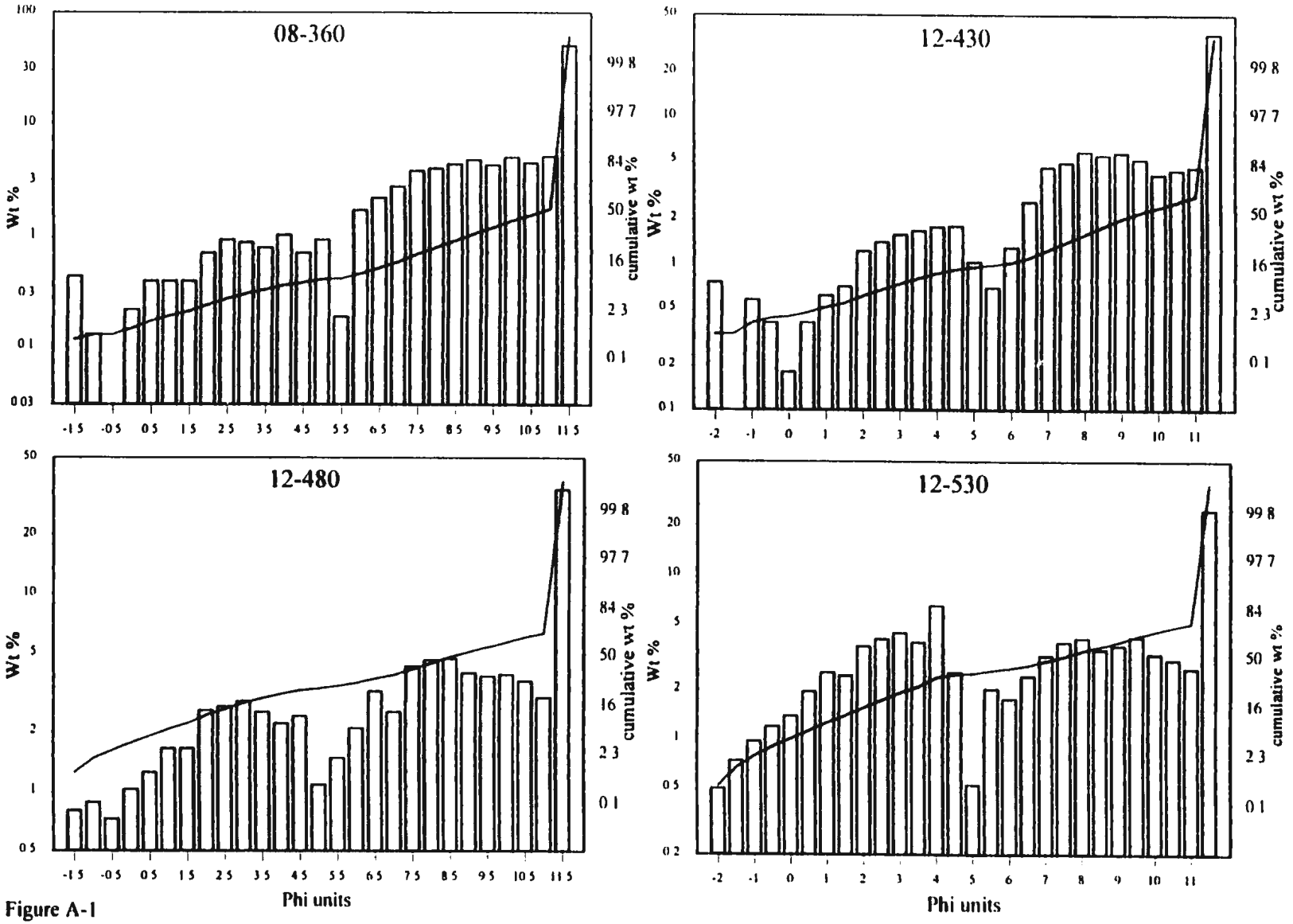

Figure A-1

Grain size distribution of the different samples analyzed in this study. Histograms show the weight percent at each phi class show on logarithmic scale. The line curve is the cumulative weight percent on a probability scale. For samples location see Table 3, Table A1, figures 6 and 11.

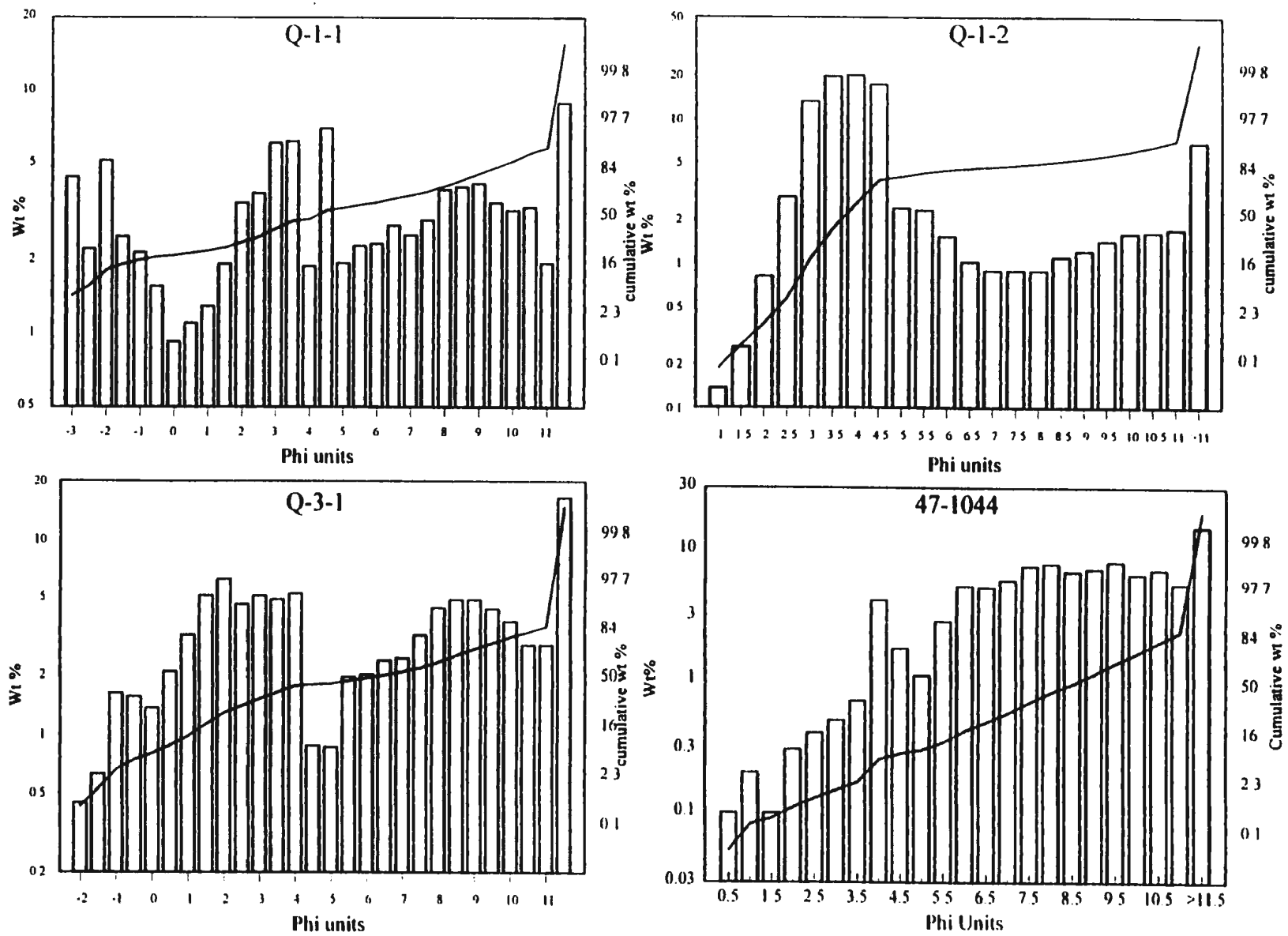

Figure A-1 (continued).

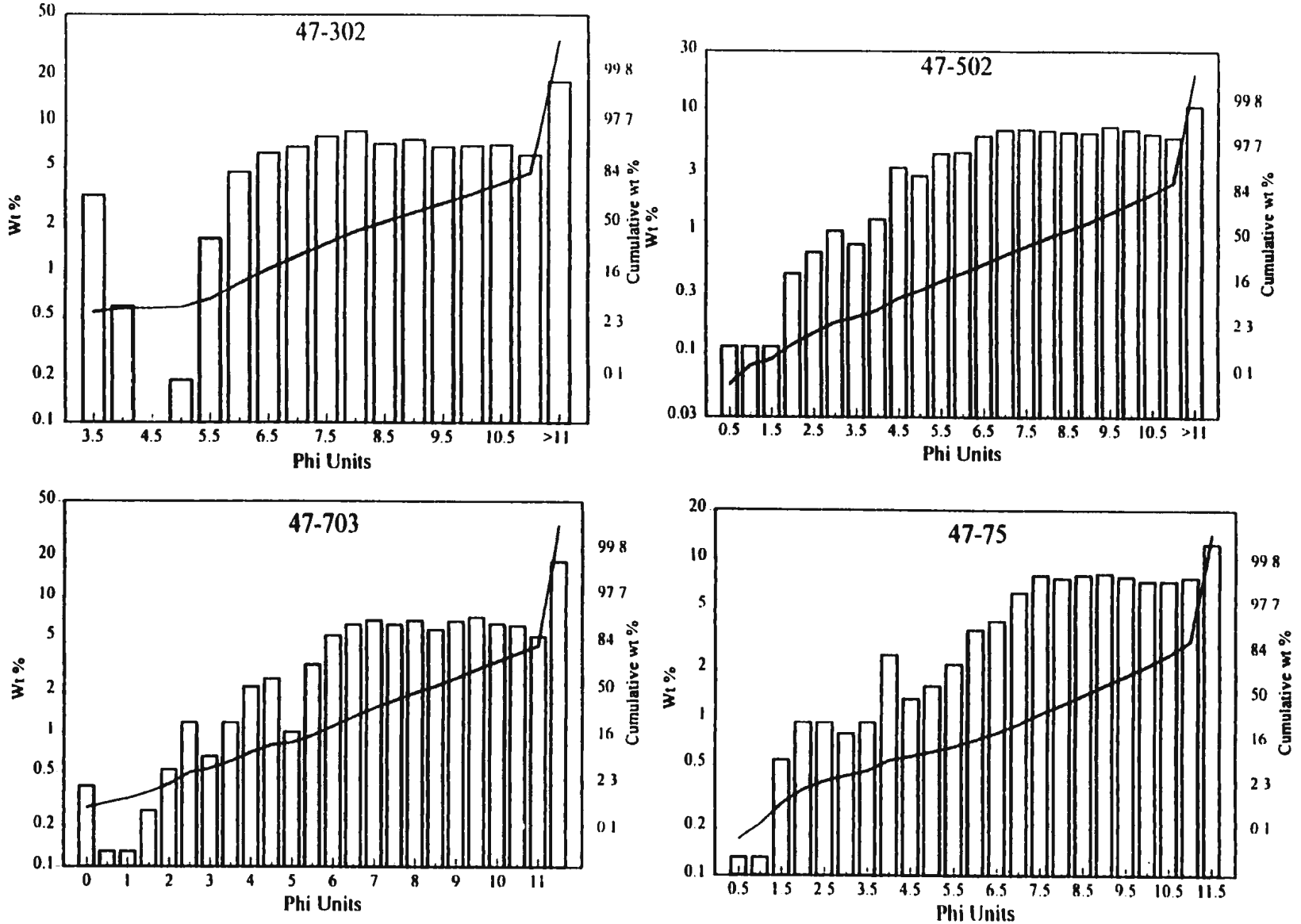

Figure A-1 (continued).

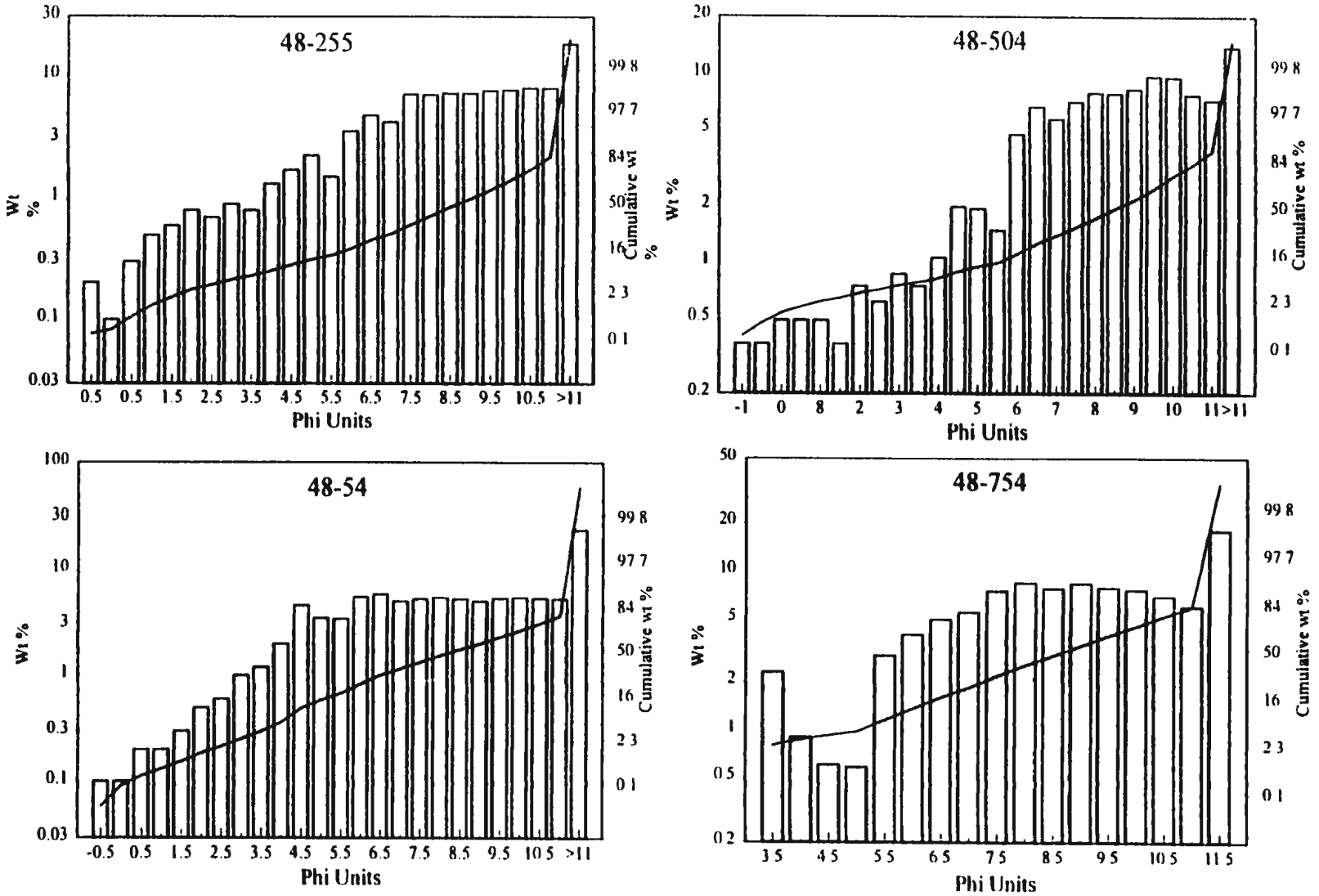

Figure A-1 (continued).

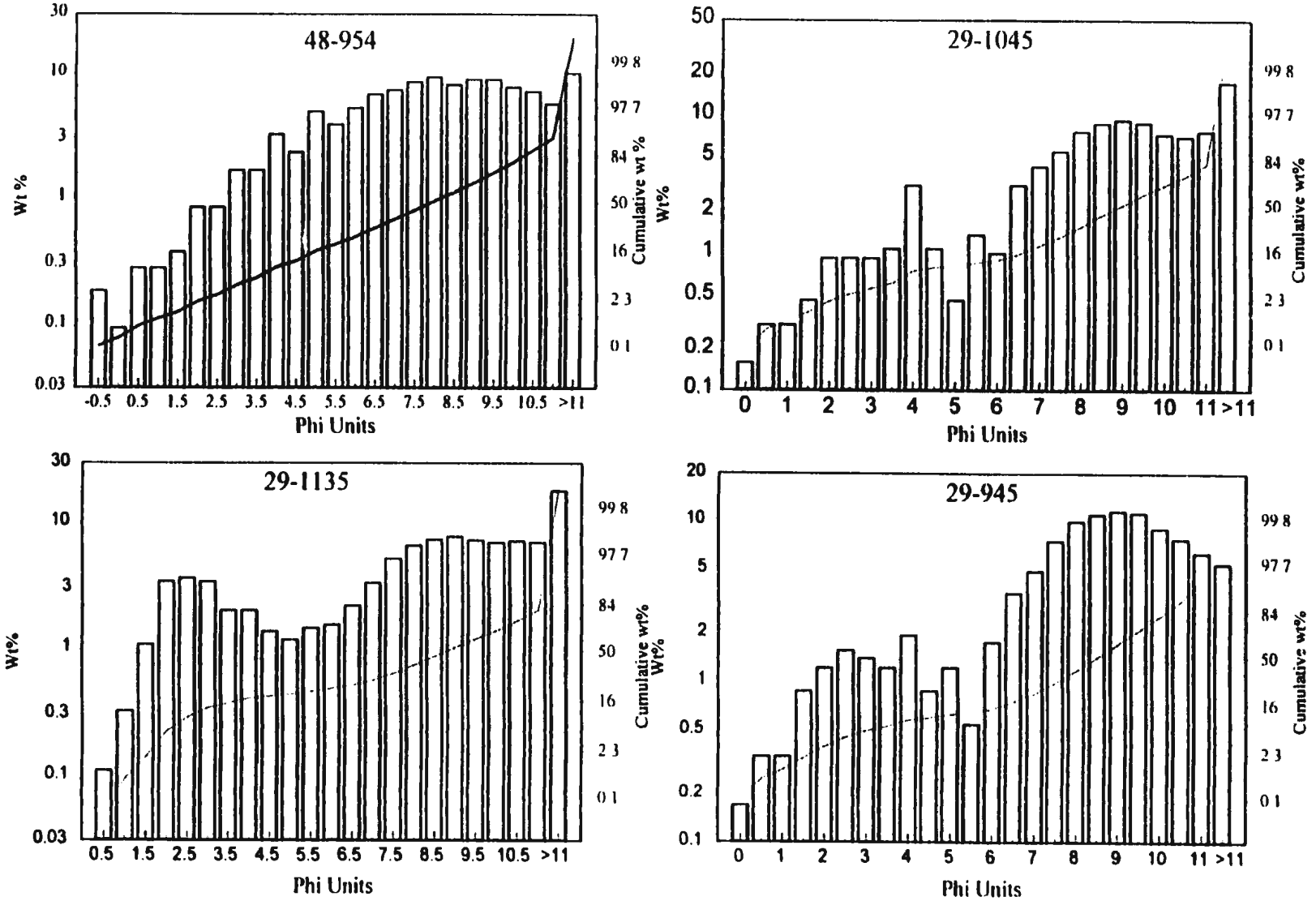

Figure A-1 (continued).

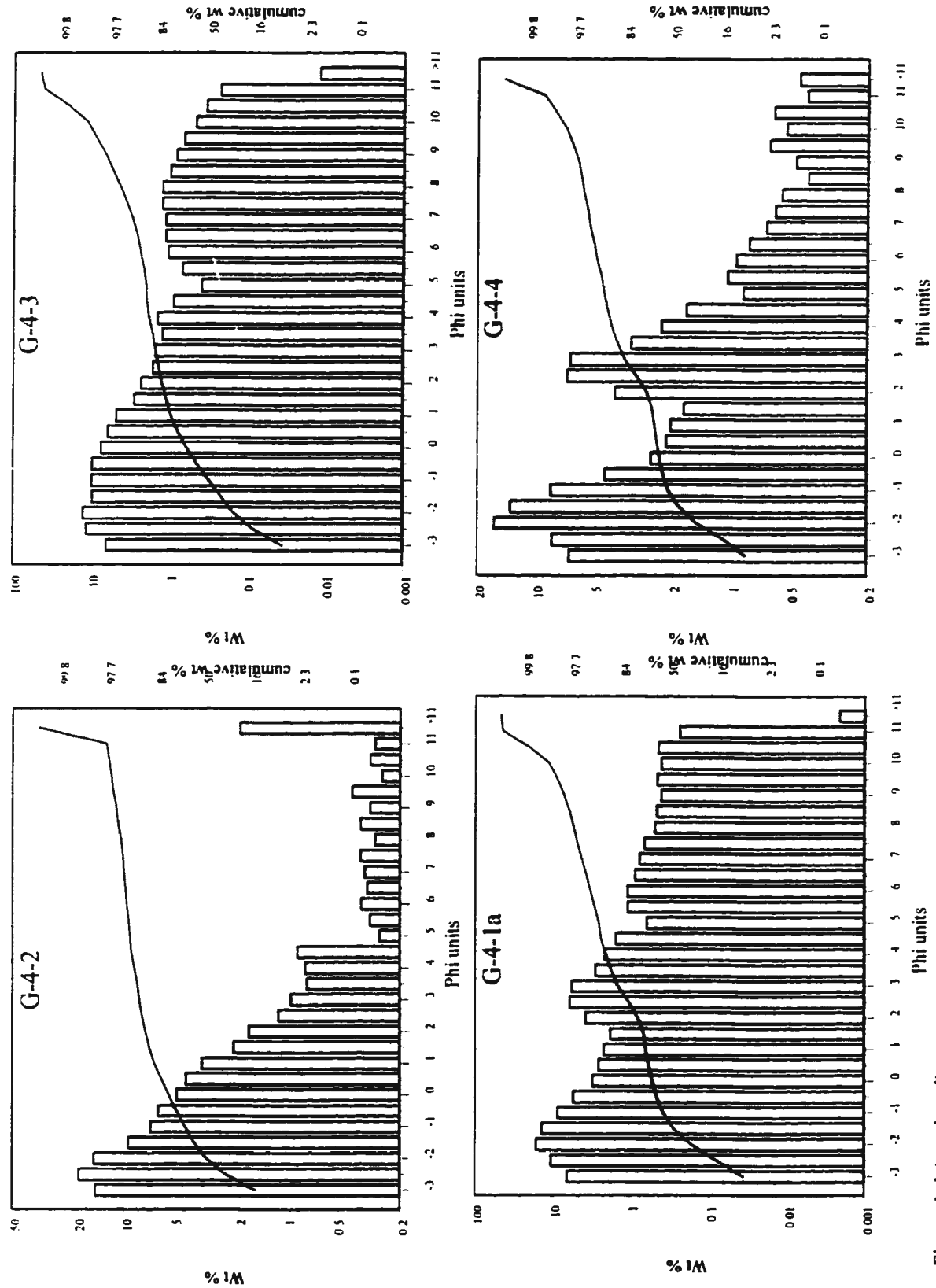

Figure A-1 (continued).

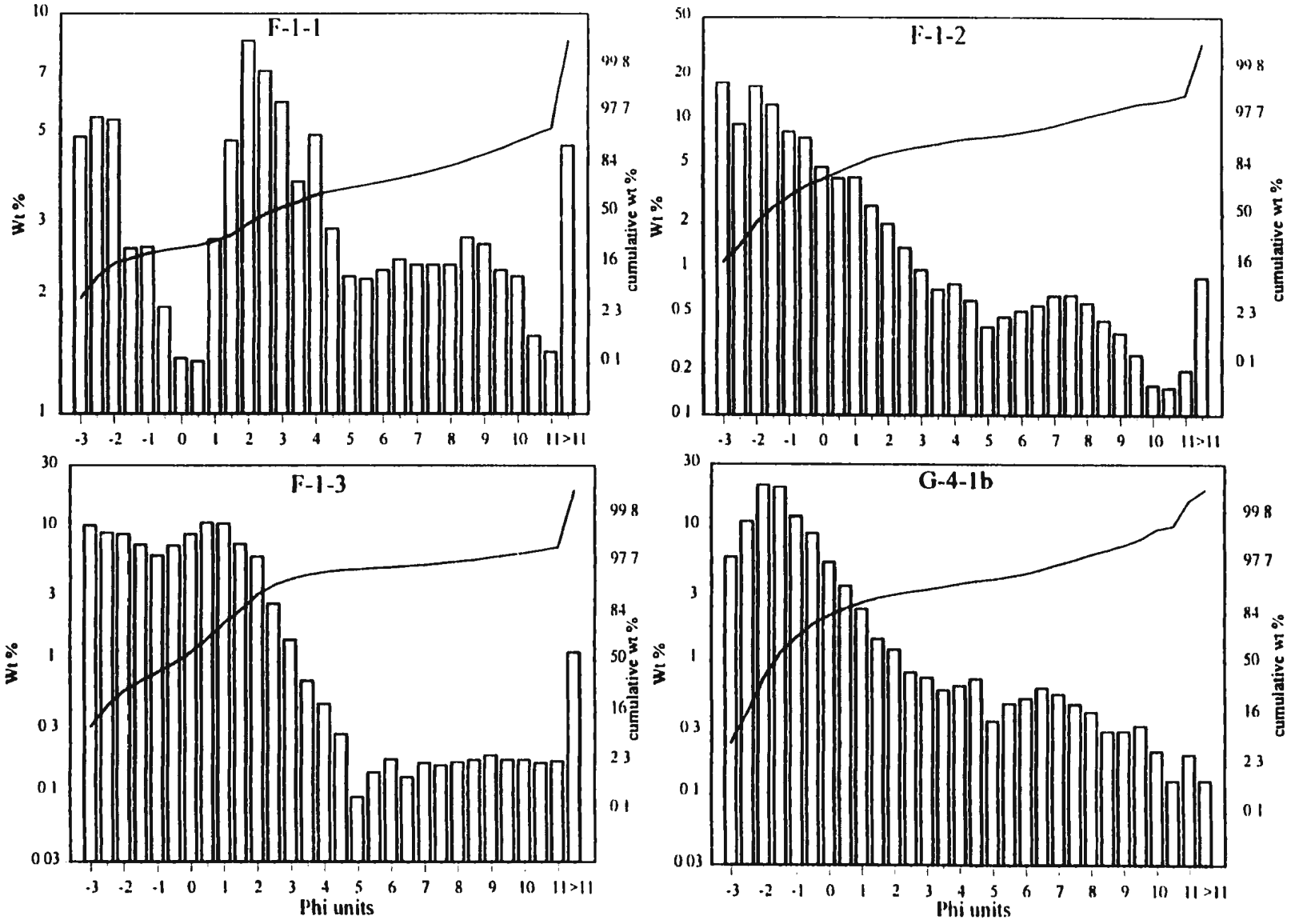

Figure A-1 (continued).

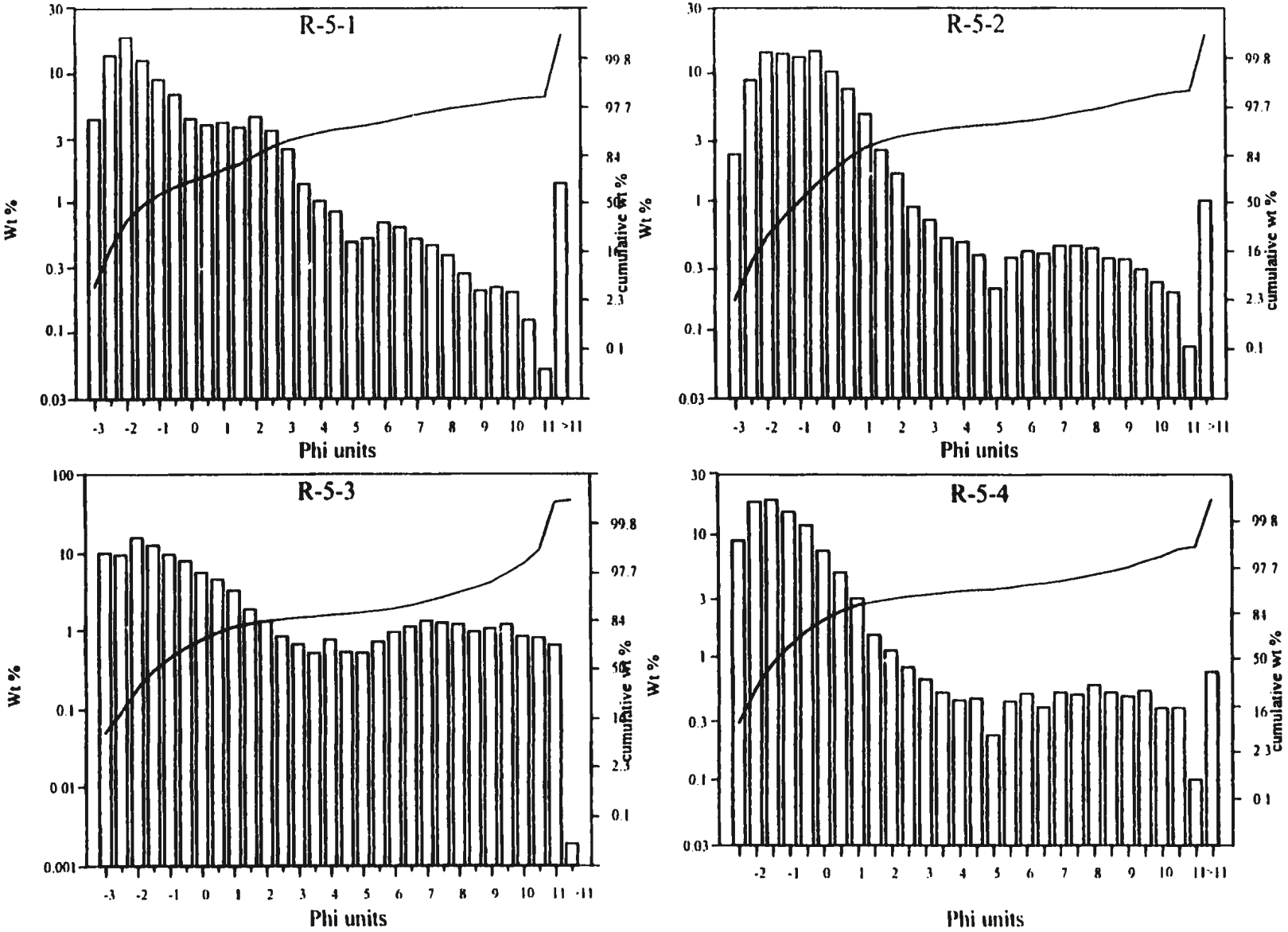

Figure A-1 (continued).

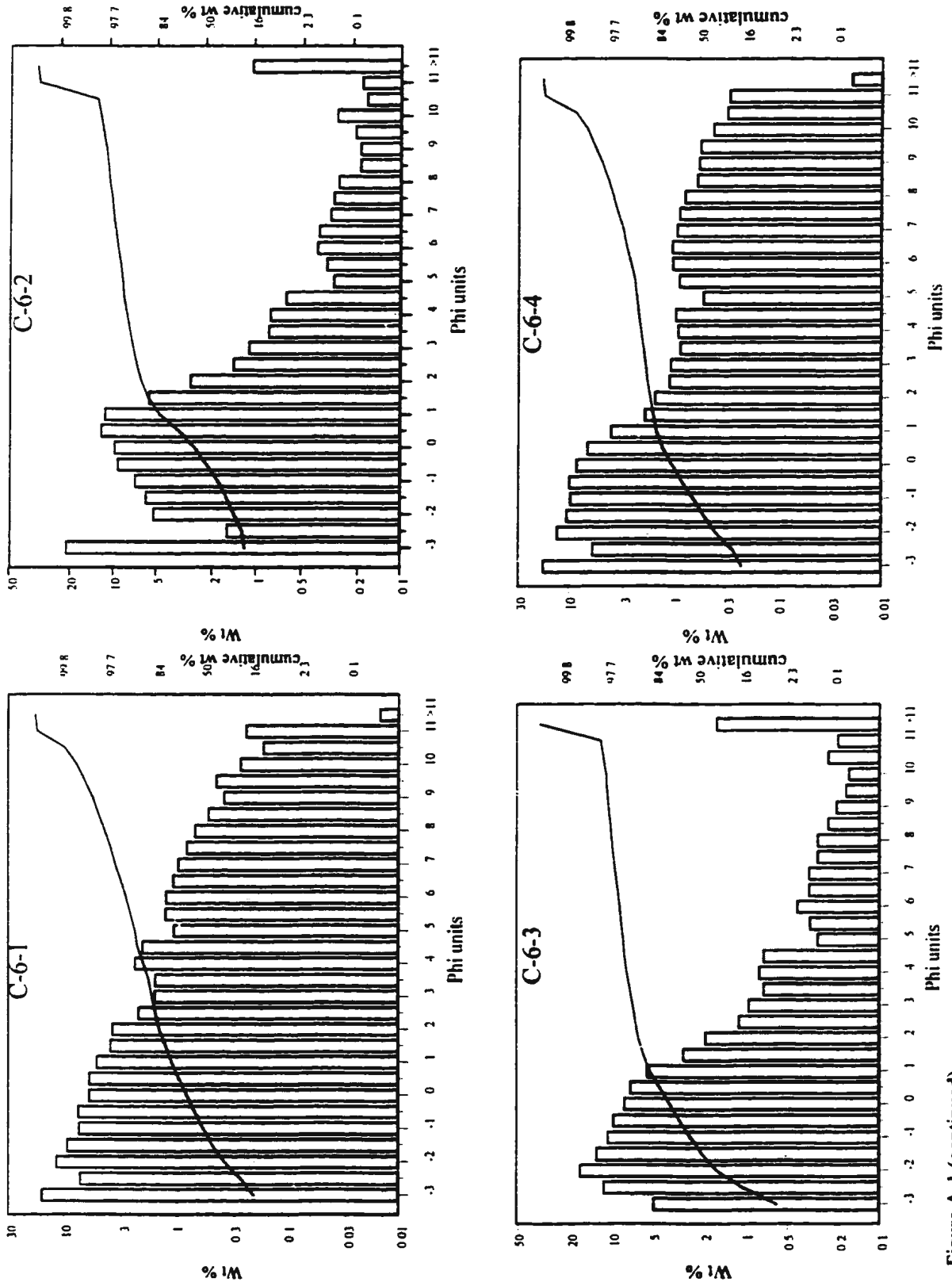

Figure A-1 (continued).

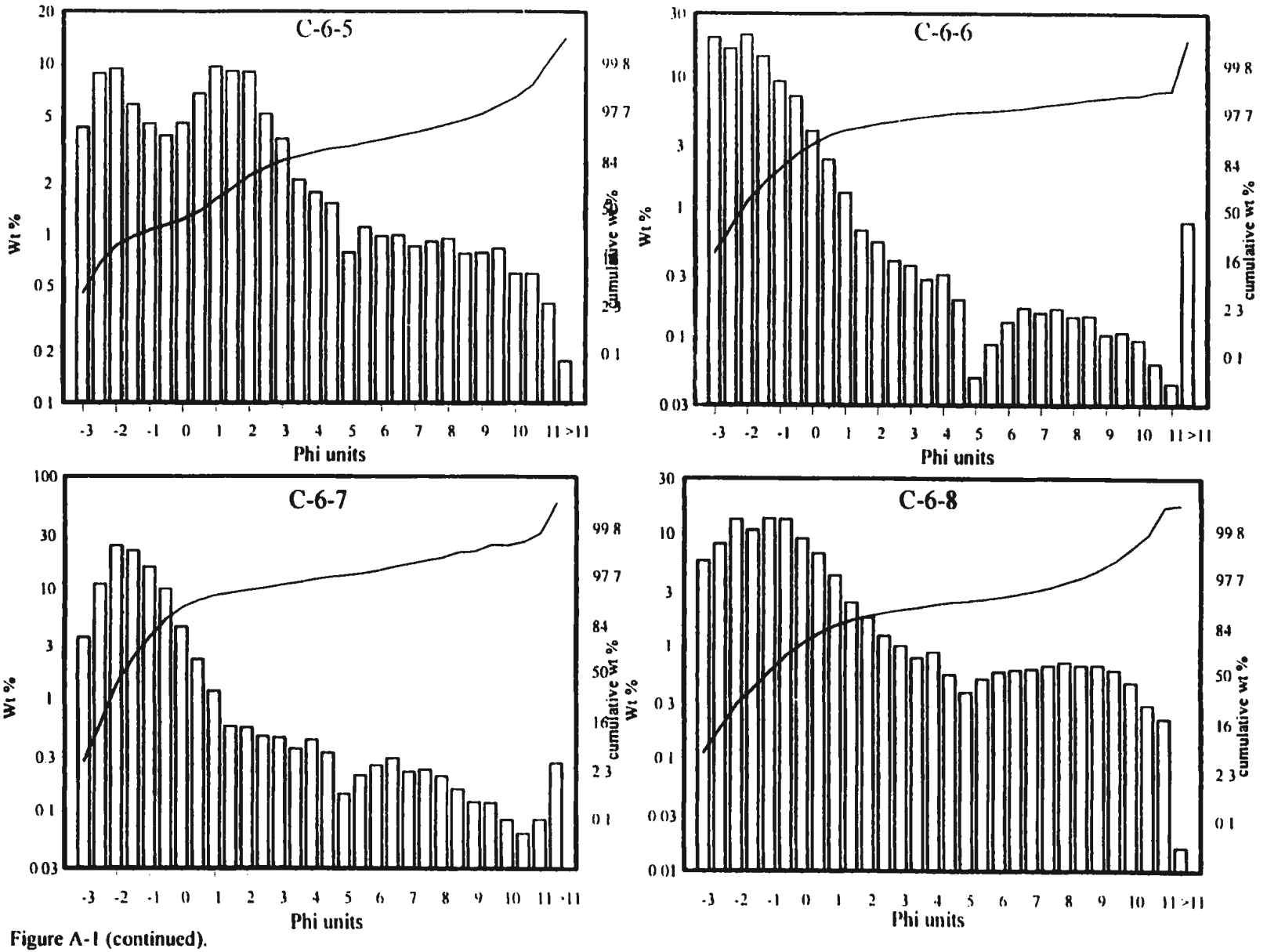

Figure A-1 (continued).

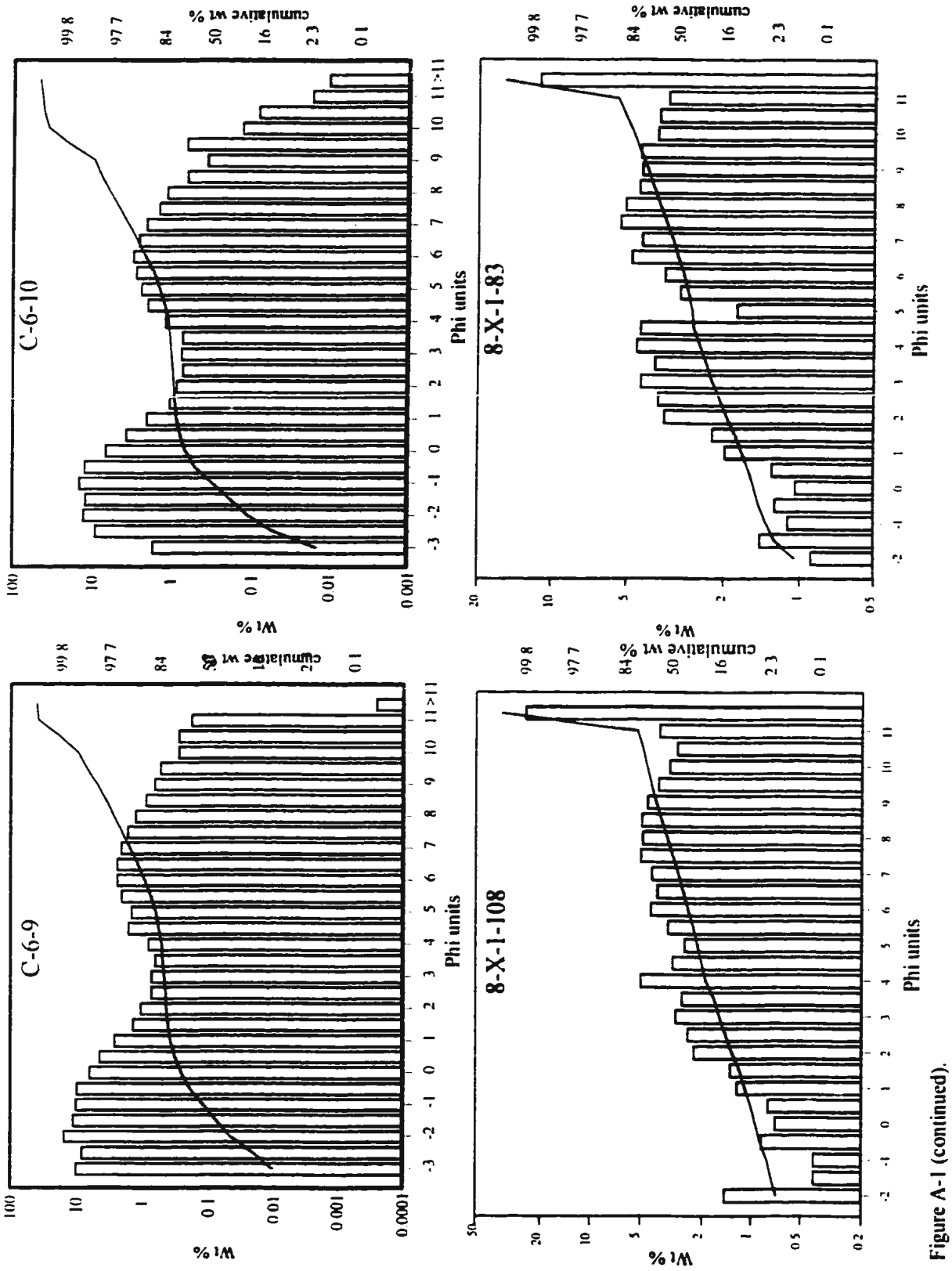

Figure A-1 (continued).

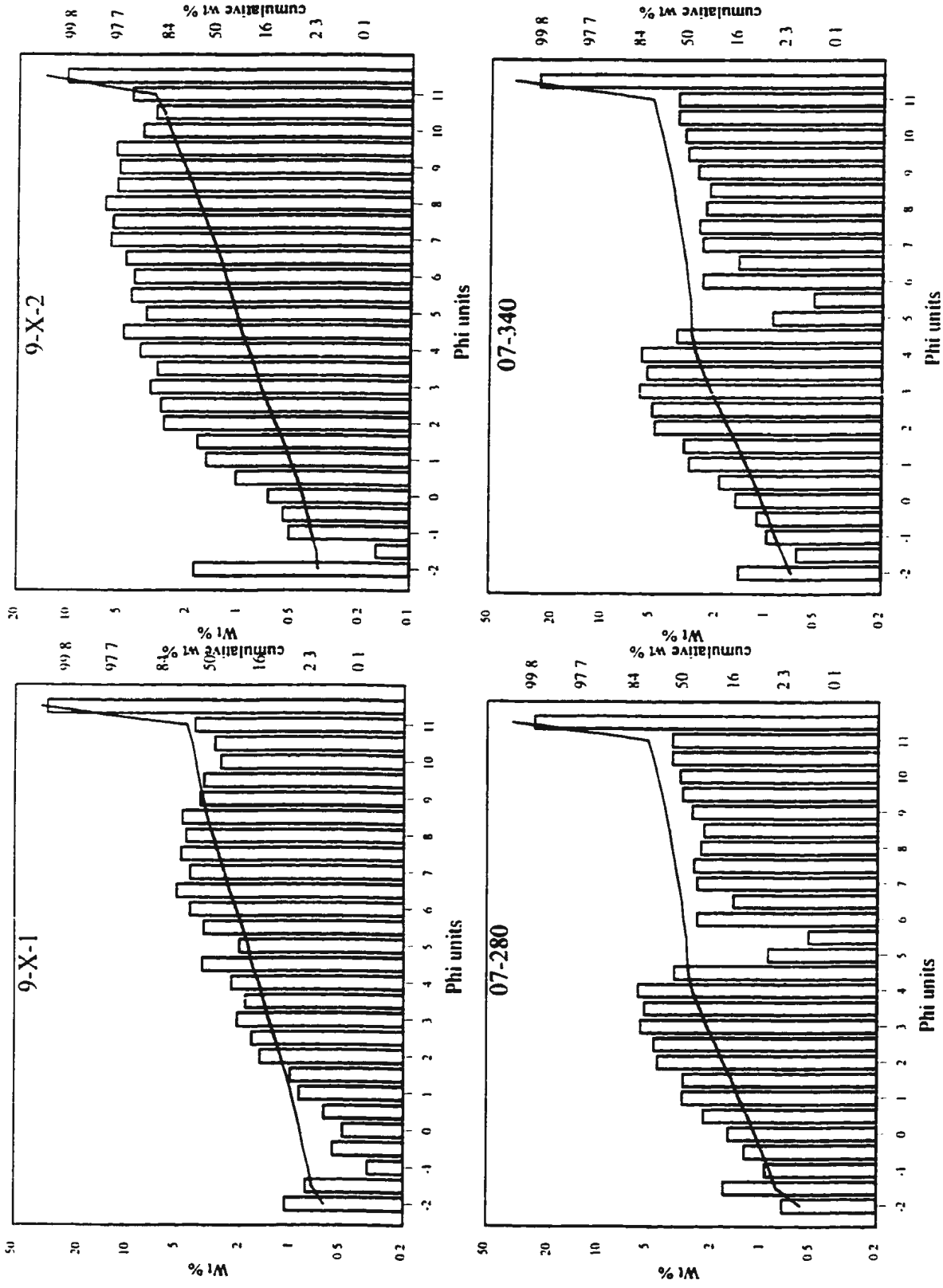

Figure A-1 (continued).

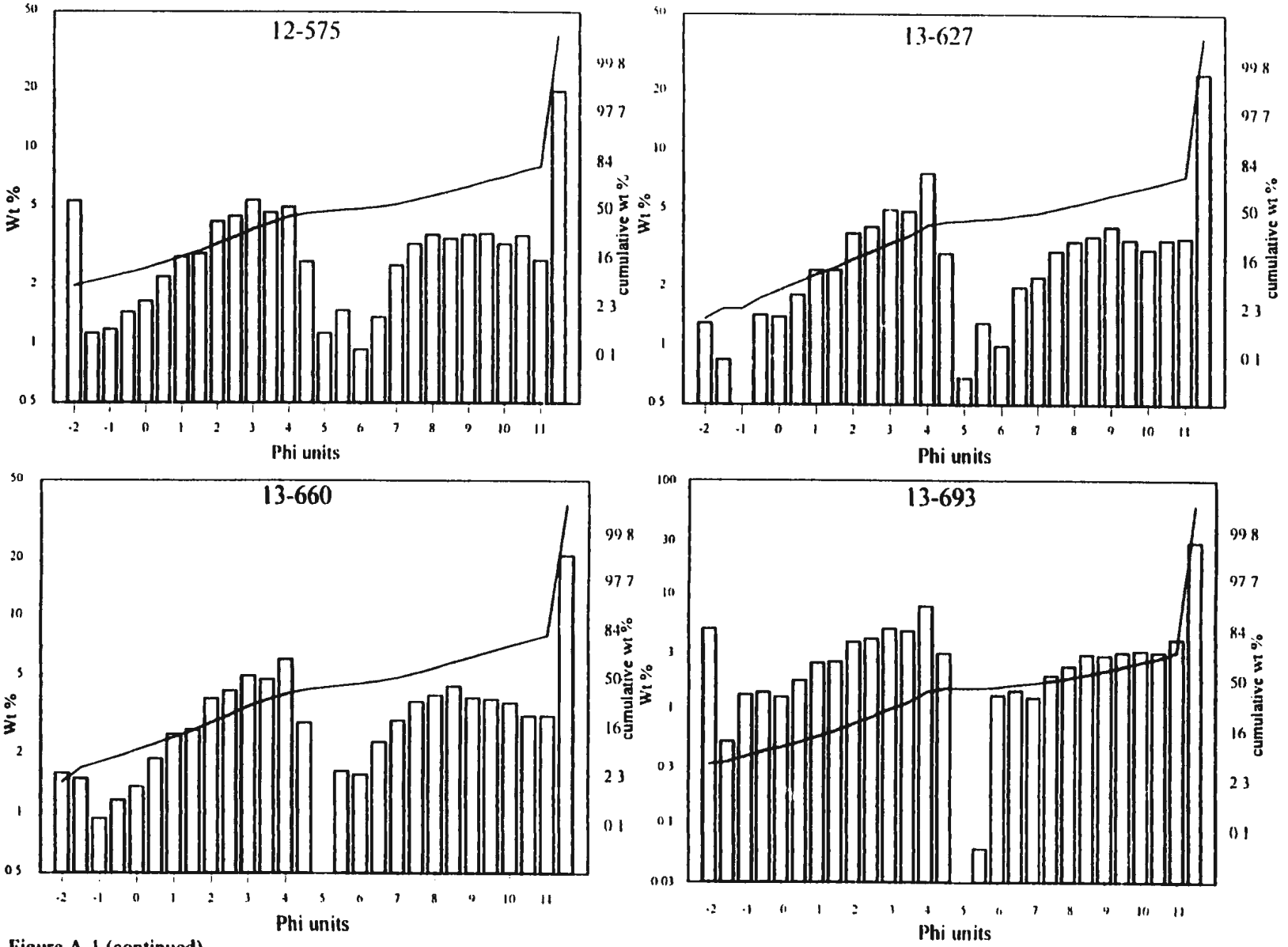

Figure A-1 (continued).

S111

Eigen values:
.519 .277 .2026
Eigen vectors:
Dip-Dir Dip
286.8 16.142
25.18 26.58
169.0 58.20
Confidence Radius
95% Signif.: 25.6 deg.
Axis:
Azim = 286.
Plng = 16.1

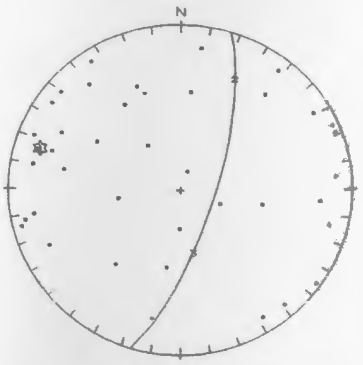

N = 40

S411

Eigen values:
.499 .415 .084
Eigen vectors:
Dip-Dir Dip
283.2 1.069
193.1 7.248
21.60 82.67
Confidence Radius
95% Signif.: 33.6 deg.
Best Fit Girdle:
Azim = 103
Dip = 88.9

N = 40

S422

Eigen values:
.621 .284 .0945
Eigen vectors:
Dip-Dir Dip
88.313 17.62
103.1 14.95
231.1 66.55
Confidence Radius
95% Signif.: 24.5 deg.
Best Fit Girdle:
Azim = 188
Dip = 72.3

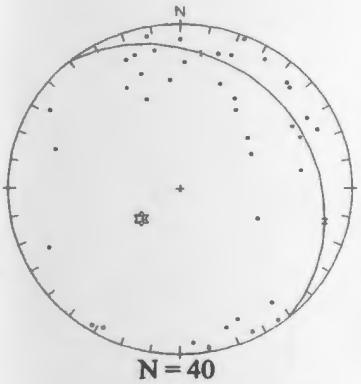

N = 40

S431

Eigen values:
.450 .369 .1797
Eigen vectors:
Dip-Dir Dip
209.2 17.65
116.6 8.143
2.916 70.43
Confidence Radius
95% Signif.: 28.0 deg.
Best Fit Girdle:
Azim = 29
Dip = 72.3

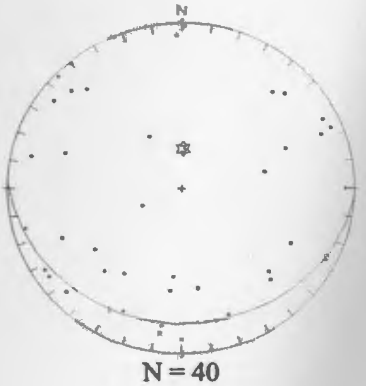

N = 40

S511

Eigen values:
.559 .375 .065
Eigen vectors:
Dip-Dir Dip
84.58 11.02
176.6 10.45
309.0 74.71
Confidence Radius
95% Signif.: 21.8 deg.
Best Fit Girdle:
Azim = 265
Dip = 78.9

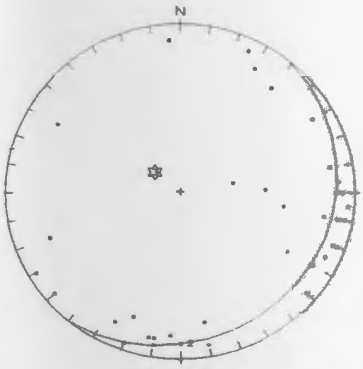

N = 40

S521

Eigen values:
.601 .310 .088
Eigen vectors:
Dip-Dir Dip
341.9 19.65
245.2 17.99
115.9 62.83
Confidence Radius
95% Signif.: 21.0 deg.
Best Fit Girdle:
Azim = 162
Dip = 70.3

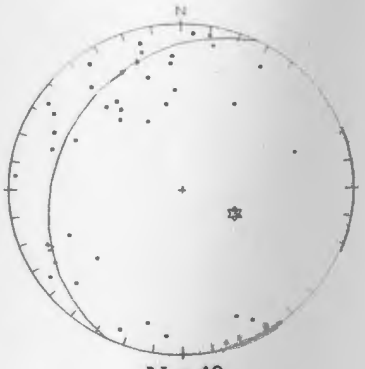

N = 40

Figure B-1. Lower hemispheric equal area stereographic projection diagrams of the clast fabric data collected from Fraser River Valley, Central Interior British Columbia.

S531

Eigen values:
.488 .392 .1182
Eigen vectors:
Dip-Dir Dip
54.06 12.24
322.1 8.860
197.0 74.80
Confidence Radius
95% Signif.: 28.5 deg.
Best Fit Girdle:
Azim = 234
Dip = 77.7

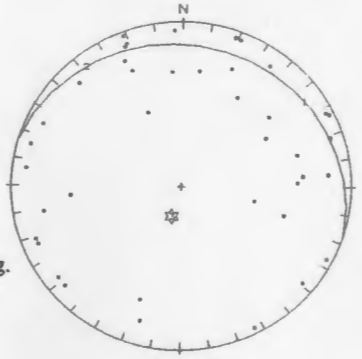

N = 40

S532

Eigen values:
.532 .303 .1641
Eigen vectors:
Dip-Dir Dip
318.6 5.402
227.9 8.029
82.27 80.30
Confidence Radius
95% Signif.: 27.6 deg.
Best Fit Girdle:
Azim = 139
Dip = 84.5

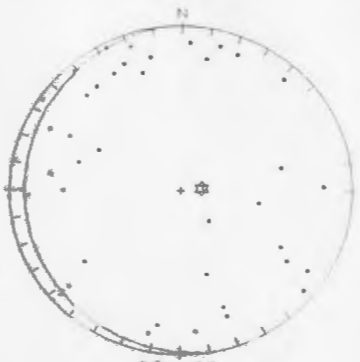

N = 40

S533

Eigen values:
.608 .283 .1077
Eigen vectors:
Dip-Dir Dip
158.8 3.547
250.1 20.24
59.32 69.42
Confidence Radius
95% Signif.: 34.3 deg.
Best Fit Girdle:
Azim = 339
Dip = 86.4

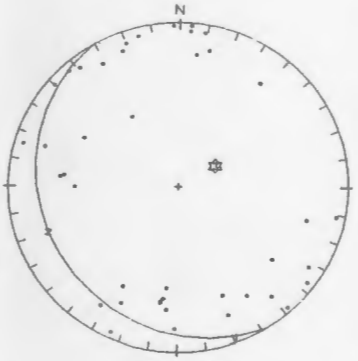

N = 40

S611

Eigen values:
.463 .383 .1525
Eigen vectors:
Dip-Dir Dip
155.0 .2997
65.00 1.389
257.3 88.57
Confidence Radius
95% Signif.: 31.9 deg.
Best Fit Girdle:
Azim = 335
Dip = 89.7

N = 40

S612

Eigen values:
.501 .437 .061
Eigen vectors:
Dip-Dir Dip
222.1 4.744
312.3 2.406
69.14 84.67
Confidence Radius
95% Signif.: 37.1 deg.
Best Fit Girdle:
Azim = 42
Dip = 85.2

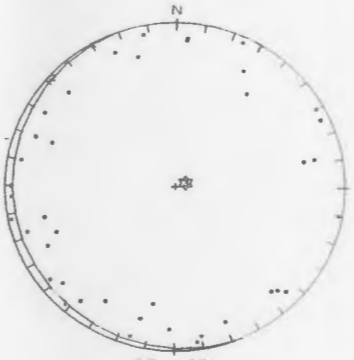

N = 40

S623

Eigen values:
.559 .360 .0799
Eigen vectors:
Dip-Dir Dip
300.9 10.21
210.7 1.606
111.8 79.66
Confidence Radius
95% Signif.: 30.4 deg.
Best Fit Girdle:
Azim = 121
Dip = 79.7

N = 40

Figure B-1. Continued.

S631

Eigen values:
.514 .317 .1680
Eigen vectors:
Dip-Dir Dip
195.6 17.02
287.1 4.675
31.97 72.30
Confidence Radius
95% Signif.: 22.7 deg.
Best Fit Girdle:
Azim = 16
Dip = 72.9

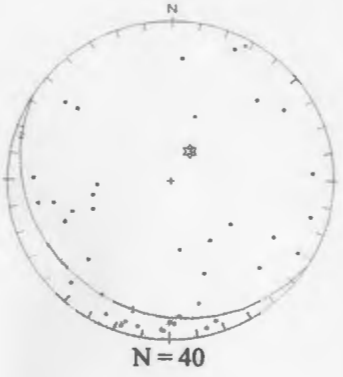

S641

Eigen values:
.600 .312 .087
Eigen vectors:
Dip-Dir Dip
112.1 8.258
205.4 21.24
2.134 67.05
Confidence Radius
95% Signif.: 24.2 deg.
Best Fit Girdle:
Azim = 292
Dip = 81.7

S651

Eigen values:
.502 .354 .1435
Eigen vectors:
Dip-Dir Dip
157.4 5.728
66.24 12.16
272.2 76.51
Confidence Radius
95% Signif.:
28.9 deg.
Best Fit Girdle:
Azim = 337
Dip = 84.2

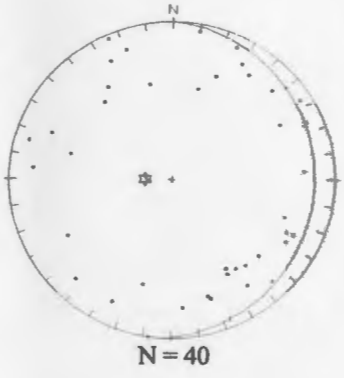

S661

Eigen values:
.554 .335 .1101
Eigen vectors:
Dip-Dir Dip
174.8 5.809
81.63 28.97
275.1 60.33
Confidence Radius
95% Signif.: 24.7 deg.
Best Fit Girdle:
Azim = 355
Dip = 84.1

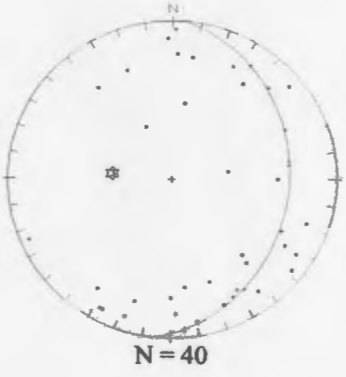

S662

Eigen values:
.559 .311 .1290
Eigen vectors:
Dip-Dir Dip
172.1 4.802
262.6 5.987
43.66 82.31
Confidence Radius
95% Signif.: 22.6 deg.
Best Fit Girdle:
Azim = 352
Dip = 85.1

SQ11

Eigen values:
.426 .334 .2391
Eigen vectors:
Dip-Dir Dip
3.670 42.09
157.6 44.86
261.3 13.32
Confidence Radius
95% Signif.: 21.0 deg.
Best Fit Girdle:
Azim = 184
Dip = 47.9

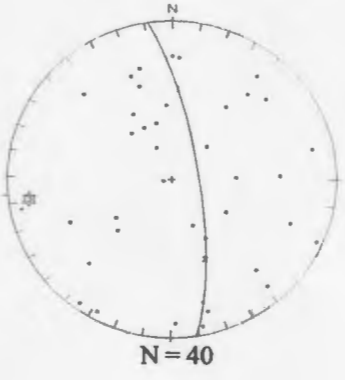

Figure B-1. Continued.